

University of Nottingham
UK | CHINA | MALAYSIA

NUMERICAL INVESTIGATION OF HEAT TRANSFER OF A MULTI-LAYERED MICROCHANNEL HEAT SINK WITH TAPERED CHANNEL

Zuo Jiawei

024020

Supervised by Dr. Wong Kok Cheong

Prof. Ng Hoon Kiat

THESIS SUBMITTED TO THE UNIVERSITY OF NOTTINGHAM FOR THE DEGREE OF DOCTOR PHILOSOPHY

Abstract

With the ever-growing development of microelectronic equipment, a more efficient heat dissipation method is in demand. The present study seeks to enhance the heat transfer characteristic in microchannel heat sink (MCHS), while maintain low power consumption by using multi-layered microchannels, different flow configurations and tapered channel profile.

The numerical study is firstly conducted on DL-MCHS with parallel and counter flow with tapered channel profile. Parametric study is then conducted to evaluate the effect of different design parameters of channel inlet width,W_i channel outlet width, W_o and channel height, H_{ch} on thermal and hydraulic performance. The results show that the designs with counter flow configuration always have better thermal performance than the designs with parallel flow configuration when volumetric flow rate is large and the difference become more significant with the decrease of W_i, the maximum difference of 0.05K/W (21.67%) can be found at design with $W_i = 50\mu m$ $W_o = 200\mu m$ at $H_{ch} = 375\mu m$. However, the DL-MCHS with parallel flow always shows better thermal-hydraulic performance as compared with counter flow with exact channel dimensions, maximum difference of 0.12(12.13%) is found between parallel and counter flow configuration for design with W_i=50μm W_o=50μm. For both parallel and counter flow, the deign W_i=150μm and W_o=200μm presents the best thermal-hydraulic performance.

The numerical study is then conducted on DL-MCHS with alternating flow. The results for DL-MCHS with alternating flow shows largely similar results of thermal resistance as compared to the DL-MCHS with counter flow configuration. The optimum DL-MCHS with alternating flow and tapered channel show about 76% better in thermo-hydraulic performance as compared with benchmark of DL-MCHS with straight channel design with inlet and outlet channel size of $50\mu m$.

Numerical study is also conducted on three-layered MCHS with parallel flow (PF), counter flow1(CF1), counter flow 2(CF2). counter flow 3(CF3) and with tapered channel profile. The CF1 exhibits better thermal performance for converging channel design and PF presents better thermal performance for diverging channel design. For all flow configurations, PF always shows best thermal hydraulic performance among different flow configurations and the design with W_i=150μm and W_o=200μm presents the best thermal-hydraulic performance among different channel designs.

Finally, the thermal resistance network for DL-MCHS with parallel flow configuration has been obtained and the correlation of local Nusselt number in terms of axial distance and channel outlet width for different channel inlet width has been proposed. Good agreement was found between correlated results and generated numerical results, which provides a more convenient tool to predict the temperature along the

flow direction for DL-MCHS with parallel flow and tapered channel profile.

Acknowledgement

I express my deepest gratitude to my supervisor, Dr. Wong Kok Cheong for all these years' guidance.

Also, I want to thank all my colleagues and friends.

The last but the most important, I convey my thanks to my parents and sister for supporting me to finish the study.

Contents

ABSTRACT ii

ACKNOWLEDGEMENT iv

CONTENTS v

LIST OF FIGURES viii

LIST OF TABLES xiii

ABBREVIATIONS AND NOMENCLATURE xiv

ABBREVIATIONS xiv

PUBLICATIONS xvii

Chapter 1. INTRODUCTION 1

1.1 Background of Research 1

1.2 Objective 3

1.3 Thesis outline 4

1.4 Novelties and contributions 5

Chapter 2. Literature review 6

2.1 Introduction 6

2.2 Experimental analysis 6

2.3 Numerical analysis 13

2.4 Correlation 33

2.5 Conclusion from literature 37

Chapter 3. Methodology 38

3.1 Introduction 38

3.2 Numerical Model 38

3.2.1 The numerical model for Dl-MCHS with parallel/counter flow 38

3.2.2 The numerical model for DL-MCHS with alternating flow..... 41
3.2.3 The numerical mode for three-layered MCHS..... 42
3.3 Governing Equation and assumptions 43
3.4 Validation and grid independence test 49
3.4.1 Validation results..... 49
3.4.2 Grid Independence Test 52
Chapter 4 Numerical investigation of DL-MCHS with tapered channel profile 54
4.1 Introduction 54
4.2 The thermal performance for DL-MCHS with different designs at various Re. 54
4.3 The hydraulic performance for DL-MCHS with different designs at various Re. 61
4.4 The overall thermal resistance for DL-MCHS with different Wo, Wi and Hch..... 64
4.4.1 The thermal resistance for DL-MCHS operating in counter flow configuration 64
4.4.2 The thermal resistance for DL-MCHS operating in parallel flow configuration 65
4.4.3 The comparison of thermal resistance between parallel and counter flow configuration. 69
4.4.4 DL-MCHS design with high thermal performance..... 76
4.5 The overall pumping power for DL-MCHS with different Wo, Wi and Hc for counter flow configuration..... 76
4.5.1 The overall pumping power for DL-MCHS operating in counter flow configuration..... 76
4.5.2 The overall pumping power for DL-MCHS operating in parallel flow configuration..... 77
4.6 The thermal-hydraulic performance for DL-MCHS with different flow configurations 80
4.6 Conclusions 82
Chapter 5 Numerical Investigation of Tapered DL-MCHS with Alternating Flow configuration ... 84
5.1 Introduction 84
5.2 Thermal performance for Dl-MCHS with alternating flow at various Re 84

5.3 The thermal and hydraulic performance for DL-MCHS with alternating flow at fixed volumetric flow rate 88

5.4 Thermo-hydraulic performance for DL-MCHS with alternating flow configuration 94

5.5 The thermal performance for Dl-MCHS with different substrate material 95

5.6 Conclusion 98

Chapter 6.Numerical investigation on Three-Layered Microchannel Heat Sink with Tapered Channel Profile……99

6.1 Introduction 99

6.2 The thermal performance for three-layered MCHS with different flow configurations at various Re. 99

6.3 The hydraulic performance for three-layered MCHS at various Re. 106

6.4 The thermal performance for three-layered MCHS with different flow configurations. 108

6.5 Temperature distribution for three-layered MCHS 110

6.6 Thermal-hydraulic performance for three-layered MCHS with different flow configurations. 112

6.7 Conclusions 115

Chapter 7. Heat Transfer Network and Correlation for a Double-Layered Microchannel Heat Sink . 116

7.1 Introduction 116

7.2 Thermal resistance correlation 116

7.3 Comparison of correlation and simulation results for DL-MCHS. 122

7.4 Nu correlation for tapered MCHS. 123

Chapter 8. Conclusion and recommendation for future work 127

8.1 Conclusion 127

8.2 Future work 130

Reference 132

List of figures

Figure 1-1 Schematic of SL-MCHS proposed by Tuckerman and Pease [5] 2

Figure 2-1 MCHS with Ω-shaped reentrant configurations in mm [15]. 8

Figure 2-2 Schematic of fractal network [18]. 9

Figure 2-3 The schematic of stacked DL-MCHS proposed by Wei et al. [29]. 11

Figure 2-4 The schematic of MCHS with uniform channel profile proposed by Xia et al. [31] 12

Figure 2-5 Photograph of MCHS with zig-zag flow passage proposed by Dai et al. [32] 12

Figure 2-6 Simulation model of interlaced and parallel microchannels [38]. 14

Figure 2-7 Schematic diagram of MCHS with Different inlet/outlet locations, head shapes and microchannel designs [39]. 15

Figure 2-8 Geometry of MCHS with curved channels. 18

Figure 2-9 Schematic of cross-view of a single U-shaped microchannel. 20

Figure 2-10 Schematic of cobweb-shaped MCHS [61]. 20

Figure 2-11 SEM photograph of reentrant porous microchannels proposed by [75] 23

Figure 2-12 The Schematic for the DL-MCHS with counter flow configuration proposed by Vafai and Zhu[7]. 23

Figure 2-13 The schematic of staggered DL-MCHS with (a) Straight channel design, (b)Wavy channel design(c) X-structure [81] 26

Figure 2-14 The schematic of DL-MCHS with truncated top channels [92] 28

Figure 2-15 The schematic of DL-MCHS with porous fins[94]. 29

Figure 2-16 The schematic of MCHS with porous substrate [95]. 30

Figure 3-1 Schematics of (a) double-layer MCHS (b) single unit of MCHS (c) computational domain. 39

Figure 3-2 Schematics of (a) width-converging channel with counter flow configuration and (b)

width-converging channel with parallel flow configuration. 40

Figure 3-3 (a) Repeating section of the DL-MCHS with alternating flow (b) Schematics of computational domain for Dl-MCHS with alternating flow 41

Figure 3-4 The schematic of (a) three-layered-MCHS (b) single section of three-layered-MCHS 42

Figure 3-5 Schematics of boundary conditions for (a) parallel flow configuration PF, (b) counter flow configuration CF1, (c) counter flow configuration CF2 and (d) counter flow configuration CF3 43

Figure 3-6 Influence of fluid properties on maximum temperatures for DL-MCHS with parallel flow and with different W_i. 44

Figure 3-7 Flow chart for nuermcai anlysis using Ansys Fluent. 47

Figure 3-8. Schematics of DLMS and computational domain[85]. 49

Figure 3-9 the graph of max thermal resistance versus the channel number valid with Lin et al. [85] 50

Figure 3-10 The schematic of (a)experimental test module (b) computational domain proposed by Wei et al [29]. 51

Figure 3-11 The graph of max temperature along the bottom surface valid with Wei et al. [29] 52

Figure 3-12 The results of (a) thermal resistance, R_t (b) pumping power, Ω for three grid sizes 53

Figure 4-1 Temperature distributions along flow direction on the bottom and symmetry plane for four designs (1,4,5 and 8) at Re=200 for DL-MCHS with parallel flow configuration. 55

Figure 4-2 Temperature distributions along flow direction on the bottom and symmetry plane for four designs (1,4,5 and 8) at Re=200 for DL-MCHS with counter flow configuration. 56

Figure 4-3 The R_t for DL-MCHS with parallel flow and with different designs at various Re. 57

Figure 4-4 The R_t for DL-MCHS with counter flow and with different designs at various Re. 57

Figure 4-5 The Nu for Dl-MCHS with parallel flow at various Re for (a) Design 1-4 (b) Design 5-8. 59

Figure 4-6 The Nu for Dl-MCHS with counter flow at various Re for (a) Design 1-4 (b) Design 5-8. 60

Figure 4-7 The velocity distribution for DL-MCHS with different designs for Re=200. 62

Figure 4-8 The pressure for DL-MCHS with different designs at various Re. 63

Figure 4-9 The thermal resistance for counter flow configuration in DL-MCHS with different W_o, Wi and H_{ch} (a) H_{ch} = 325 μm, (b) H_{ch} = 350 μm, (c) H_{ch} = 375 μm, and (d) H_{ch} = 400 μm. 66

Figure 4-10 The thermal resistance for parallel flow configuration in DL-MCHS with different W_o, Wi and H_{ch} (a) H_{ch} = 325 μm, (b) H_{ch} = 350 μm, (c) H_{ch} = 375 μm, and (d) H_{ch} = 400 μm. 68

Figure 4-11 Comparison of thermal resistance between parallel and counter flow configuration for H_{ch} =325μm and (a) W_o =50μm, (b) W_o =100μm, (c) W_o =150μm (d) W_o =200μm 70

Figure 4-12 Comparison of thermal resistance between parallel and counter flow configuration for H_{ch} =350μm and (a) W_o=50μm, (b) W_o =100μm, (c) W_o =150μm (d) W_o =200μm 71

Figure 4-13 Comparison of thermal resistance between parallel and counter flow configuration for H_{ch} =375μm and (a) W_o=50μm, (b) W_o =100μm, (c) W_o =150μm (d) W_o =200μm 72

Figure 4-14 Comparison of thermal resistance between parallel and counter flow configuration for H_{ch} =400μm and (a) W_o =50μm, (b) W_o =100μm, (c) W_o =150μm (d) W_o =200μm 73

Figure 4-15 Temperature distribution along the bottom surface of the DL-MCHS for parallel flow and counter flow configuration. 74

Figure 4-17 Temperature distribution along the bottom surface of the DL-MCHS for parallel flow and counter flow configuration for H_{ch} =325μm and Wo=50μm 75

Figure 4-18 The overall pumping power for counter flow configuration in DL-MCHS with different Wo, Wi and H_c (a) H_c = 325 μm, (b) H_c = 350 μm, (c) H_c = 375 μm, and (d) H_c = 400 μm 78

Figure 4-19 The overall pumping power for parallel flow configuration in DL-MCHS with different Wo, Wi and H_{ch} (a) H_{ch} = 325 μm, (b) H_{ch} = 350 μm, (c) H_{ch} = 375 μm, and (d) H_{ch} = 400 μm. 79

Figure 4-20 The FOM for DL-MCHS with parallel flow configuration. 81

Figure 4-21 The FOM for DL-MCHS with counter flow configuration. 81

Figure 4-22 The comparison of FOM between Dl-MCHS with parallel and counter flow configuration. 82

Figure 5-1 Temperature distribution for four designs at Re=200. 85

Figure 5-2 R_t for DL-MCHS with alternating flow and with different Re ranging from 100-1000. 86

Figure 5-3 Nu for DL-MCHS with alternating flow and with different Re r for (a) Design 1-4 (b) Design 5-8 87

Figure 5-4 The thermal resistance for DL-MCHS with alternating flow configuration. 88

Figure 5-6 The pressure drop for DL-MCHS with alternating flow configuration 89

Figure 5-7 The comparison of Rt between DL-MCHS with alternating and parallel flow configuration. 90

Figure 5-8 The comparison of Rt between DL-MCHS with alternating and counter flow configuration. 90

Figure 5-9 The ΔTb for DL-MCHS with alternating flow configuration 91

Figure 5-10 Temperature distribution for DL-MCHS with alternating flow configuration with (a) Straight channel design (b) tapered channel design with fixed Wi of 50μm (c) tapered channel design with fixed Wo of 50μm 93

Figure 5-11 FOM for DL-MCHS with alternating flow configuration 95

Figure 5-12 The R_t for DL-MCHS with alternating flow and different substrate materials for W_o of (a)50μm, (b)100μm, (c)150μm and (d)200μm. 97

Figure 6-1 Temperature distribution for three-layered MCHS with different flow configurations for Design 1 100

Figure 6-2 Temperature distribution for three-layered MCHS with different flow configurations for Design 4 101

Figure 6-3 Temperature distribution for three-layered MCHS with different flow configurations for Design 5 102

Figure 6-4 Temperature distribution for three-layered MCHS with different flow configurations for Design 8 103

Figure 6-5 The R_t for three-layered MCHS with PF at various Re. 104

Figure 6-6 The R_t for three-layered MCHS with CF1 at various Re. 104

Figure 6-7 The R_t for three-layered MCHS with CF2 at various Re. 105

Figure 6-8 The R_t for three-layered MCHS with CF3 at various Re. 105

Figure 6-10 The △P for three-layered MCHS for (a) design 1-4 (b) design 5-8. 107

Figure 6-11 Comparison of thermal resistance among PF, CF1, CF2 and CF3 flow configurations for (a)$Wo = 50\mu m$, (b)$Wo = 100\mu m$, (c)$Wo = 150\mu m$ and (d)$Wo = 200\mu m$ 109

Figure 6-12 Comparison of $T_{y,max}$ among 4 flow configurations for case of (a) converging channel with $Wi = 200\mu m$ $Wo = 50\mu m$, (b) straight channel with $Wi = 50\mu m$ $Wo = 50\mu m$ and (c) diverging channel with $Wi = 50\mu m$ $Wo = 200\mu m$ 111

Figure 6-13 FOM for three-layered MCHS with PF. 112

Figure 6-14 FOM for three-layered MCHS with CF1. 112

Figure 6-15 FOM for three-layered MCHS with CF2. 113

Figure 6-16 FOM for three-layered MCHS with CF3. 113

Figure 6-17 The comparison of FOM between three-layered MCHS with PF, CF1, CF2 and CF3. 114

Figure 7-1.The heat transfer flow within DL-MCHS. 117

Figure 7-2 (a) shows the thermal resistance network proposed by Wei et al. [16] and (b) The thermal resistance after delta-wye conversion for DL-MCHS 120

Figure 7-3 The comparison of ΔT_y for DL-MCHS with different Wch. 123

Figure 7-4 The comparisong between generated and correlated Nu_y for W_i=50μm. 125

Figure 7-5 The comparisong between generated and correlated Nu_y for W_i=100μm. 125

Figure 7-6 The comparisong between generated and correlated Nu_y for W_i=150μm. 125

Figure 7-7 The comparisong between generated and correlated Nu_y for W_i=200μm. 125

List of tables

Table 1-1: Classification of Channels [8]. 3

Table 2-1 The summarized correlations. 34

Table 3-1 Material properties used in simulation[124]. 39

Table 3-2 The W_i and W_o for different designs. 40

Table 3-3 Different geometries of DL-MCHS of for parametric studies 41

Table 3-4 The microchannel dimensions $\times 103$(m) proposed by Wei et al [29]. 51

Table 5-1 The material properties of Aluminum, copper and silicon[29]. 96

Table 7-1 The constant used in Eq. (7.17) for different W_i and corresponding R^2. 124

Abbreviations and nomenclature

Abbreviations

DL-MCHS	Double-layered microchannel heat sink
DRIE	deep reactive ion etching technique
FOM	Figure of merit
FSM	Fractional Step Method
FVM	Finite Volume Method
MCHS	Micro-channel heat sink
PDE	Partial Differential Equations
RIE	reactive ion etching
SIMPLE	Semi-Implicit Method for Pressure Linked Equations
SIMPLEC	Semi-Implicit Method for Pressure Linked Equations-Consistent
SL-MCHS	Single-layered microchannel heat sink

NOMENCLATURE

Variables

A	Area (m^2)
$\mathbf{c_p}$	Specific heat, (J kg^{-1} K^{-1})

H	Height (m)
h	Heat transfer coefficient, W/(m^2°C)
K	Thermal conductivity, (W/m/K)
L	Length (m)
N	Channel number
P	Pressure, (Pa)
Q	volumetric flow rate, (ml/min)
$\boldsymbol{q}''$	Heat flux (W/cm^2)
$\boldsymbol{R_T}$	Thermal resistance (K/W)
T	Temperature (℃)
v	Velocity(m/s)
W	Width (m)
$\boldsymbol{y}^*$	Dimensionless axial distance
δ	Thickness(m)
ρ	Density (kg/m^3)
Ω	pumping power, (W)
μ	Viscosity (kg/m/s)

Subscript

b	base
ch	channel
f	fluid
in	inlet
m	mean
max	maximum
min	minimum
out	outlet
r	rib
s	solid
z	z −direction
x	x −direction
y	y −direction

Dimensionless number

Nu	Nusselt Number
Pr	Prandtl Number
Re	Reynolds Number

Publications

ZUO, J.-W., WONG, K.-C. and NG, H.K., 2019. Heat transfer network and correlation for a double-layered microchannel heat sink Journal of Advanced Research in Fluid Mechanics and Thermal Sciences. 56(1), 88-99

ZUO, J.-W., WONG, K.-C. and NG, H.K., 2019. The thermal performance of three-layered microchannel heat sink with tapered channel profile Journal of Advanced Research in Fluid Mechanics and Thermal Sciences. 56(1), 147-156

ZUO, J.-W., WONG, K.-C. and NG, H.K., 2019. Numerical investigation of tapered DL-MCHS with alternating flow configuration CFD Letters. 11(12), 1-12

K.-C.WONG, J.W.ZUO and H.K. NG, 2017. The thermal performance of Double Layer Microchannel Heat Sink with tapered channel profile In: ICENS-Summer August 23-25, 2017, Sapporo, Japan.

Chapter 1. Introduction

1.1 Background of research

With the fast development of microelectronic equipment, the number of transistor on integrated circuit doubles almost every other year [1]. The heat removal becomes a serious problem to meet the demand for the thermal performance required. The overheating for electronic equipment may lead to some fundamental problems, such as: reduced lifespan, increased operating cost, reduced reliability, reduced performance and higher manufacturing cost.

Various electronic cooling solutions has been proposed to meet the growing heat dissipation requirement. Piezoelectric fans are ultra-low power air movers, which uses actuator to induce resonance in the blade, forms vortex through disturbing surrounding air with high frequency and amplitude oscillation and creates downstream wind velocities in blade [2]. However, due to the low thermal conductively of air, the cooling efficiency is relatively low. A Heat pipes is a heat transfer device that uses phase transition and thermal conduction to transfer heat between two solid interfaces. When heat is applied to the system, the volatile liquid in contact with the hot surface turns into vapor though thermal conduction. The change in pressure gradient causes vapor travels to the cold regions, where the vapor condenses back in liquid and returns to the hot interface through capillary action, centrifugal force or gravity and forms a close-loop [3-4]. The heat pipes are high effective thermal conductors due to the high heat transfer coefficient for boiling and condensation. The heat transfer can also be enhanced by placing a conductive thick metal plate (cold plate) between heat source and cold flowing fluid. The cold plate method has advantages of no additional pumping power and no extra heat transfer surface area required. As an attempt to solve the problem of high heat flux over small area, Tuckerman and Pease[5] first proposed the design of micro-channel heat sink (MCHS) in 1981,which is shown in Fig 1-1, by using silicon as substrate material and deionized water as coolant, the maximum thermal resistance can achieve 0.09 ℃/W when subjected to uniform heat flux of 790 W/cm^2.

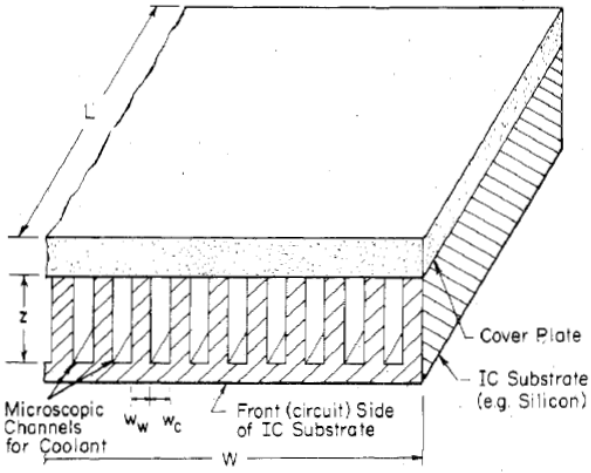


Figure 1-1 Schematic of SL-MCHS proposed by Tuckerman and Pease [5]

The decrease of the channel size has greatly improved the heat sink's thermal performance due to its high area to volume ratio, but also increase the pressure drop dramatically. To compare the thermal-hydraulic performance between different MCHS designs, Figure of merit (FOM) is applied to determine the improvement of one design in terms of heat transfer and pumping power at the same time and has been widely used by researchers. Compared with MCHS with uniformed rectangular channel profiles, it was found that the thermal performance can be enhanced by changing channel profile along the flow direction and/or insert ribs, but normally with the sacrifice of higher pressure drop. However, by adjusting the design parameters, the overall thermo-hydraulic performance can be enhanced.

For SL-MCHS, the maximum local temperature normally increases with the flow direction, with the peak temperature occurs at near the outlet position and temperature difference can reach 36℃ when subject to uniform heat flux of 100 W/cm^2 [6]. To reduce the temperature gradient along axial-direction, Vafai and Zhu [7] proposed the concept of DL-MCHS which is a substantial improvement over a conventional SL-MCHS. They pointed out that when compared with SL-MCHS design, the DL-MCHS with counter flow configuration shows much lower temperature rise at on the base surface and substantially smaller pressure drop.

To differentiate the micro-channels to the conventional channels, Kandlikar and Grande [8] proposed the class of channels based on different hydraulic diameter range, which is listed in Table 1-1. So, in the

present study, the parametric study is conducted within this range.

Table 1-1: Classification of Channels [8]

Class of Channel	**Range of Hydraulic Diameter D_H**
Conventional Channels	Dh > 3mm
Minichannels	3mm ≥ Dh > 200μm
Microchannels	200μm ≥ Dh > 10μm
Transitional Channels	10μm ≥ Dh > 0.1μm
Transitional Microchannels	10μm ≥ Dh > 1μm
Transitional Nanochannels	1μm ≥ Dh > 0.1μm
Molecular Nanochannels	Dh ≤ 0.1μm

1.2 Objective

This study has carried out the analysis of thermal, hydraulic and thermo-hydraulic performance on multi-layered MCHS with different tapered channel designs and with different flow configurations.

- To study the thermal and hydraulic performance for DL-MCHS with parallel, counter and alternative flow configuration and with different design parameters (channel inlet width, channel outlet width and channel height). Provide the design with best thermo-hydraulic performance.
- To study the thermal and hydraulic performance for three-layered MCHS with parallel flow (PF), counter flow 1(CF1), counter flow 2(CF2) and counter flow 3(CF3) configuration and with different design parameters. Provide the design with best thermo-hydraulic performance.
- To generate the local Nusselt number for tapered microchannels and use generated Nusselt number and proposed thermal resistance model to obtain a correlation of local thermal

resistance for heat transfer of a DL-MCHS with parallel flow configuration and tapered channel design.

1.3 Thesis outline

This thesis contains 8 chapters. After the introduction of research in this chapter, the following chapters of the thesis are described briefly below:

Chapter 2 presents the literature review on this research topic in terms of experimental, numerical and analytical studies on MCHS.

Chapter 3 presents the overview of research methodology for numerical simulation in chapters 4 to chapter 7.

Chapter 4-6 presents the thermal and hydraulic performance for DL-MCHS and three-layered MCHs with different channel design and different flow configuration.

Chapter 7 presents the correlation of Nu and the thermal resistance model to predict the temperature distribution along flow direction for multi-layered MCHS.

Chapter 8 contains the conclusions of this research and the recommendations for the future work.

1.4 Novelties and contributions

The novelties and contributions of current study is presented below:

Multiple novel numerical studies were developed which considered new geometry of microchannel heat sinks as follows:

a. DL-MCHS with tapered channel designs
b. 3L-MCHS with tapered channels

in which different flow configurations of parallel flow, counter flow and alternating flow between layers of channels were investigated for their thermal and hydraulic performance.

1) The research output provided new understanding of the thermal and hydraulic performance of the DL-MCHS and 3L-MCHS with tapered channel designs under the mentioned flow configurations in terms of:
   a) Coupled effects of geometry and flow configurations on temperature uniformity
   b) Coupled effects of geometry and flow configurations on both high thermal and hydraulic performance
2) A new thermal-resistance model for DL-MCHS with tapered channel design capable of predict the local thermal resistance were developed, which is useful for the design and optimization of MCHS.

Chapter 2. Literature review

2.1 Introduction

This chapter presents a literature review to show the knowledge gap in this field of study. At the beginning, the chapter discusses the previous experimental work for MCHS in Section 2.2. Then the previous numerical study on analysing the fluid flow and heat transfer characteristic for MCHS is presented in Section 2.2. Section 2.4 discusses the previous studies on predicting heat transfer performance for SL- and DL-MCHS based on thermal resistance model. Lastly, the research gaps are identified and presented in Section 2.5.

2.2 Experimental analysis

In 1981, Tuckerman and Pease [5] experimentally studied the performance for silicon-based SL-MCHS. Channel size of 50μm in height and 50μm in width were etched vertically by using an orientation dependent etching technology. Based on their experimental results, they concluded that for laminar flow within confined channels, the convective heat transfer coefficient is inversely proportional to the channel width and high aspect ratio can effectively reduce the thermal resistance. This indicated that the MCHS design with smaller channel size gives higher heat transfer coefficient and better thermal performance and the thermal performance can be enhanced by properly adjusting the geometrical parameters.

After their pioneer's work, Wu and Little [9-10] experimentally studied the friction factor and heat transfer characteristics for MCHS with gas flow for both laminar and turbulent regime. The channel dimension of width ranging from 130-200μm and height ranging from 30-60um was fabricated through photolithographic technique for both glass and silicon based MCHS. They pointed out that both fraction factor and heat flux are highly dependent on the channel shape, size, and roughness. The increase of channel roughness led to better heat transfer coefficient with the sacrifice of friction factor. In addition, they claimed that flow transits to from laminar to turbulent flow occurred at a Reynolds number of 1000.

Lee and Garimella [11] performed an experimental study of a copper-based microchannel with different channel sizes (with hydraulic diameters of 318–903μm). Both laminar and turbulent flow with Re ranging from 300 to 3500 were considered to investigate the heat transfer and fluid flow for single-phase flows in the thermally developing laminar regimes. The results showed that the thermal performance enhanced with the decrease of channel size. Moreover, they proposed numerical predictions based on a classical,

continuum approach and good agreement was found between predictions and experimental data.

The fluid flow and heat transfer characteristic of manifold MCHS was numerically and experimentally studied by Zhou et al. [12]. It was found that hierarchical manifold MCHS produced a uniform flow distribution, exhibited lower overall thermal resistance and pressure drop as compared to the typical manifold MCHS at volumetric flow rate ranging from 0.12-1.17L/min. The maximum value of cooling efficient of performance of 19480 was found for hierarchical manifold MCHS at the volumetric flow rate of 0.6L/min and heat flux of 260Wcm^2.

Shkarah et al. [13] numerically studied the effect of channel shapes and substrate material on thermal performance for SL-MCHS. Different substrate material of aluminium, silicon, and graphene and three sets of channel shapes with channel width ranging from 44-56μm and channel height ranging from 287-320μm were used for investigation under different heat fluxes and different volumetric flow rates. They found that graphene exhibited best thermal performance in terms of thermal resistance as compared with silicon and aluminium at same volumetric flow rate.

Mansoor et al. [14] employed 3D simulations of a rectangular cross-sectional copper-based MCHS using single-phase laminar flow to predict the heat transfer characteristic. Different coolant velocities with Re ranging from 500-2000 and different heat flux ranging from 45-130W/cm^2 were considered. A commercial CFD software - FLUENT were employed to solve the 3D conjugate model and good agreement was found as compared with previous experimental and numerical data. This indicated that FLUENT was a good option to perform the numerical study for MCHS. Moreover, they found that the value of heat transfer coefficient increased with the increase of the applied heat flux. In addition, High Reynolds led fluid flow transited from single-phase to two-phase flow and the criteria increased with the increases of heat flux applied.

An experimental study of flow boiling performance on copper based MCHS with Ω-shaped reentrant configurations was conducted by Deng et al. [15] as shown in Figure 2-1. The comparison of flow boiling performance between Ω-shaped reentrant microchannels and rectangular microchannels with same hydraulic diameter were investigated with different coolants of ethanol and deionized wate. The results indicated that the Ω-shaped reentrant microchannels exhibited better heat transfer performance at large inlet subcooling and moderate to high hat flux and lower pressure drop for all cases studied as compared with rectangular microchannels. Moreover, the results showed that water presented better heat transfer performance than ethanol for both Ω-shaped reentrant microchannels and rectangular microchannel designs.

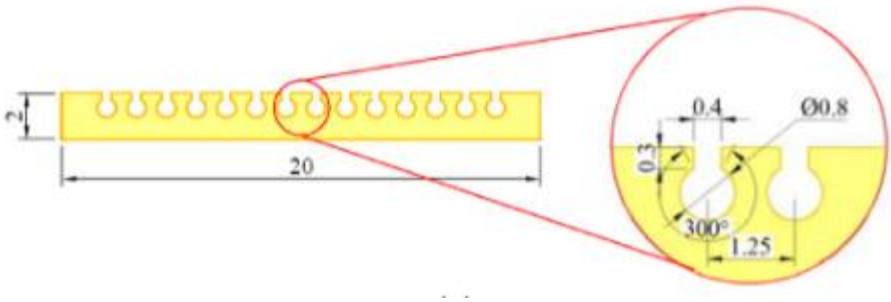


Figure 2-1 MCHS with Ω-shaped reentrant configurations in mm [15].

Zheng et al. [16] numerically and experimentally studied the thermal and hydraulic performance for hierarchical MCHSs with Reynolds number ranging from 1500 to 5500. Better heat transfer performance and minor increase in pressure drop was observed in the proposed design. The experimental results, as well as the numerical results, showed that the proposed design can dissipated heat load up to 700 W/cm^2 with maximum temperature rise lower than 52K.

Pandey et al. [17] experimentally studied the thermal and hydraulic characteristic of copper-based parallel microchannel and pin-fin heat sinks. The results showed that the thermal resistance decreases with the increase of pumping power for both designs, but the parallel microchannel design always presents better thermal resistance and higher pumping power as compared to the pin-fin design with same heat flux conditions.

Silicon based fractal tree-shaped MCHS with different bifurcation angles, as shown in Figure 2-2, were experimentally studied by Ji et al. [18] under different inlet Reynolds number of 500 to 1700. It was found that the fractal MCHS can greatly enhance both thermal and hydraulic performance as compared with traditional straight MCHS. The results showed that the pressure drop can be reduced by up to 92% and the heat transfer coefficient can be increased up to 1.5 times when compared to the straight MCHS with same flow rate. The optimized bifurcation angle of the fractal network was found to be 30°and the coefficients of performance was found to be 12-13 times at this angle.

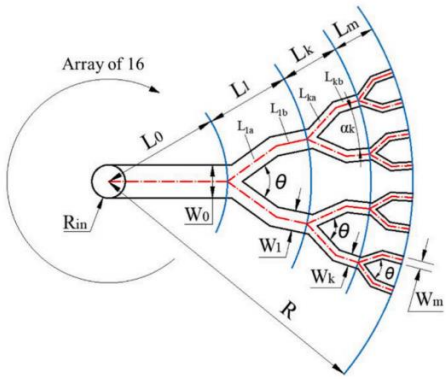


Figure 2-2 Schematic of fractal network [18].

Zhang et al. [19] numerically and experimentally studied the effect of structure parameters and arrangement ways of internal fins in MCHS. The numerical results showed good agreement with experimental results with relative error within 2%. Moreover, the proposed design presented lower maximum temperate, average temperature, temperature uniformity and pressure drop as compared to the straight channel design.

To find the MCHS with best thermal performance and lowest power consumption with low cooling volume, Parlak et al. [20] numerically and experimentally investigated the effect of channel spacing, channel height and channel thickness on thermal and hydraulic performance for MCHS. Good agreement was found between numerical results and experimental results. Moreover, it was found that the thermal resistance is highly depending on the channel thickness and spacing. The design with channel height of 2mm has the optimized overall performance.

MCHS with inline and staggered open-ring pin fins was numerically and experimentally studied by Zeng et al. [21]. Flow channels of internal separated and merged passages (ISMP) and external convergent-divergent passages (ECDP) was considered for Re ranging from 160-694. It was found that the proposed design exhibited noticeably enhancement in Nu as compared to the conventional straight channel, which was mainly due to the periodic flow separation and convergence, successive flow mixing and periodic interruptions and redevelopment of boundary layers induced by the open-ring fins. Moreover, the proposed design exhibited better overall thermal-hydraulic performance and the advantage becomes more obvious at high heat flux.

Qu and Mudawar [6] numerically and experimentally studied the heat transfer and pressure drop characteristic for MCHS with single-phase water-cooled flow. The microchannel with height of 231μm and depth of 713μm was fabricated on an oxygen-free copper. They found the early transition from laminar to turbulent was not observed within the tested Reynolds number ranging from 139 to 1672. Increasing Reynolds number greatly reduces the outlet temperature of coolant and MCHS maximum temperature at the expense of larger pressure drop. Temperature distribution and pressure drop of the experimental results are in good agreement with the corresponding predictions, which proves that the conventional Navier-Stokes equation and energy equation can be used to predict the thermal performance for MCHS.

Kohl et al. [22] conducted an experimental study on the pressure drop for MCHS with both compressible and incompressible fluid flow. Different channel hydraulic diameters ranging from 25μm to 100μm were fabricated on silicon wafer through reactive ion etching (RIE) technique. They pointed out that the friction factor can be accurately determined based on experimental results for standard large channels.

Other than studies of MCHS with rectangular microchannel profile, Wu and Cheng [23] experimentally studied the convective heat transfer and pressure drop for laminar flow in 13 different trapezoidal silicon microchannels. They found that Nusselt number and apparent friction factor increase with the increase of surface roughness and surface hydrophilic property and the increase becomes more significant with the increase of Reynolds number.

Qu et al. [24] and Qu et al. [25] experimentally studied the heat transfer characteristic and flow characteristic of water through trapezoidal silicon microchannels with wide range of hydraulic diameters. Compared with the numerical results, the experimental results show a much lower value of Nusselt number and a higher value of pressure gradient. They pointed out that the difference may because of surface roughness of microchannel wall.

By inserting ribs and grooves inside microchannels, Wang et al. [26] conducted an experiment study on the performance of MCHS with micro-scale ribs and grooves. The micro-scale ribs and grooves were fabricated by using different surface-micromaching micro-electro-mechanical system processes. Compared with the smooth rectangular microchannel at Reynolds number ranging from 100 to 1000, the MCHS with ribs and grooves gives higher values of Nusselt number and friction factor, which can up to 1.55 and 4.09 times, respectively.

To investigate the MCHC with different flow passage, Dede [27] and Liu [28] experimentally and numerically studied the thermal resistance and pressure drop performance of a multi-pass branching

aluminium MCHS. The single-phase ethylene-glycol/water cooled MCHS was investigated at wide range of Reynolds number varies from 1070 to 6370. The multi-pass branching consists of two layers. Each layer was fabricated by micro-machining and bonded through diffusion bonding technique. They found that the multi-pass branching microchannels gives low thermal resistance and negligible penalty of pressure drop due to the compound jet and channel-based characteristics of the design plus the multiple passes through the branching microchannels. The optimized design of multi-pass branching MCHS shows low thermal resistance (0.34 cm^2 K/W) and low pressure drop (19.5 kPa at 1 L/min) when subjected to high heat flux of 100 W/cm^2.

By putting one layer of microchannels on top of another one, Wei et al. [29] experimentally and numerically studied the thermal performance of liquid cooled multilayer stacked MCHS. The stacked MCHS consists of 5 layers as shown in Figure 2-3, among which the two microchannel layers at the bottom are used to provide cooling, the two manifold layers above the microchannel layers are used to provide fluid distribution and the fifth layer at the top is used to provide inlet and outlet ports. The microchannels, manifolds and inlet/outlet ports are fabricated using deep reactive ion etching technique (DRIE) and all the five layers of MCHS are bonded into a watertight stack through silicon-silicon direct bonding. Based on the experimental results, they found that DL-MCHS with counter flow configuration shows better temperature uniformity, while the DL-MCHS with parallel flow configuration has lower peak temperature. The bottom layer of DL-MCHS has better heat removal ability compared to the top layer, since it is closer to the heat source. The thermal resistance as low as 0.09°C/(W/cm^2) was found for both parallel and counter flow configuration.

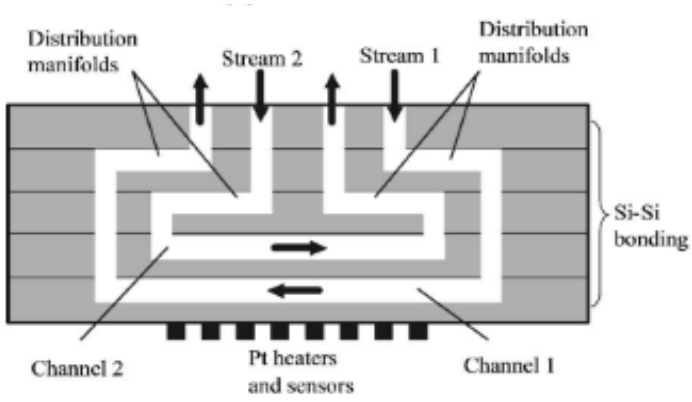


Figure 2-3 The schematic of stacked DL-MCHS proposed by Wei et al. [29].

Lu et al. [30] experimentally studied the liquid flow characteristic and heat transfer performance for both single-layered and double-layered MCHS. They concluded that the DL-MCHS shows similar heat transfer performance but much lower pressure drop compared with SL-MCHS.

In addition to the experimental studies on MCHS with uniform channel profile, Xia et al. [31] also experimentally and numerically studied the thermal behaviour and pressure drop for MCHS with complex structure. The schematic of microchannel with complex structure is shown in Figure 2-4. When flow rate is larger than 100ml/min, the MCHS with complex structure shows lower maximum and average temperature at the channel walls, better temperature uniformity and higher pressure drop compared with the equivalent rectangle MCHS. They pointed out that the enhanced heat transfer may due to the heat transfer area enlarged, thermal boundary interrupted and redeveloped, chaotic advection, hot and cooling fluid better mixed by vortex formed in the reentrant cavity. Compared with rectangle MCHS, the pumping power can reduce 18.99% when the total thermal resistance equals to 0.446 K/W and the thermal enhancement factor can reach 1.24 for Reynolds number of 611.

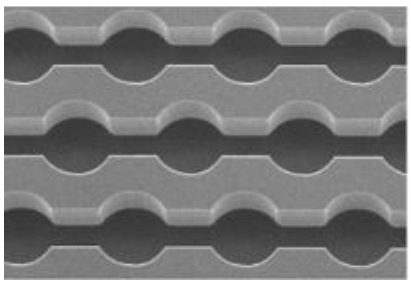


Figure 2-4 The schematic of MCHS with uniform channel profile proposed by Xia et al. [31]

Dai et al. [32] conducted an experimental investigation on single-phase water-cooled zig-zag MCHS with semi-circular cross-section as shown in Figure 2-5. They observed a transition from a steady flow to a time-dependent oscillatory flow with a few dominant frequencies through time-resolved measurements.



Figure 2-5 Photograph of MCHS with zig-zag flow passage proposed by Dai et al. [32]

Duryodhan et al. [33], Duryodhan et al. [34] and Duryodhan et al. [35] conducted an experimental study on fluid flow and heat transfer performance through MCHS with diverging and converging channels. As for thermal performance, they found that the heat transfer coefficient in converging microchannel is 35% higher than that in diverging channels and less pumping power is required compared with uniform cross-section microchannel. When it comes to the hydraulic performance, the results show that the pressure drop in converging microchannel varies non-linearly with the volume flow rate and inversely with the convergence angle and hydraulic diameter. They proposed an equivalent hydraulic diameter to predict the overall pressure drop through the converging microchannels and diverging microchannels, which is located at 1/3.6th of the total length from the narrowest width of the microchannel for converging microchannel and 1/3rd for the diverging microchannel.

The experimental results proposed by various researchers show that the MCHS has excellent heat removal ability. Moreover, increasing the surface area and developing secondary flow in microchannels, using different substrate material, using high thermal conductivity coolant can help enhance the thermal performance, but normally with the sacrifice of higher pressure drop.

2.3 Numerical analysis

The limitation of conducting experimental studies on MCHS is the difficulty of manufacturing micro-channels and the high cost to manufacture it. The numerical study based on certain assumptions solves the Navier-stoke equation through commercial computational fluid dynamic (CFD) software, provides a good tool to investigate the performance for microchannels with complex shapes without much error.

Monavari et al. [36] numerically studied the effects of particle shape (cylinder, brick, platelet, blade and oblate spheroid) on the thermohydraulic performance of a boehmite nanofluid in a aluminium based SL-MCHS with circular, rectangular, hexagonal and triangular cross sections at four different Reynolds numbers ranging from 400-1600. They found that the MCHS with triangular microchannels exhibited best thermal performance while the MCHS with circular microchannels showed the best thermo-hydraulic performance. Moreover, the temperature uniformity and thermal resistance reduced, while the heat transfer coefficient, pressure drop, and pumping power increased with the increase of Reynolds number for all nanoparticle shapes and channel cross-sections.

Sohel et al. [37] numerically investigated the thermal performance for circular shaped copper based SL-MCHS using three different types of nanofluids (Al_2O_3–Water, TiO_2–water and CuO–water) with different volume fractions ranging from 0.5 vol.% to 4 vol.% and at a constant inlet velocity of 1.5 m/s. They found

that the thermal performance in terms of heat flux was enhanced 13.15% for MCHS using 4 vol.% CuO–water nanofluid as compared with using pure water, followed by Al_2O_3–Water and TiO_2–water. However, the additional pumping power required was not considered.

Ling et al. [38] proposed the interlaced microchannel design, which two side walls of the microchannel are served as the main heat transfer surface as shown in Figure 2-6. The effect of different geometric parameters of depth, width and spacing on thermal and hydraulic performance were numerically investigated by using full-size conjugate heat transfer model. They found that the Nusselt number of the interlaced microchannel can increase up to 65.4% compared to the parallel microchannel, and the JF factor can reach 1.43. They pointed out that the thermal and hydraulic performance of the interlaced microchannel are improved with the increase of the depth and width of microchannel due to the heat transfer area in the first and second heat transfer directions are increased.

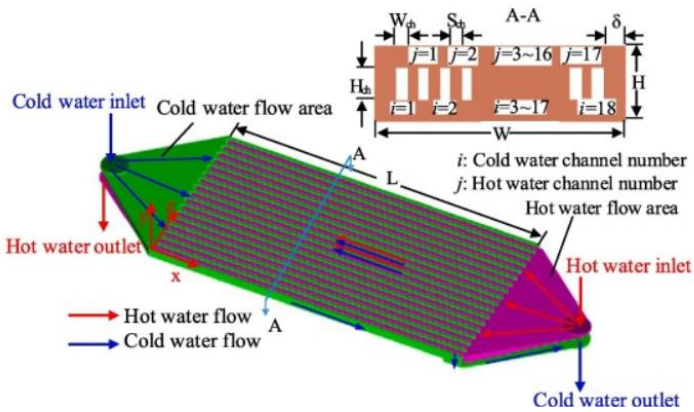


Figure 2-6 Simulation model of interlaced and parallel microchannels [38].

Xia et al. [39] numerically studied the fluid flow and heat transfer characteristics of microchannel heat sink with different inlet/outlet locations of I, C and Z types and different header shapes of triangular, trapezoidal and rectangular as shown in

Figure 2-7. Three microchannel cross-section shapes (the conventional rectangular microchannel, the microchannel with offset fan shaped reentrant cavities and the microchannel with triangular reentrant cavities) were also considered. The results showed that the I-type inlet/outlet location and rectangular header shape has the best flow velocity uniformity. And the microchannel with offset fan-shaped reentrant cavities and the microchannel with triangular reentrant cavities has better heat transfer performance as

compared to the conventional rectangular microchannel, which is mainly due to the e jetting and throttling effect.

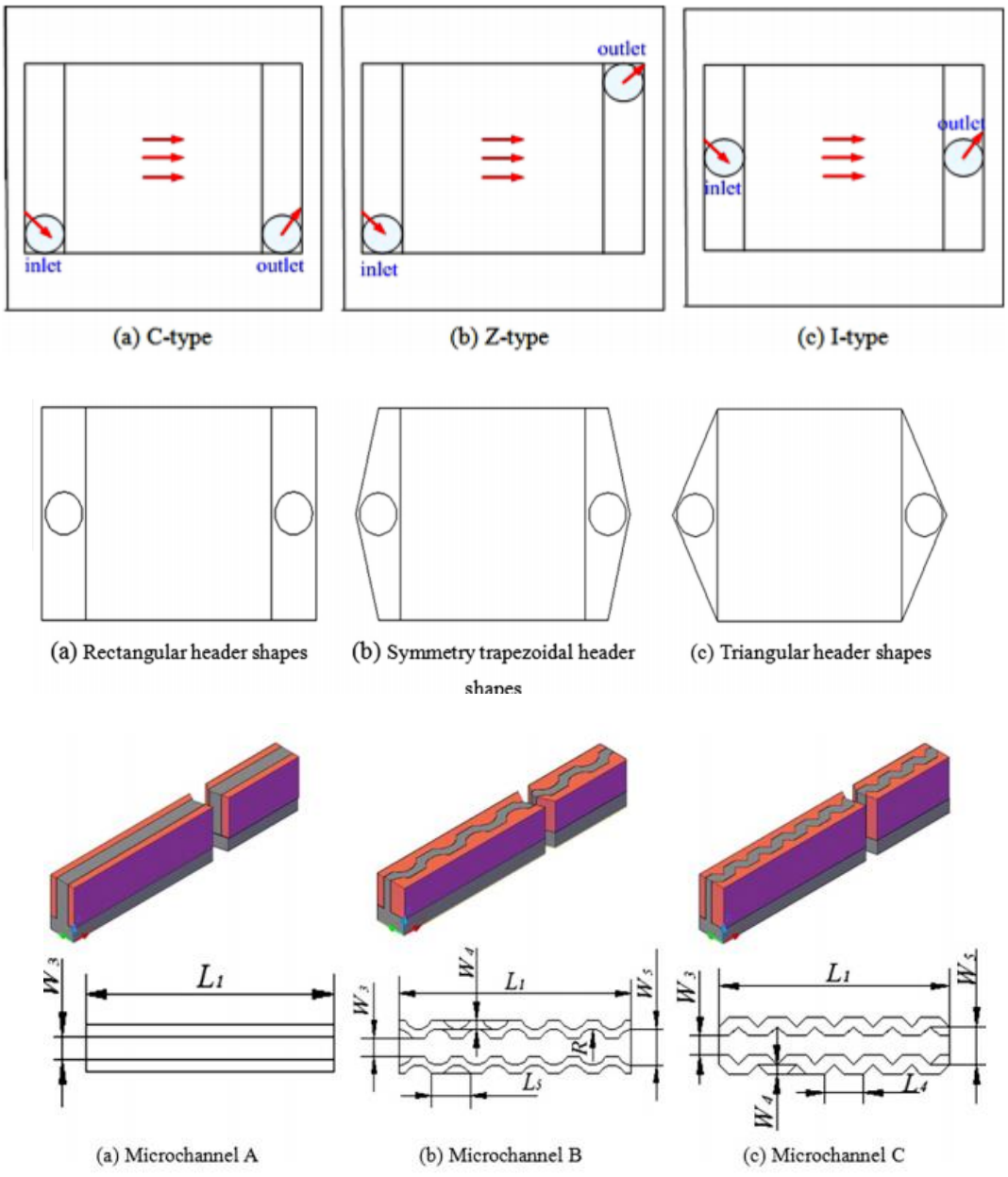


Figure 2-7 Schematic of MCHS with Different inlet/outlet locations, head shapes and microchannel designs [39].

Not only liquid can be used as working fluid, Balaj et al. [40] studied the effect of shear stress in micro and nanochannel with constant heat flux by using gas as coolant. Direct simulation Monte Carlo solver and modified iterative technique was implemented to investigate the effect of rare-friction property variations and compressibility. The results showed that the shear stress on walls greatly affects all aspects of the fluid flow and heat transfer performance. It was also found that the viscous dissipation affects the heat flux applied and at the cooling conditions.

Ghasemian et al. [41] numerically studied the laminar forced convection heat transfer of water based Fe_3O_4 ferrofluid in mini channel with magnetic field. Transverse non-uniformed magnetic field produced by current carrying wires was applied to the mini heat sink with size of 20mm x 2mm. The finite volume approach was implemented to solve the governing equations and the two-phase mixture model. The found that the heat transfer performance can be enhanced by applying magnetic field and this becomes more significant when the magnetic field source was placed in the fully developed region. Moreover, the results showed that the heat transfer enhancement due to the magnetic field is more significant at lower Reynolds numbers and the optimum frequency for transfer enhancement increased with the increase of Reynolds number.

Pan et al. [42] studied the influence of complex manifold geometries on the flow distribution between microchannels through an analytical model and an equivalent electrical resistance network model. They also proposed an optimization procedure to optimize the manifold geometries and dimensional variations to find relatively ideal flow distribution between microchannels. It was found that t the microchannel width has the most significant effect on optimization results.

Zhu et al. [43] proposed the design of MCHS with periodic gradual-expansion and sudden-constriction cross-sections by arranging backward right-angled trapezoidal grooves in channel sidewalls. The found that the proposed design presents significant improvement in heat transfer performance and overall performance with the expense of hydraulic performance in terms of pressure resistance and viscous resistance.

Zhu et al. [44] numerically studied the flow and heat transfer characteristics of MCHS with water droplet cavities and rib columns channel design. Five different shaped rib columns of triangular, rectangular, diamond, elliptical and trapezoidal rib columns were considered. They found that that the use of rib columns enhanced the heat transfer performance and the use of cavities reduced the pressure drop, and thus the proposed design greatly enhanced the overall performance. It was found that the hydrothermal performance was greatly depended on the rib column shape and the design with water droplet cavities and

elliptical rib columns has the best overall performance, which can up to 1.513 at Re of 331.32.

To enhance the heat transfer efficiency in laminar flow condition, Zhan et al. [45] proposed the type of heat transfer enhancement techniques by viscoelastic fluid pulsating. They pointed out that the overall heat transfer performance can be greatly enhanced by applying viscoelastic fluid pulsating flow and the optimal frequency with the best overall performance locates nearby the characteristic frequency of viscoelastic fluid flow.

Cheng et al. [46] conducted an parametric study to evaluate the effect of four different geometric parameters of width of the offset ribs, depth of the offset ribs, incline angle of the offset ribs, and distance between the adjacent offset ribs on heat transfer enhancement, friction loss, and performance evaluation criteria through orthogonal experimental design method and fuzzy grey relational analysis. They found that depth, width and incline angle have the most effect on heat transfer enhancement, friction loss and performance evaluation criteria, respectively.

To solve the problem of uneven distribution of temperature along flow direction in MCHS, Rajalingam and Shubhankar [47] proposed the design MCHS with gradual and sudden variation of flow passage. The results showed that the channel designs with channel cross-section reduces to a minimum one (at the throat) and then increases have lower overall performance as compared to the straight channel design, the channel designs with channel cross-section sudden contraction and then expansion can have better overall performance when channel sections with larger cross-section area is connect by a channel with smaller cross-section. Moreover, better thermal performance and hydraulic performance was observed with the increase number of expansion and contraction in the design with multiple sudden expansion and sudden contraction.

The thermal and hydraulic performance of wavy MCHS with a variety of geometric fan-shaped ribs was studied by Liu et al. [48]. It was found that the heat transfer performance is highly depends on the geometric parameters of ribs and Reynolds number. Moreover, there always exists a channel design with best overall performance.

An parametric study was carried out by Kose et al. [49] to study the effect of different design variables on thermal and hydraulic performance for MCHS with rectangular, triangular and trapezoidal channel design under same hydraulic diameter. It was found that the both heat transfer performance and power consumption increase with the decrease aspect ratio for rectangular channel design and the rectangular microchannel was found to be the most effective channel design among three designs in terms of thermal

and hydraulic performance.

MCHS with curvature added to the geometry pf rectangular was studied by Bhatt et al. [50], as shown in Figure 2-8. The results showed that the proposed design has better heat removal ability, lower temperature difference between inlet/outlet and higher heat transfer coefficient as compared with straight channel design. Moreover, better performance was observed in design with smaller hydraulic diameter.

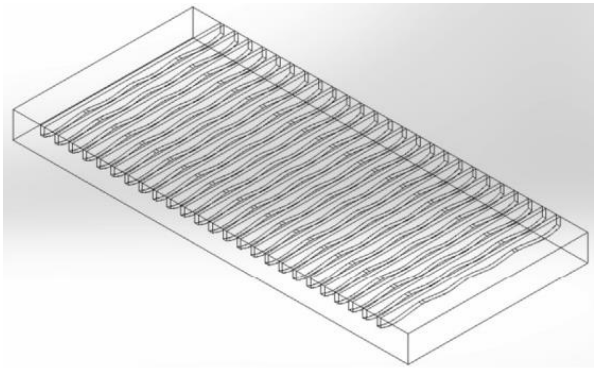


Figure 2-8 Geometry of MCHS with curved channels [50].

To improve the poor numerical stability caused by the traditional Topology Optimization, Zhou et al. [51] proposed the Contour Extraction Based on Topology Optimization method, which can optimize the geometry of the fins based on a threshold velocity and improve the hydrothermal performance of MCHs under high Re. The results showed that the heat sink generated by the proposed method has better interaction of fluid with walls and better uniform velocity distribution as comparted with heat sink generated by the traditional method.

Pan et al. [52] numerically studied the flow and heat transfer characteristic of MCHS with cylindrical pin-fin manifold. It was found that the proposed design has heat transfer performance and higher pressure drop as compared to the straight channel design with same heat flux. However, the proposed design presented better thermal performance and less mass flux as compared to the straight channel design with same pressure drop.

Jamshidmofid and Bahiraei [53] numerically investigated the performance for MCHS with rectangular ribs and sinusoidal cavities and using water-based nanofluid containing reduced oxide-cobalt oxide hybrid nanocomposite as coolant. The results showed that the thermal performance was greatly enhanced for the proposed design with moderate pressure drop increase as compared to the design without nanofluid, which

led to an increase in overall performance.

Microchannels with turbulators were numerically investigated by Khan et al. [54]. Different turbulators locations on the channel wall and channel widths were considered with different heat fluxes. The design with turbulators located on 75% of channel length was found to have best thermal performance and the design with turbulator location neat channel exit exhibits lowest thermal performance.

Hajmohammadi et al. [55] demonstrated a parametric study to investigate the effect of coolant passage widths and heights with or without porous material on average heat coefficient and pumping power. The results indicated that the heat transfer coefficient reduces and pumping power increases by applying the porous material, which contrasted with the effect of channel width increase.

The design of Silicon-diamond MCHS was proposed by Ansari and Jeong [56], which silicon was used for low heat flux zone and diamond was used for high heat flux zone . Different flow rates, heating schemes and hotspot sizes were considered. The proposed design showed advantage in both thermal and hydraulic performance as compared to the design without composite.

Farahani and Hajian [57] numerically studied the performance for MCHS with square, circular and flattened channel design and using porous material, phase changing material and nanofluid. They indicated that there always exists a critical thickness of porous substrate material design that can have minimum thermal performance. The thermal performance decreased with the increase of Darcy number, porosity coefficient, nanoparticle diameter and phase change material thickness. And the design with square geometry exhibited best thermal performance among all channel designs. Moreover, the thermal performance can be enhanced by applying porous material, nanofluid and phase change material.

Ali et al. [58] numerically investigated the hydraulic and thermal performance for MCHS with nanofluid and fins. Al_2O_3 nanofluid coolant with a nanoparticle volume fraction ranging from 0 to 3% and fins shape of rectangular, twisted and zig-zag were considered at Re ranging from 100 to 350. The result showed that the design with twist fins presented lower pressure drop as compared to the design with straight fins and the design with zig-zag fin and 3% Al_2O_3 nanofluid exhibited best thermal performance.

Copper based MCHS with rectangular U-shaped microchannels, as shown in Figure 2-9, was numerically studied by Mieczkowski et al. [59]. The Entropy Generation Minimization criterion was applied to find the optimal geometric structure based on over 130 various geometrical configurations with five different design parameters. The results showed that over 35% reduction of irreversibility losses can be achieved for the optimal heat sink as compared with initial geometry.

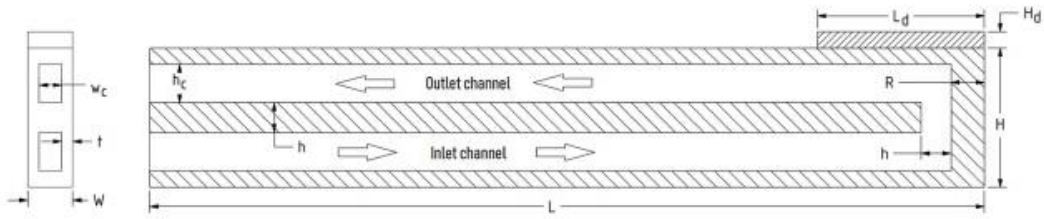


Figure 2-9 Schematic of cross-view of a single U-shaped microchannel [59].

Pourhammati and Hossainpour [60] numerically studied the fluid flow and heat transfer performance for wavy MCHS with different relative wave amplitude and wave length. The results indicated that the proposed design exhibited better performance at higher Re and the design with larger wavelength and channel height presented better overall performance. Maximum overall performance of 1.38 and minimum total resistance of 0.607K/W was found foe MCHS with certain value of wavelength and height.

Qiu et al. [61] numerically investigated the flow boiling heat transfer performance for cobweb-shaped MCHS with horizontal/inclined inlet and outlet, which was shown in Figure 2-10. It was found that the heat transfer coefficient was enhanced and wall temperature was reduced for both cobweb-shaped MCHS design as compared to the straight channel design, which was mainly due to the flow disturbance and heat transfer area increasement. Moreover, the design with horizontal inlet and outlet exhibited better heat transfer performance and stable flow boiling behaviour as compared to the design with inclined inlet and outlet.

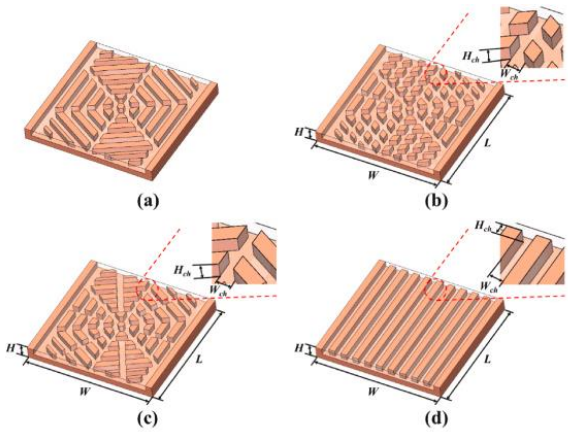


Figure 2-10 Schematic of cobweb-shaped MCHS [61].

The hydraulic and heat transfer performance of silicon-based circular MCHS using swirl and Al_2O_3 nanofluid with Re ranging from 100-350 was numerically studied by Ali et al. [62]. The swirl fluid was induced by a twisted tape and nanoparticle volume fractions of 1,2 and 3% was considered. The results indicated that the MCHS with swirl flow and with highest nanoparticle volume fractions exhibited the lowest thermal resistance and contact temperature, but it also presented highest flow resistance among all designs. This indicated that the design parameters play important roles in presenting thermal/hydraulic performance, the design with certain combination of design parameters can performed required performance in balance of increase of thermal performance and increase of pressure drop at same time.

Central jetting MCHS was designed and studied by Liu et al. [63] to meet the high heat flux of 150W/cm^2 for laser crystals. The design has narrow width and extended length as compared to the tadeonal MCHS. The results showed that the heat transfer performance was enhanced by jet impingement and generally 15% enhancement in thermal performance was found in the central region as compared to traditional MCHS.

Lori and Vafai [64] numerically investigated the fluid flow and heat transfer of MCHS with periodic vertical porous and solid ribs with different geometrical shapes of rectangular, elliptical, isosceles triangular, backward triangular and forward triangular on the walls. The results showed that the design with porous ribs exhibited less pressure drop and better thermal-hydraulic performance as compared to the design with solid ribs at same increase of Nu.

Zhu et al. [65-67] numerically studied the heat transfer and flow characteristic of MCHS with different rib shapes and grooves shapes. Ribs shapes of rectangular, diamond, hexagonal and elliptic and periodic grooves shapes of rectangular, triangular, trapezoidal, water-droplet, and semi-circular were considered. When consider ribs and grooves separately, the results showed that the overall performance can be greatly enhanced by arranging grooves on channel sidewalls for most grooves shapes exclude rectangular. The design with triangles grooves shape revealed best heat transfer performance enhancement, but in sacrifice with the highest increase in pressure drop when Re ranging from 194 to 610. The design of water-droplet sharped grooves was pointed out to be the optimum design, since it produced effective heat transfer enhancement at high Re and produced lowest pressure drop at low Re. Moreover, they found that the transfer efficiency was highly depend on the rib shape, dimension, and configuration. When combine ribs and grooves at same time, they found that the overall performance can be greatly improved. This was due to the advantages of ribs to increase flow disturbance and to enhance heat transfer, and the advantages of grooves to increase flow area and to reduce pressure drop. The design with rectangular ribs and rectangular grooves exhibited best overall performance at Re of 500.

MCHS with symmetric and parallel wavy microchannels was numerically studied by Wang et al. [68]. The results showed that the design with symmetric configuration exhibited higher Nu but slightly lower overall performance as compared with the design with parallel configuration. Adding serval traverse gaps into ribs can significantly enhance the thermal performance and overall performance.

To enhance the flow mixing, Alihosseini et al. [69] proposed the design of MCHS with wavy and oblique grooved microchannels. It was found that the secondary flow generation causes the thermal boundary layer redevelop at each fin and hence enhanced the thermal performance.

Zhong et al. [70] numerically studied the entropy generation, heat transfer, and Fe_3O_4-water ferro-nanofluid flow within a porous ribbed MCHS with constant magnetic field. It was found that entropy generation by heat transfer decreases and entropy generation by friction increases with the increase of Re.

Symmetric and asymmetric divergent-convergent MCHS was studied by Liu and Jing [71]. The results showed that symmetric divergent-convergent MCHS presented lower thermal resistance and higher pressure drop at smaller inlet-to-middle width ratio and/or at smaller outlet-to-inlet width. The increase of middle cross-section width can enhance the thermal performance with the sacrifice of higher pressure drop when other design parameters were fixed. All design proposed exhibited worse thermal-hydraulic performance as compared with conventional parallel MCHS.

Pfahler et al. [72] and Harley et al. [73] conducted an experimental study on the fluid flow through three rectangular microchannels with cross-section area varying from 80 to 7200 μm^2. They found that the Poiseuille number increases with the increase of Reynolds number, but is normally lower than the predicted value by Navier-Stokes equations.

Lee et al. [11] conducted an experimental study on the thermal behaviour for single-phase MCHS with channel width ranging from 194μm to 534 μm and channel depth five times the width. They pointed out that the experimental data were in good agreement with the numerical predictions when entrance and boundary conditions are properly matched.

Xu et al. [74] experimentally studied the liquid flow in MCHS with channel size ranging from 30μm to 344 μm at Reynolds number ranging from 20 to 4000. Based on their results, they pointed out that the characteristics of flow in microchannels agree with conventional behaviours predicted by Navier-Stokes equations in the region of those dimensions tested.

By using porous material as substrate material, Deng et al. [75] presented a porous heat sink with reentrant microchannels by using traditional sintering fabrication method. The SEM photograph of reentrant porous

microchannels is presented in Fig. 2-11. Compared with solid microchannels with the same reentrant configuration, the porous one shows great thermal enhancement in terms of wall superheat and mitigation of two-phase flow instabilities.

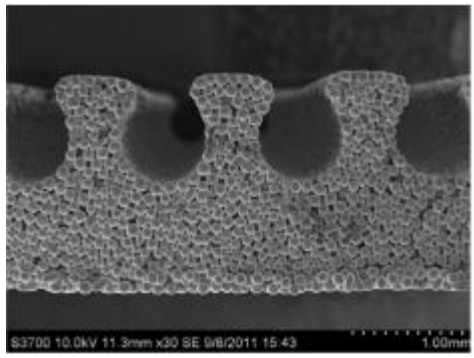


Figure 2-11 SEM photograph of reentrant porous microchannels proposed by [75]

For SL-MCHS, the local thermal resistance keeps increasing along the flow direction, which causes considerable temperature difference between inlet and outlet. In order to reduce the temperature variation along the flow direction, Vafai and Zhu [7] firstly proposed the design of double-layered microchannel heat sink (DL-MCHS), which was a kind of design that one layer of microchannels was on top of another. The schematic of DL-MCSH was shown in Figure 2-12. They found that the temperature variation along the flow direction for DL-MCHS was found only 1/3 as compared with SL-MCHS with exact dimensions and at same Reynolds number of 143.6. Based on their results, they claimed that DL-MCHS design was a substantial improvement over conventional SL-MCHS design.

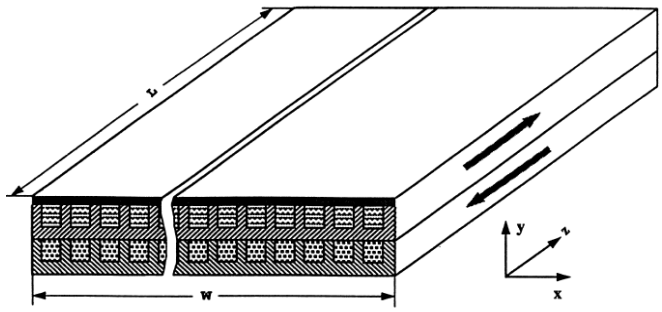


Figure 2-12 The Schematic for the DL-MCHS with counter flow configuration proposed by Vafai and Zhu[7].

Follow by their studied, many researchers have numerically investigated the performance for conventional DL-MCHS. Hung et al. [76] numerically studied the effects of substrate materials (copper, alumina, silicon, and steel), coolants (water, ethylene glycol, and glycerol), and geometric parameters(channel number, channel width ratio, channel aspect ratio, substrate thickness, pumping power) on the temperature distribution, pressure drop, and thermal resistance for DL-MCHS with counter flow. They pointed out that for DL-MCHS design, the substate material with high thermal conductivity and coolant with high thermal conductivity and low dynamic viscosity always exhibited better thermal performance, while the design with small channel aspect ratio and channel width ratio normally exhibited lower pressure drop. When compared to SL-MCHS with same geometric dimensions and under same pumping power, the DL-MCHS showed better thermal performance by an average of 6.3%.

Wong and Muezzin [77] numerically studied the thermal performance for DL-MCHS with both parallel and counter flow configurations for various aspect ratios. Different Reynolds number ranging from 500-2000 were used for investigation. They found that the parallel flow configuration showed better heat transfer performance at low Reynolds number and low channel aspect ratio.

Levac and Soliman [78] numerically studied the performance for DL-MCHS with parallel and counter flow configuration at low Reynolds number of 116 and high Reynolds number of 1160, respectively. They found the DL-MCHS with counter flow exhibited significantly improvement in thermal performance, about 30% sacrifice of hydraulic performance and about 5% enchantment in overall thermal performance as compared with SL-MCHS.

Xie et al. [79] numerically investigated the laminar heat transfer and pressure loss of silicon based DL-MCHS with both parallel and counter flow configurations under several sets of inlet flow rates. They found that DL-MCHS have both better thermal characteristic and less pressure drop as compared with SL-MCHS under same pumping power. Moreover, they pointed out that the DL-MCHS with parallel flow showed better thermal performance when flow rate was low.

For conventional DL-MCHS, the cooling effectives for upper layer was normally lower than the bottom layer due to the distance to the heat source, Authors [80-81] tried to enhance the performance for top layer by swapping the fluid flow in the top and bottom channels.

Shen et al. [80] proposed the design of silicon based DL-MCHS with swap upper/lower channel design for both straight and wavy channel configuration, which was illustrated in Figure 2-13(a) and (b), respectively. Different velocities (Re ranging from 175-345) were considered to investigate the thermal

and hydraulic performance for the proposed design with both parallel and counter flow configuration. A uniform heat flux of 100W/cm^2 was applied at the bottom surface of the heat sink as the heat source. The results showed that the re-developing of flow field caused by swap upper/lower design can greatly enhance the thermal performance at upper channel. Moreover, the wavy channel design can slightly enhance the thermal performance, but with dramatically pressure drop penalty. When consider thermal performance and hydraulic performance simultaneously, the DL-MCHS with straight staggered channel design and counter flow configuration presented the best overall thermal performance among all designs considered.

Shen et al. [82-83] further studied the effect of numbers staggered structures, position of staggered structures and flow direction within the staggered structures on performance of DL-MCHS. They found that adding more numbers of staggered structures can effectively enhance the thermal performance, but with large pressure penalty. While changing the position of the staggered structures can greatly improve the thermal performance with inapparent pressure penalty and place the staggered structures in the middle of MCHS presented best overall thermal performance.

Shen et al. [81] improved the design of staggered DL-MCHS and proposed the design of X-structured DL-MCHS, which enlarged the staggered section in DL-MCHS. The schematic of X-structured is illustrated in Figure 2-13. They found that the proposed X-structured DL-MCHS presented higher entropy generation number and better temperature uniformity when compared with traditional DL-MCHS.

In order to enhance the performance and to find the DL-MCHS design with best overall performance, optimization based on different geometrical and physical parameters are normally occupied by using different algorithms. Shen et al. [5] used Elitist Non-dominated Sorting Genetic Algorithm (NSGA-II) optimization algorithm to optimize the height ratio of the two layers and length of the upper layer for DL-MCHS with counter flow configuration.

Hung et al. [84] occupied a simplified conjugate-gradient method to find the design with lowest overall thermal performance based on four different variables of number of channels, channel width ratio, lower channel aspect ratio, and upper channel aspect ratio. The thermal resistance of the optimized DL-MCHS was about R_T = 0.12 °C/m^{2}W when subjected to a uniform heat flux of 100 W/cm^2 and a fixed pumping power of 0.1W.

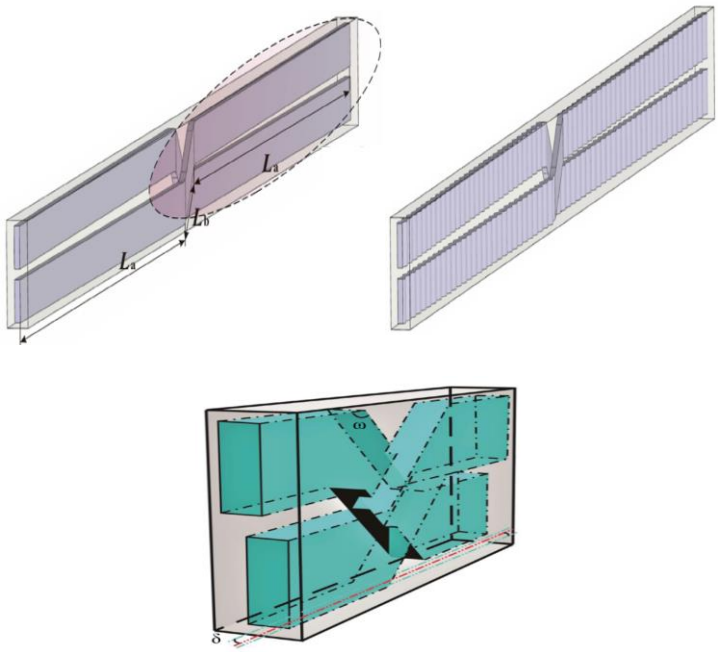


Figure 2-13 The schematic of staggered DL-MCHS with (a) Straight channel design, (b)Wavy channel design(c) X-structure[81]

Lin et al. [85] also adopted the simplified conjugate-gradient method coup[led with a three-dimensional conjugate model to optimize the flow and heat transfer in a water-cooled, silicon-based DL-MCHS. Six different design variables of channel number, bottom channel height, vertical rib width, thicknesses of two horizontal ribs, and coolant velocity in the bottom channel were used to find the optimum global thermal resistance for DL-MCHS at fixed pumping powers, coolant volumetric flow rates, and pressure drops, respectively. The optimal design with thermal resistance of $0.089KW^{-1}$ at fixed pressure drop of 100kPa.

Chamoli et al. [86] employed a multi-objective genetic algorithm to find the optimum ratio of the thermal resistance of the modified case over base case and ratio of the total pumping power of the modified case over base case based on design variables of relative axial ridge length, relative transverse ridge length, and relative channel length ratio.

Leng et al. [87] performed a simplified conjugate-gradient method to optimize the performance for DL-MCHS with four different variables of channel number, channel width, bottom channel height, and bottom coolant inlet velocity.

Kulkarni et al. [88] adopted a multi-objective genetic algorithm to find the optimum design for DL-MCHS with rectangular wedge-shaped cross section. Water with variable thermo-physical properties was used as coolant. Two geometric variables related to the channel cross section and a ratio of flow rates in the upper and lower channels were selected as design variables to find the optimum combination for thermal resistance and pumping power.

Leng et al. [89] employed a multi-parameter optimization to find the optimum design for DL-MCHS with truncated top channel. Different variables of channel number, channel height, channel width, and the dimensionless truncation length of top channels were evaluated to find the optimum overall thermal performance at various fixed pumping powers and fixed coolant volumetric flow rates, respectively.

Derakhshanpour et al. [90] numerically investigated the characteristic of laminar fluid flow and forced convection heat transfer through SL- and DL-MCHS with cylindrical ribs. They found that DL-MCHS achieved 30%-60% convection heat transfer coefficient as compared with SL-MCHS at same mass flow rate and DL-MCHS exhibits better thermal performance with the increase of mass flow rate.

Zhai et al. [91] numerically investigated the performance for silicon based Dl-MCHS with staggered flow(the fluid staggers flow along each layer). The distribution of the total temperature, average bottom temperature, maximum temperature difference and thermal resistance for DL-MCHS with flow 1 (the fluid flows along the x direction at the first layer, while fluid staggers along the y direction at the second layer) and flow 2(the fluid flows along the x direction at the second layer, while fluid staggers along the y direction at the first layer) were numerical studied and compared with DL-MCHS with counter flow. They pointed out that the changing flow direction can greatly enhance the thermal performance in terms of thermal resistance and temperature uniformity.

Conventional DL-MCHS shows great potential to improve the temperature uniformity through temperature compensation between the two layers through conduction. However, the temperature of the coolant in top channels is always higher than that in bottom channels at inlet region, which inversely heat up the temperature of coolant in bottom channels. To reduce the amount of heat transfer from top channel coolant to bottom, Leng et al. [92] numerically studied the effect of bottom channel length, channel number, channel-to-pitch width ratio, and total pumping power on the performance of silicon-based DL-MCHS with truncated top channels, which was shown in Figure 2-14. They pointed out that the design with truncated top channels presented better overall thermal resistance and temperature uniformity as compared with original DL-MCHS design.

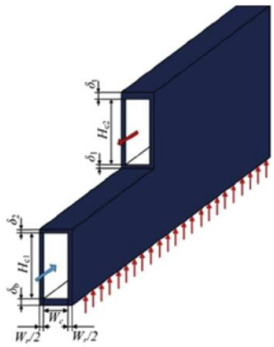


Figure 2-14 The schematic of DL-MCHS with truncated top channels [92]

Debbarma et al. [93] proposed the design of DL-MCHS with partly diverged channel in top layer, which enlarged the contact surface between solid and fluid for top channels. They pointed out that the addition of bigger flow area at upper section of top layer due to diverged portion can produce much lower pressure drop as compared with conventional straight channels and the advantage was more obvious at high Reynolds number.

Wang et al. [94] proposed the design of DL-MCHS utilizing porous copper fins instead of solid fins, which was shown in Figure 2-15. The overall thermal performance and pumping power of the proposed design are investigated at Reynolds number ranging from 65-200 and with a uniform heat flux of 100W/cm^2. They found that the DL-MCHS design with porous fins has 45.3%-48.5% reduction in pumping power but 14.8%-16.2% increment in thermal resistance as compared with DL-MCHS design with solid fins at same Re. The enhancement of the hydraulic performance was mainly due to the “slip effect” of coolant on the porous fin walls, where the non-zero velocity is observed at sloid-fluid interface. The DL-MCHS with porous fins showed 10% reduction in thermal resistance as compared to the design without porous fins.

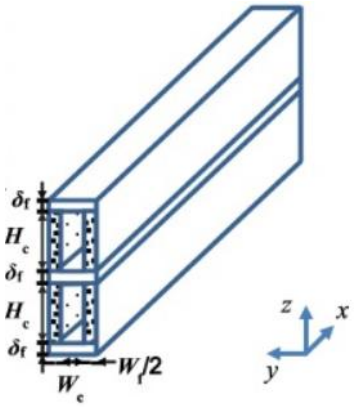


Figure 2-15 The schematic of DL-MCHS with porous fins[94].

Ali et al. [95] proposed the design of DL-MCHS by adding steel porous substrate between the solid ribs and coolant, as shown in Figure 2-16. They numerically studied the thermal performance and pumping power of proposed DL-MCHS at different Re of 20-170 and a uniform heat flux of 100W/cm^2. Different porous substrate and solid fin thickness were evaluated to find the optimized design with best thermo-hydraulic performance. They found that the solid-porous fin thickness of the bottom channel was more important than top channel when evaluate the thermal performance. This indicated that the bottom layer channels have better heat removal ability as compared with top layer channels. Moreover, they found that the thermal resistance and pumping power of DL-MCHS can be reduced simultaneously by properly adjust the design parameters and porous DL-MCHS always has better thermo-hydraulic performance as compared with conventional DL-MCHS.

Li et al. [96] numerically studied the thermal performance and flow characteristics of DL-MCHS with copper based porous substrate at Reynolds number varying from 194-389. Five different designs of solid-ribs single-layered, porous-ribs single-layered, solid-ribs double-layered, porous-ribs double-layered and top channel with porous ribs and bottom channel with solid ribs double-layered designs were considered. The results confirmed that the DL-MCHS has better temperature uniformity as compared with SL-MCHS and the design with mixed porous and solid ribs has lowest thermal resistance and best temperature uniformity among five designs at both fixed Re and fixed pumping power. This was mainly due to the combination of better thermal conductivity of the solid ribs and lower pressure drop of the porous ribs.

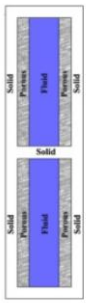


Figure 2-16 The schematic of MCHS with porous substrate [95].

Wang et al. [97] utilizing a multi-objective and multi-parameter genetic optimization method to find the design with best thermo-hydraulic performance for DL-MCHS with copper based semi-porous-ribs at fixed volumetric flow rate. The optimum design can have thermal resistance and pumping power of 0.09348 K/W and 0.02888 W, respectively. When compared with DL-MCHS with solid ribs, the proposed design can have 14.06% enhancement in thermal performance and 16.40% in hydraulic performance. They pointed out that compromise mediation between the hydraulic performance of the upper channel and the thermal performance of the lower channel yielded best thermo-hydraulic performance, which can be evidenced from Li et al. [96].

Recently authors [98-99] have investigated the performance for DL-MCHS with nanofluid. Compare to deionized water, the nanofluid has higher thermal conductivity and viscosity, which increases the convective heat transfer and pressure drop simultaneously. However, when consider overall performance, the nanofluid still shows superiority.

Hung and Yan [98] numerically studied the performance for silicon based DL-MCHS with various nanofluid and geometric parameters. Three types of nanofluid (aluminium oxide, copper oxide, and titanium oxide) and six nanoparticle volume fractions ranging from 0.5% to 5% were considered. They found that the thermal resistance is highly depends on the type of nanofluid, particle volume fraction, channel number, channel width ratio, channel aspect ratio and pumping power. And the thermal performance of the channel can usually be improved by decreasing the channel number or channel aspect ratio, or increasing the channel width ratio.

Sakanova et al. [100] numerically studied the performance for Cu-based DL- and double-sided MCHS with waster as coolant. The effects of inlet velocity, inlet temperature and heat flux were investigated to

find the optimum design with best thermal performance. The optimized double-sided MCHS design showed 59%, 52% and 53% enhancement in thermal performance as compared with SL-MCHS, DL-MCHS with parallel flow and DL-MCHS with counter flow, respectively. Moreover, they found that the nanofluids at a higher concentration yield a better cooling performance by about 17.3% at 5% concentration while 10.6% at 1% concentration.

Ahmed et al. [101] experimentally studied the performance for aluminium DL-MCHS with rectangular and triangular channel and round corners designs. Two different nanofluids of Al_2O_3–H_2O and SiO_2–H_2O with different nanoparticles concentration were used as coolant at Reynolds numbers ranging from 50 to 300. They found that the DL-MCHS with both rectangular and triangular channel designs showed better thermo-hydraulic performance as compared with SL-MCHS for varies channel dimensions, nanoparticles concentrations, nanoparticles types and pumping powers investigated. Moreover, the nanofluid with higher nanoparticle concentration showed better thermal stability for both nanofluids and the design by using Al_2O_3–H_2O nanofluid (0.9 vol.%) showed the best thermal performance with temperature difference of 1.6 °C and lowest thermal resistance of 0.13 °C/W·m^2 was found.

Sarvar-ardeh et al. [102] numerically studied the heat transfer performance in DL-MCHS at constant Reynolds number and constant flow rate. Different coolant of Al2O3-Cu/water and Al2O3-SiO2/water hybrid nanofluids with temperature-dependent properties and different volumetric concentrations were considered. They found that the thermal resistance was decreased by using both nanofluids as coolant as compared to the water as coolant at same Reynolds numbers and increasing the volumetric concentration of both nanofluids reduces the thermal resistance but raises the pumping power consumption.

Hajmohammadi and Toghraei [99] performed a numerical study to optimize the design of DL-MCHS cooled with Al_2O_3–water nanofluid. Different design parameters of thicknesses of the DL-MCHS ribs, the number of channels, height and width of the channels, and the inlet coolant velocities in each layer were used to find the design with lowest thermal resistance at fixed pumping power and fixed volumetric flow rate. They pointed out that the DL-MCHS design with nanofluid as coolant has great improvement in thermal performance, which shows 10% lower thermal resistance as compared with optimized DL-MCHS proposed by Lin et al. [85].

Combined the effect of truncated top channels and nanofluid, Ali et al. [103] numerically studied the laminar flow and heat transfer of nanofluid water/single-wall carbon nanotubes in a truncated DL-MCHS. The design with different truncated lengths of 0, 0.4, 0.8 and 1 were investigated at Reynolds numbers of 500, 1000 and 2000, respectively. They pointed out that the thermal resistance, temperature uniformity

decreases with the increase of nanoparticles volume fraction and the decrease of truncated lengths. Moreover, increase volume fraction of nanoparticles can enhance the thermo-hydraulic performance effectively.

Zhai et al. [104-106] numerically studied the characteristics of entropy generation and heat transfer for DL-MCHS with triangular cavities and ribs for both parallel and counter flow configuration. They pointed out that DL-MCHS with complex structure in top channel has better heat dissipation and pressure drop than DL-MCHS with triangular cavities and ribs in both top and bottom channel. Moreover, the DL-MCHS with triangular ribs and triangular cavities exhibited better thermal performance as compared with conventional SL- and DL-MCHS with same volumetric flow rate.

Wong and Ang [107] numerically investigated thermal and hydraulic performance for DL-MCHS with vertically tapered channel design. They found that the DL-MCHS with vertically tapered channel design was not an appropriate solution as compared with conventional DL-MCHS.

Debbarma et al. [108] numerically studied the performance for DL-MCHS with protrusions mounted on sidewalls. They found that the design with protrusions mounted on sidewalls shows better thermal performance at all range of Re investigated.

Elqady et al. [109] studied the performance for DL-MCHS with concentrator photovoltaic cell and they pointed out that counter flow has better temperature uniformity as compared with parallel flow when mass flow rate ranging from 200-1200ml/hr.

Xie et al. [110-111] numerically investigated the laminar flow and heat transfer for DL-MCHS with wavy channels for both parallel and counter flow. They found that DL-MCHS with wavy channels can reduce pressure drop and overall thermal resistance simultaneously as compared with SL-MCHS with wavy channel at same flow rate. Moreover, the wavy DL-MCHS with counter flow exhibited better overall thermal performance at high flow rate where the DL-MCHS with parallel showed advantage when flow rate is low.

Cheng [112] performed an numerical study of a stacked DL-MCHS with enhanced mixing passive microstructure. They found that the thermal performance improved by changing the ratio of embedded structure height to microchannel height from 0.13 to 0.26 at fixed Reynolds number of 14.8.

Srivastava et al. [113] numerically studied the thermal and flow characteristic of silicon based DL-MCHS with bifurcation under parallel and counter flow configuration for Re ranging from 50 to 900. They found that the DL-MCHS with bifurcation has about 28% lower of overall thermal resistance as compared with

non-bifurcated MCHS with sacrifice of hydraulic performance. The Nusselt number for parallel flow is higher than counter flow for all cases investigated, wherever the counter flow shows better temperature uniformity.

2.4 Correlation

To conduct experiments for fluid flow through heated MCHS is difficult and expensive, whereas running simulations for MCHS require long preparation and waiting time. Therefore, establishing correlation provides an easy way to predict the performance of MCHS.

Tuckerman and Pease [5] proposed the correlation of maximum thermal resistance for SL-MCHS as the sum of three components: a) the conductive thermal resistance from the circuits through the substrate, package and heat sink interface, b) the convective thermal resistance from the heat sink to the coolant, and c) the thermal resistance due to the heating of fluid. Based on their results, the correlation results give good prediction of thermal performance in terms of maximum thermal resistance. Normally, the conductive thermal resistance can be very small by locating the heat source very near to the heat exchanger and the thermal resistance because the heating of the fluid can be greatly reduced by using coolant of high volumetric heat capacity. So, the convective thermal resistance is the main concern for the MCHS design, which is highly dependent on the convective heat transfer coefficient.

In order to predict the convective heat transfer coefficient accurately, it needs to identify proper boundary conditions first. For most applications used in MCHS, a uniform heat flux is applied at the bottom surface of the heat sink. To simplify the full three-dimensional conjugate heat transfer model, the computational domain can be restricted to include only the fluid region with one of the following thermal boundary conditions applied to the channel walls: H1 (circumferentially constant wall temperature and axially constant wall heat flux), H2 (uniform wall heat flux, both axially and circumferentially), and T (uniform wall temperature, both axially and circumferentially) [114]. Compared with full three-dimensional conjugate heat transfer model, such approaches are more computationally economical, since the conduction in the substrate is not included and can be applied to simulate MCHS model with a wide range of dimensions, de-coupled from details of the substrate.

Lee at al. [11] experimentally studied the heat transfer performance of MCHS with uniformed heat flux applied at the bottom surface of the heat sink by using copper as substrate material. Through comparing experimental results with the simulation results obtained from simplified model with H1, H2 and T thermal boundary conditions on the channel wall, the simulation results from the H1 boundary condition give the

best agreement with the full three-dimensional conjugate heat transfer model, in which the maximum difference is found to be 1.3%. They concluded that the H1 thermal boundary condition is most suitable for the simplified analysis when the full conjugate heat transfer model is unavailable.

By applying H1 thermal boundary condition, Lee and Garimella [115] numerically investigated the laminar flow and heat transfer in the thermal entrance region of rectangular ducts with different aspect ratios ranging from 1 to 10. The temperature and heat flux distributions on the channel walls are obtained by using finite volume approach to calculate the local and average Nusselt number in the entrance region as a function of the dimensionless axial distance and channel aspect ratio. The proposed local and average Nusselt numbers in the entrance region shows good agreement compared with both predictions from correlations and experiment data of MCHS, and can be used to calculate the convective thermal resistance mentioned by Tucker and Pease [5]. Incropera et al. [116] conducted an experimental study on the convective heat transfer from a single source by using water and FC-77 as coolants for a wide range of channel Reynolds number varying from 1000 to 14,000. Based on the predictions from two-dimensional model and experimental results, they concluded that the substrate conduction and boundary-layer effects can be neglected.

Wang and Peng [117-118], Peng and Peterson [119] experimentally studied the singe-phase forced flow and boiling characteristics through microchannels with rectangular cross section. They pointed out that the geometric configuration has a significant effect on the single-phase convective heat transfer and flow characteristics and the fully developed turbulent convection that starts at about Re from 100 to 1500. Based on their experimental results, they proposed the correlation for fully developed turbulent heat transfer by using modified Dittus-Boelter correlation and concluded that the laminar and transition heat transfer performance is highly dependent on the coolant temperature, velocity and microchannel dimension. The proposed correlations are summarized in Table 2-1.

Table 2-1 The summarized correlations

Reference	**Correlation**
Tuckerman and Pease [5]	The Nusselt in the developing region: $\mathrm{Nu} \propto \left(\frac{x}{D_h \cdot Re \cdot Pr}\right)^{-1/3}$ for $\frac{x}{D_h \cdot Re \cdot Pr} \leq 0.02$

	The Nusselt in the fully developed region $Nu \cong Nu_{\infty}$ for $\frac{x}{D_h \cdot Re \cdot Pr} > 0.02$
Lee and Garimella [115]	The local Nusselt number as a function of dimensional axial distance: $Nu_z = \frac{1}{C_1 (z^*)^{C_2} + C_3}$ for $1 \le \alpha \le 10,\ z^* < z^*_{th}$ $C_1 = -3.122 \times 10^{-3}\alpha^3 + 2.435 \times 10^{-2}\alpha^2 + 2.143 \times 10^{-1}\alpha + 7.325$ $C_2 = 6.412 \times 10^{-1}$ $C_3 = 1.589 \times 10^{-4}\alpha^2 - 2.603 \times 10^{-3}\alpha + 2.444 \times 10^{-2}$ $C_4 = 7.148 - 1.328 \times \frac{10^1}{\alpha} + 1.515\frac{10^1}{\alpha^2} - 5.936/\alpha^3$ Where α is the aspect ratio The average Nusselt number as a function of dimensional axial distance: $Nu_{ave} = \frac{1}{C_1 (z^*)^{C_2} + C_3}$ for $1 \le \alpha \le 10,\ z^* < z^*_{th}$ $C_1 = -2.757 \times 10^{-3}\alpha^3 + 3.274 \times 10^{-2}\alpha^2 - 27.464 \times 10^{-5}\alpha + 4.476$ $C_2 = 6.391 \times 10^{-1}$ $C_3 = 1.604 \times 10^{-4}\alpha^2 - 2.622 \times 10^{-3}\alpha + 2.568 \times 10^{-2}$ $C_4 = 7.301 - 1.311 \times \frac{10^1}{\alpha} + 1.519\frac{10^1}{\alpha^2} - 6.094/\alpha^3$
Wang and Peng [117]	For 1500>Re>100 $Nu = 0.00805 Re^{4/5} Pr^{1/3}$
Wang and Peng [118]	For laminar flow: $Nu_f = 1.86 Re^{\frac{1}{3}} Pr^{\frac{1}{3}} \left(\frac{d_e}{l}\right)^{\frac{1}{3}} \left(\frac{\mu_f}{\mu_w}\right)^{0.14}$

	For transition flow: $$Nu_f = 0.116(Re_f^{\frac{2}{3}} - 125) \cdot Pr^{\frac{1}{3}}[1 + \left(\frac{d_e}{l}\right)^{\frac{2}{3}}](\frac{\mu_f}{\mu_w})^{0.14}$$ Where μ_f and μ_w represents dynamic viscosity of fluid and wall
Peng and Peterson [119]	For laminar flow: $$Nu = 0.1165\left(\frac{D_h}{W_c}\right)^{0.81}(\frac{H}{W})^{-0.79}Re^{0.62}Pr^{\frac{1}{3}}$$ For Turbulent flow: $$Nu = 0.0072\left(\frac{D_h}{W_c}\right)^{1.15}[1 - 2.42 \cdot (2 - 0.2)^2]Re^{0.8}Pr^{\frac{1}{3}}$$

Mital [120] proposed to use semi-empirical correlations in the model to calculate the effective nanofluid thermophysical properties inside MCHS by using the thermal resistance model proposed by Tuckerman and Pease [5], Nusselt number proposed by Lee and Garimella [115] and friction factor proposed by Yilmaz [121]. The proposed predictions are in good agreement with the experimental results with the maximum difference of 5% found. The validated model used to predict the thermal resistance and pumping power is calculated in terms of channel width, wall width, coolant velocity and particle volume fraction.

Zhai et al. [122] validated the related empirical correlation of lamina factor, Nusselt number, different thermal resistances, etc. Li et al. [123] validated the laminar flow and heat transfer performance in rectangular MCHS with hydraulic diameter of 0.333m at Re varying from 101 to 1775 in terms of friction factor and convective heat transfer coefficient by using inlet, average and variable thermal properties.

Wei and Joshi [124] proposed the thermal resistance model for multi-layered stacked MCHS. To solve the thermal resistance model, heat flux at the bottom surface is set as input and the temperature at the top surface of the MCHS through fin theory and energy balance. Since some of the boundary conditions are part of solutions, the solutions require many iterations.

As a conclusion, the correlation studies provide a more convenient method to predict the thermal performance in MCHS.

2.5 Conclusion from literature

A comprehensive literature review has been conducted in this chapter to understand the knowledge gap in published studies on microchannel heat sink.

- The increasing of heat flux in electronics demands heat dissipation method with small size and high heat removal ability.
- All studies in the literatures proved that the MCHS with non-uniform channel profile show better thermal performance, which is mainly due to the increase of surface area and developing of secondary flow. However, the non-unform channel profile always exhibits higher pressure drop penalty.
- The multi-layered MCHS proved to have better temperature uniformity as compared to single-layered MCHS with same channel design.
- The tapered(converging/diverging) channel profile has been studied in the literature. However, the micro-sized channels have seldom been investigated. Moreover, the correlation of Nu in tapered channel remains blank.

As presented in the literature, there is a knowledge gap on DL-MCHS with non-uniformed channel profile. Therefore, present study focuses on the investigation of thermal and hydraulic performance of multi-layered MCHS with tapered channel profile and different flow configurations at various design parameters.

Chapter 3. Methodology

3.1 Introduction

As discussed in Literature Review, computational fluid dynamics (CFD) has been widely used to investigate the performance for MCHS to save the cost and time. In this chapter, the numerical model, boundary conditions, governing equations, and assumptions for multi-layered MCHS with tapered channel designs are presented. The generated numerical results are then validated with experimental results proposed in open literatures and the accuracy is verified through grid independence test.

3.2 Numerical model

3.2.1 The numerical model for Dl-MCHS with parallel/counter flow

The schematic of DL-MCHS with dimension of $L_x = 10\text{mm}$, $L_y = 1\text{mm}$ and $L_z = 10\text{mm}$ is shown in Figure 3-1(a). The heat sink consists of 40 channels, and it can be divided into 40 repeated sections with each section width W of 250 μm, the schematic of single unit is shown in Figure 3-1(b). For the purpose of simulation, a half-symmetry single section illustrated in Figure 3-1(c) is used as the computational domain. Both left and right surface of the computational domain is set to be symmetry, bottom wall is set subjected to the uniform heat flux, all the surfaces between solid domain and fluid domain are set to be solid-fluid interface, other surfaces in computational domain are assumed have no heat loss and set to be adiabatic. The substrate material is silicon and the coolant used is water. The properties of these materials used in simulation is shown in Table 3-1, which are referenced to the experimental data given by Wei et al. [124]. The numerical study is first conducted on DL-MCHS with 8 different channel design at various Re. The channel dimensions used are list in Table 3-2. Parametric studies are then carried out to determine the critical geometrical factor that contribute toward heat dissipation and identify geometries of MCHS that likely to have optimal thermal-hydraulic performance. The geometrical parameters studied and presented in this report are the inlet channel width W_i , outlet channel width, W_o and the channel height, H_{ch} as illustrated in the single section of MCHS in Figure 3-1(b). Based on these variables, total 128 geometries were generated with the combination of parameters specified in Table 3-3 for parallel and counter flow configuration. The geometry can be classified into three types with changing the value of W_o and W_i:

- Channel with converging tapering profile ($W_o < W_i$)

- Straight channel ($W_o = W_i$) / conventional design
- Channel with diverging tapering profile ($W_o > W_i$).

Based on the 64 different geometries for parallel flow configuration and 64 different geometries for counter flow configuration, simulations were conducted by using CFD software. For parallel flow configuration, the fluid flow for both upper channels and bottom channels is along the same direction. While for the counter flow configuration, the fluid in the upper channels flows opposite to fluid flow direction in the lower channels. The schematic of flow conditions for width-converging MCHS are shown in Figure 3-2(a) and Figure (b). Therefore, a total of 128 simulations were conducted. All the cases are subjected to the same boundary conditions of a uniform heat flux of 100 W/cm^2 at the bottom surface of the heat sink, inlet temperature of 300K, and an overall volumetric flow rate of 200 ml/min for easy comparison.

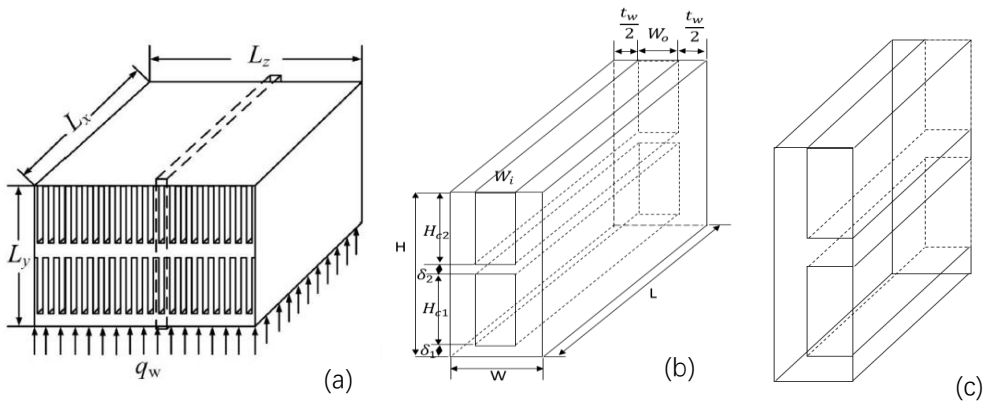


Figure 3-1 Schematics of (a) double-layer MCHS (b) single unit of MCHS (c) computational domain.

Table 3-1 Material properties used in simulation[124].

Materials	Density, ρ (kg/m^3)	Specific heat, C_p (J/kg/K)	Thermal conductivity, K (W/m/K)	Viscosity, μ (kg/m/s)
Silicon	2329	710	148	-
Water	998.2	4182	0.6	0.001003

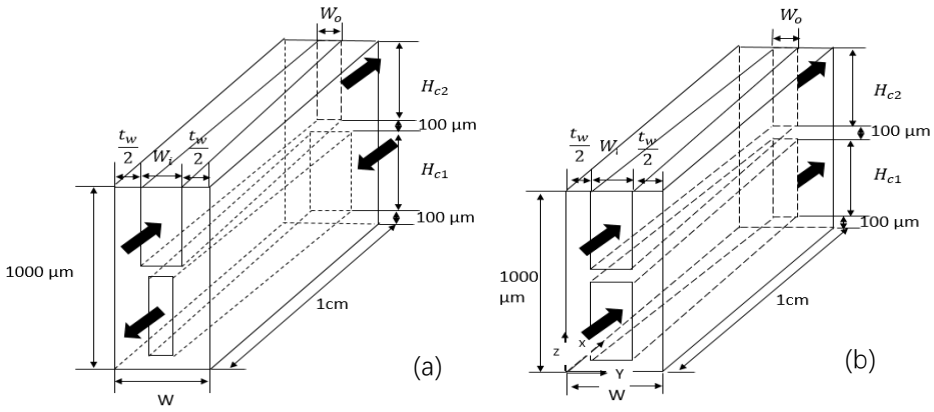


Figure 3-2 Schematics of (a) width-converging channel with counter flow configuration and (b) width-converging channel with parallel flow configuration.

Table 3-2 The W_i and W_o for different designs.

No.	W_i(µm)	W_o(µm)	Channel Type	W_o/ W_i
Design 1	50	50	Straight	1
Design 2	50	100	Diverging	2
Design 3	50	150	Diverging	3
Design 4	50	200	Diverging	4
Design 5	200	50	Converging	1/4
Design 6	200	100	Converging	1/3
Design 7	200	150	Converging	1/2
Design 8	200	200	Straight	1

Table 3-3 Different geometries of DL-MCHS of for parametric studies

Parameters	Values
Channel inlet width, $\mathbf{W_i}$ (μm)	50, 100, 150, 200
Channel outlet width, $\mathbf{W_o}$ (μm)	50, 100, 150, 200
Channel height, $\mathbf{H_{ch}}$ (μm)	325, 350, 375, 400

3.2.2 The numerical model for DL-MCHS with alternating flow

The numerical model for DL-MCHS with alternating flow is presented here. The heat sink also consists of 40 repeated sections with each section width W of 250μm. The geometrical parameters for a single unit used for Dl-MCHS with alternating flow is shown in Figure 3-3(a). Each unit has identical top and bottom layer dimensions and each unit can be divided into left and right part. Each layer has channel height,H_{ch} of 375μm and horizantal rib thickness,t of 125μm. For the left part and right part, the fluid flows along y-direction and negative y-direction, respectively. The computational domain of the single section is illustrated in Figure 3-3(b). The performance is first evaluated based on different design at various Re and then proceed to the parametric study to understand the effects of geometrical parameters W_i and W_o. In present study, W_o and W_i are both varied from 50μm to 200μm with step size of 10μm. So totally, 256 cases are investigated at various channel designs.

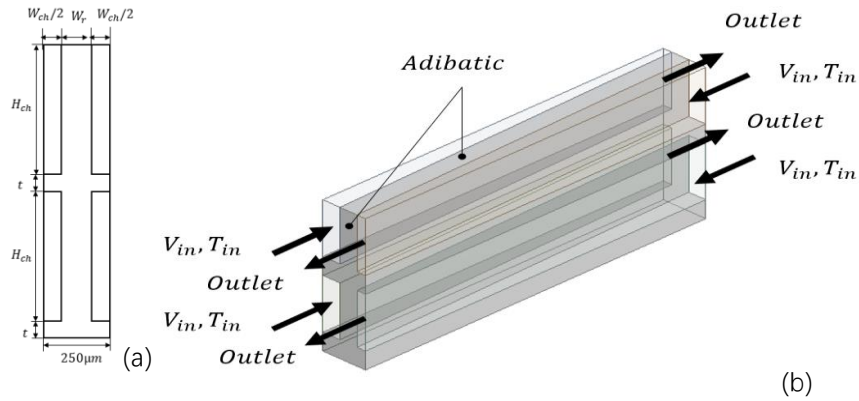


Figure 3-3 (a) Repeating section of the DL-MCHS with alternating flow (b) Schematics of computational domain for Dl-MCHS with alternating flow

3.2.3 The numerical mode for three-layered MCHS.

The physical model of the three-layered MCHS is illustrated in Figure 3-4(a) with an overall width, length and height of 10mm, 10 mm and 1 mm, respectively. The heat sink consists of 40 repeated sections with each section width W of 250μm. The schematic of half of a single section is shown in Figure 3-4 (b). The three-layered MCHS can be divided into top, middle and bottom layers with each layer consist of substrate materials and a channel. The present study considers 4 different flow configurations. One of them is the parallel flow configuration as illustrated in Figure 3-5(a). The rest are 3 different counter flow configurations, namely CF1, CF2 and CF3 as illustrated in Figure 3-5 (b), Figure 3-5 (c) and Figure 3-5 (d), respectively. The substrate material used in the study is silicon and the coolant used is water. Note that the flow directions are illustrated with arrows in Figure with fluid entering the channel inlets at different locations and with fluid exiting the channel outlets.

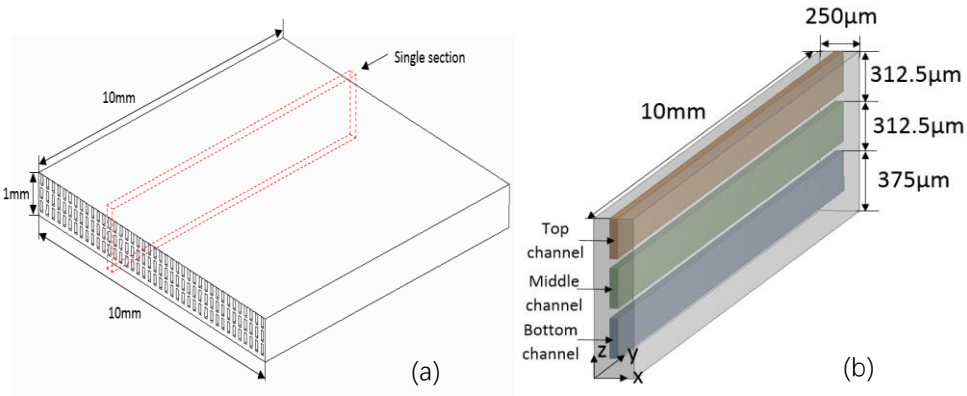


Figure 3-4 The schematic of (a) three-layered-MCHS (b) single section of three-layered-MCHS

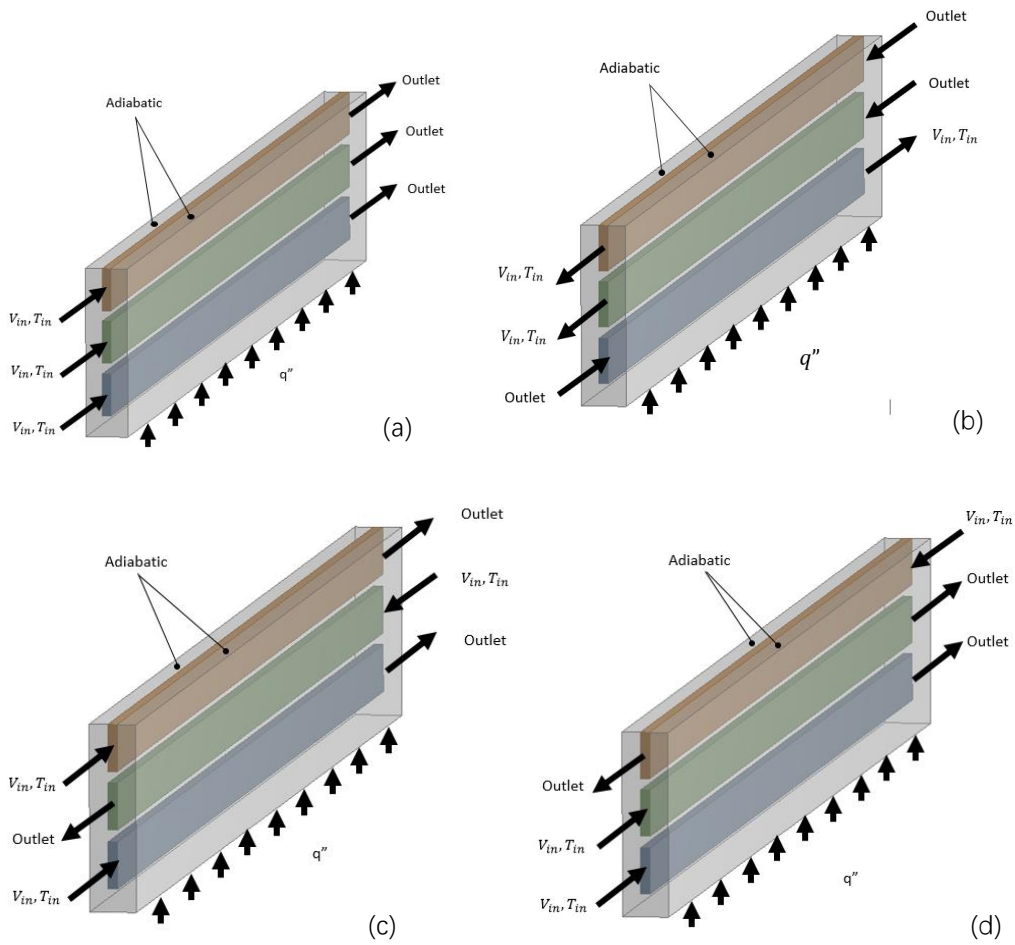


Figure 3-5 Schematics of boundary conditions for (a) parallel flow configuration PF, (b) counter flow configuration CF1, (c) counter flow configuration CF2 and (d) counter flow configuration CF3

3.3 Governing equation and assumptions

The Froude number, Fr is the ratio of convective forces to external forces (normally represents gravity), which is defined as:

$$\mathrm{Fr} = \frac{\mathrm{u_{in}}}{\sqrt{\mathrm{gD_h}}} \tag{3.1}$$

In present study, the Fr calculated is ranging from 19.37 to 84.34, which indicates that the effect of external

field (normally the gravity filed) is much smaller and can be neglected as compared with convective force. So, the effects of gravity and other forms of body forces can be assumed negligible.

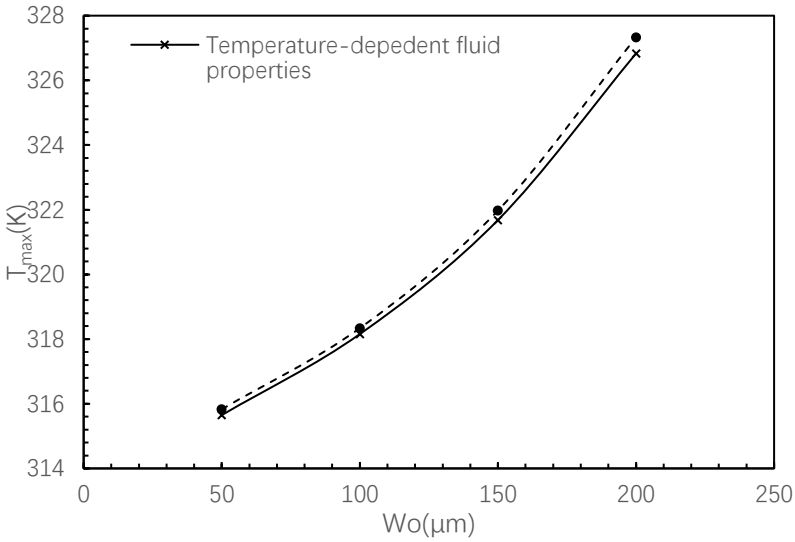


Figure 3-6 Influence of fluid properties on maximum temperatures for DL-MCHS with parallel flow and with different W_i.

Figure 3-6 presents the differences between the influences of using temperature-dependent fluid properties and using fluid properties with the inlet temperature of 20°C on the maximum temperatures for DL-MCHS with parallel flow configuration. The designs with W_o of 200μm and with different W_i of 50μm, 100μm, 150μm and 200μm are used for example. The temperature-dependent fluid properties used in simulation are presented in Equation 3.1-3.4. The Maximum temperature difference is found to be 0.5K(0.15%), which indicates that the influence of using temperature-dependent fluid properties on thermal performance is neglected and the fluid properties with fixed inlet temperature can be used to save the simulation cost.

$$\rho_f = 1000 \times \left[1 - \frac{(T_L - 4)^2}{11900 + 1365 \times T_L - 4 \times {T_L}^2}\right] \quad (3.2)$$

$$k_f(T_L) = 0.56112 + 0.00193 \times T_L - 2.60152749 \times 10^{-6} \times {T_L}^2 - 6.08803 \times 10^{-8} \times {T_L}^3 \quad (3.3)$$

$$\mu_f(T_L) = 0.00169 - 4.25263 \times 10^{-5} \times T_L + 4.9255 \times 10^{-7} \times {T_L}^2 - 2.09935 \times 10^{-9} \times {T_L}^3 \quad (3.4)$$

$$C_{p,f}(T_L) = 4217.629 - 3.20888 \times T_L + 0.09503 \times {T_L}^2 - 0.00132 \times {T_L}^3 + 9.415 \times 10^{-6} \times {T_L}^4 - 2.5479 \times 10^{-8} \times {T_L}^5 \quad (3.5)$$

Three-dimensional solid-fluid conjugate model is created to solve the heat transfer between fluid, channels and ribs. The following assumptions are made to make sure the applicability:

- The effects of gravity and other forms of body forces are negligible.
- The fluid flow and heat transfer are in steady-state.
- The flow is assumed to be incompressible (Coolant used in present study is water).
- The properties of fluid and solid assumed to be constant
- Since thermal radiation is much smaller than thermal conduction and thermal convection, Heat losses of the MCHS to the ambient are ignored.

Based on the assumptions above,the governing equations are as follows [66][125]:

Continuity equation:

$$\nabla \cdot \vec{\mathbf{V}} = \frac{\partial \mathrm{u}}{\partial \mathrm{x}} + \frac{\partial \mathrm{v}}{\partial \mathrm{y}} + \frac{\partial \mathrm{w}}{\partial \mathrm{z}} = 0 \quad (3.6)$$

Where $\vec{\mathbf{V}}$ is the velocity vector

Momentum equation:

$$\rho_f(\vec{\boldsymbol{V}} \cdot \nabla)\vec{\boldsymbol{V}} = -\nabla p + \mu_f \nabla^2 \vec{V} \quad (3.7)$$

Where ρ_f and μ_f are the coolant density and viscosity, p is the coolant pressure.

Energy equation for fluid:

$$\rho_f c_{p,f}(\vec{\mathbf{V}} \cdot \nabla)\mathrm{T_f} = \mathrm{k_f}\nabla^2\mathrm{T_f} \quad (3.8)$$

Where $\mathrm{T_f}$ is the coolant temperature, $c_{p,f}$ and $\mathrm{k_f}$ are the specific heat and thermal conductivity of the coolant.

Energy equation for solid part:

$$k_s \nabla^2 T_s = 0 \tag{3.9}$$

Where k_s and T_s are the thermal conductivity and temperature for solid.

The boundary conditions for these equations are stated as follows:

at inlets:

$$v = V_{in}, u = w = 0, T_f = T_{in} \tag{3.10}$$

at outlets:

$$P = P_{out}\ , \ \frac{\partial T_f}{\partial y} = 0 \tag{3.11}$$

For Fluid-solid interface:

$$\vec{V} = 0, \quad T_s = T_f, \quad k_s \nabla T_s = k_f \nabla T_f \tag{3.12}$$

For the bottom wall[126][127]:

$$q'' = 100 W/cm^2 \tag{3.13}$$

For the other outside walls except the right side (symmetry surface):

$$\nabla T_s = 0 \tag{3.14}$$

The equations (3.6-3.14) were solved by using SIMPLE (Semi-Implicit Method for Pressure Linked Equations) scheme, which is widely used to solve the Navier-Stokes equations. Least squaares cell based is applied to the gradient. Both momentum ,energy equation and pressure equation is solved by using second order upwind. The convergence criterion is the maximum dimensionless temperature difference between two successive time-steps lower than 10^{-6}. The basic steps to run the simuation is presented in folliwng flow chart in Figure 3-7.

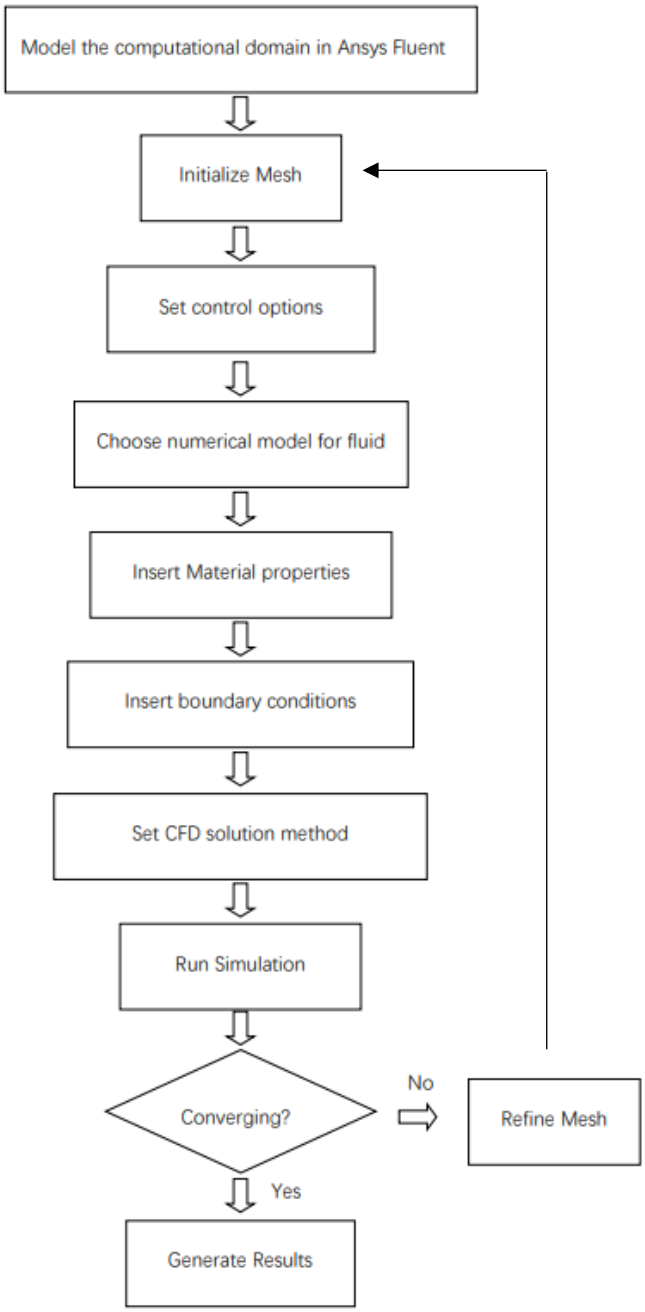


Figure 3-7 Flow chart for numerical analysis using Ansys Fluent.

Other parameters used to evaluate the performance of MCHSs are described as follows:

Total pumping power:

$$\Omega = \dot{Q}_{bottom}\Delta P_{bottom} + \dot{Q}_{top}\Delta P_{top}$$

$$= v_{in,bottom}W_{ch}H_{ch}\Delta P_{bottom} + v_{in,top}W_{ch}H_{ch}\Delta P_{top} \quad (3.15)$$

Average heat transfer coefficient, h_m:

$$h_m = \frac{q''}{(\overline{T}_b - T_{in})} \quad (3.16)$$

Thermal resistance, R_t, which assesses the heat dissipation capability of MCHSs:

$$R_t = \frac{T_{b,max} - T_{in}}{q'' L_x L_y} \quad (3.17)$$

Maximum temperature difference on the bottom surface of the heat sink, ΔT_b, which represents the cooling uniformity of MCHSs:

$$\Delta T_b = T_{b,max} - T_{b,min} \quad (3.18)$$

Where $\overline{T}_b$ is the average wall temperature wall temperature along the centerline of the bottom surface of the MCHS. $T_{b,max}$ and $T_{b,min}$ are the maximum and minimum bottom wall temperature on the bottom surface of the heat sink.

Nusselt number, NU, which represents the ratio of convective to conductive heat transfer at a boundary in a fluid.

$$Nu_m = \frac{h_m D_{h,m}}{k_f} \quad (3.19)$$

Where k_f is the thermal conductivity of the fluid

To compare the thermal-hydraulic performance between different MCHS designs, Figure of merit (FOM) is applied to determine the improvement of one design in terms of heat transfer and pumping power at the same time:

$$FOM = \frac{(h_{m,new}/h_{m,base})}{(\Omega_{new}/\Omega_{base})^{1/3}} \quad (3.20)$$

3.4 Validation and grid independence test

3.4.1 Validation results

The numerical work is validated with the numerical work by Lin et al.[85] under identical geometric dimensions and boundary conditions as shown in Figure 3-8. The geometric dimensions used for validation are: overall heat sink size of 1cm x 1cm, bottom channel height of 400μm, rib width of 150μm, bottom horizontal rib of 120μm, middle horizontal rib of 90μm and bottom channel inlet velocity of 0.7m/s. The simulations are conducted at fixed pumping power of 0.05W and a uniform heat flux of 100W/cm^2. The solid region of MCHS is made of silicon with $k_s = 148\ W/m/K$. The coolant used is pure water with $k_f = 0.587\ W/m/K$, $\mu_f = 0.001155\ kg/m/s$, $\rho_f = 999 kg/m^3$ and $c_{p,f} = 4187 J/kg/K$. The trend shows that the R_t decreases and then increases rapidly with the increase of channel number. The reason is that the overall rib width increases but channel width decreases with the increase of channel number. The increase of overall rib width decreases the contact surface area between bottom channel and coolant and thus weakens the thermal performance, while the decrease of channel width leads to the increase of upper channel velocity (bottom channel velocity is fixed) and thus enhances the thermal performance at meantime. The trend shows the balance between these two effects. The present work shows good agreement with the numerical results obtained by Lin et al. [85] with a maximum difference of 6.47% in overall thermal resistance was found as shown in Figure 3-9.

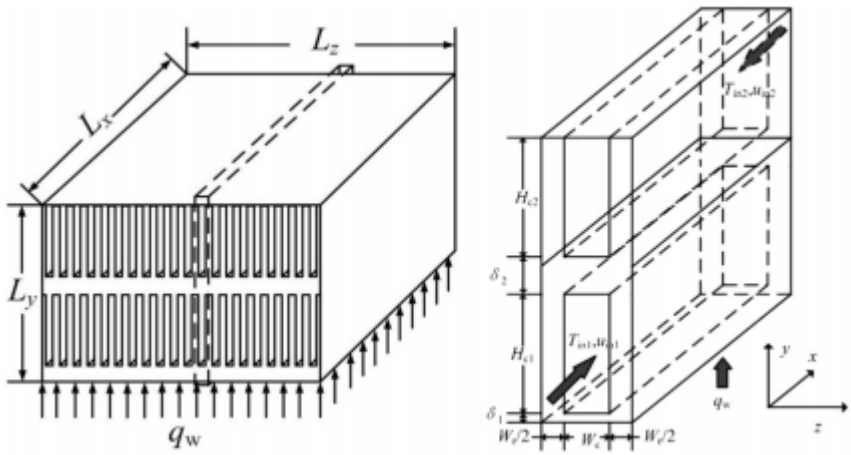


Figure 3-8. Schematics of DLMS and computational domain[85].

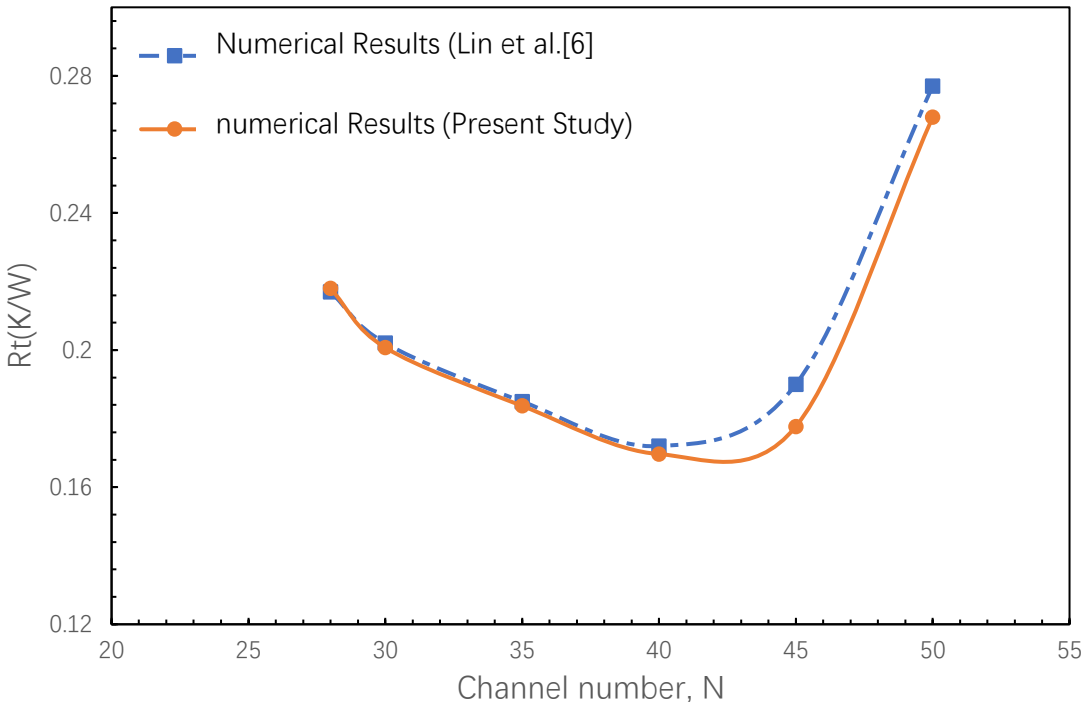


Figure 3-9 the graph of max thermal resistance versus the channel number valid with Lin et al. [85]

The numerical work is also validated with the experimental and numerical work by Wei et al [29] with the temperature along the bottom surface under same geometry and boundary conditions. The experimental model and numerical domain proposed by Wei et al. is shown in Figure 3-10(a) and(b), respectively. The experimental model consists of five layers of silicon: two microchannels at bottom to provide the cooling, two manifold layers in middle for fluid distribution and one layer in top for fluid connection. The five layers of silicon are fabricated using deep-active ion etching technique and bonded into a watertight stack through silicon-silicon direct bonding method. The numerical model takes a single channel in consideration and the dimensions used are listed in Table 3-4. Total flow rate of 83ml/min and heat flux of 100W/cm^2 is applied and good agreement was obtained and can be seen form Figure 3-11.

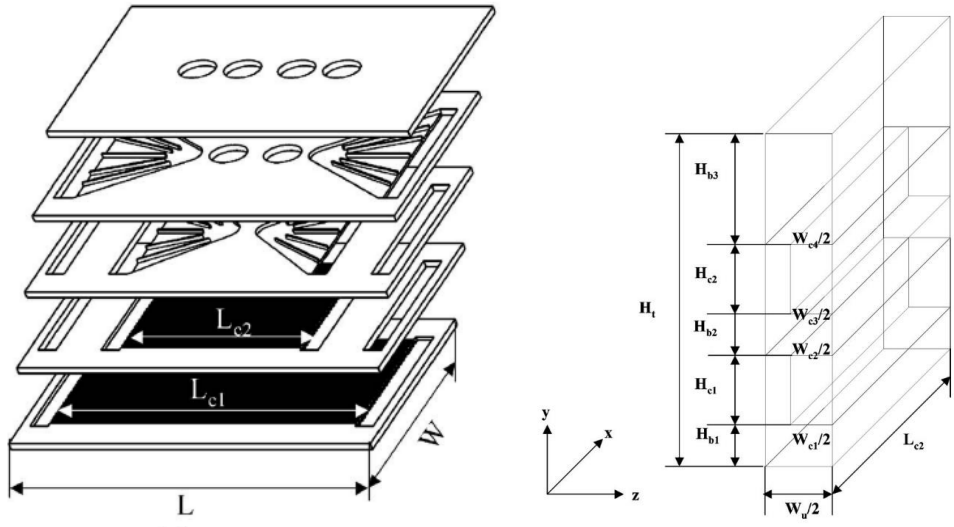


Figure 3-10 The schematic of (a)experimental test module (b) computational domain proposed by Wei et al [29].

Table 3-4 The microchannel dimensions $\times 10^3$(m) proposed by Wei et al [29].

L_{c2}	w_u	w_{c1}	w_{c2}	w_{c3}
10	0.1	0.056	0.054	0.061
w_{c4}	H_{c1}	H_{c2}	H_{b1}	H_{b2}
0.053	0.284	0.243	0.216	0.257

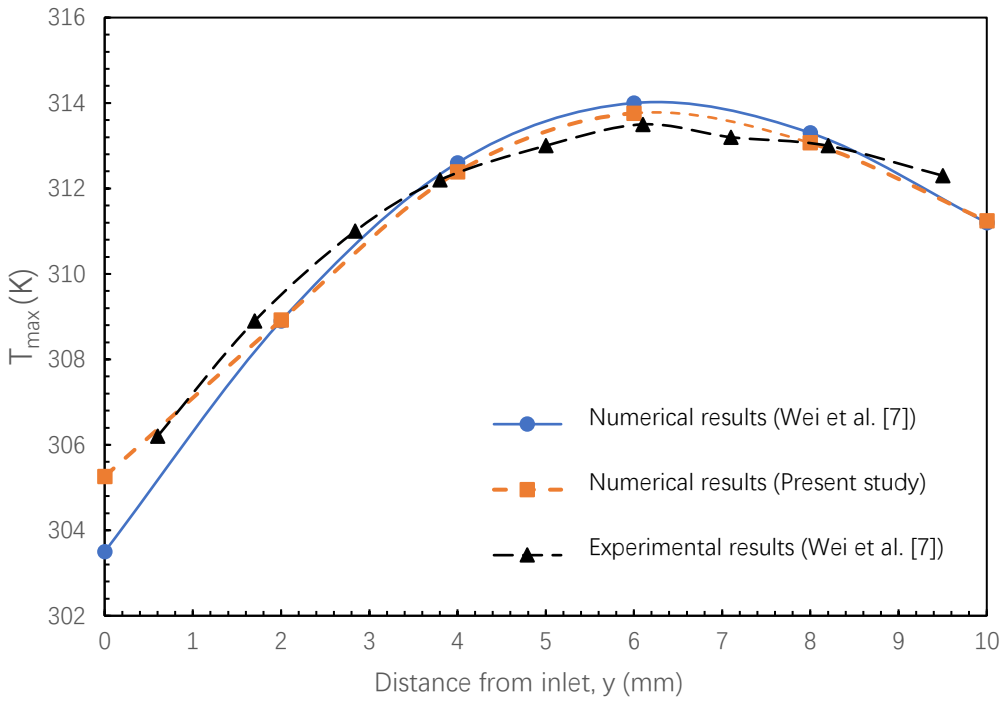


Figure 3-11 The graph of max temperature along the bottom surface valid with Wei et al. [29]

3.4.2 Grid Independence Test

To ensure the solution is not influenced by the grid size, three different grid sizes of 40×128×100, 29×98×76 and 20×66×50 is applied to all cases. The comparison of maximum thermal resistance, R_t and overall pumping power, Ω between three different grid sizes for case Wi=50μm Wo=50μm is plotted in Figure 3-12 (a) and (b), respectively. Based on calculation, difference of 0.3% and 2.53% is found between grid size of 40×128×100 and 20×66×50 for R_t and Ω, respectively. This indicates the solution has become steady and can be used for analysis without much error. For all the cases investigated in this study, the biggest relative error between fine and coarse mesh when comparing R_t and Ω is only 1% and 5%, respectively. The grid size of 40×128×100 for all cases is used for discussion to minimize the error.

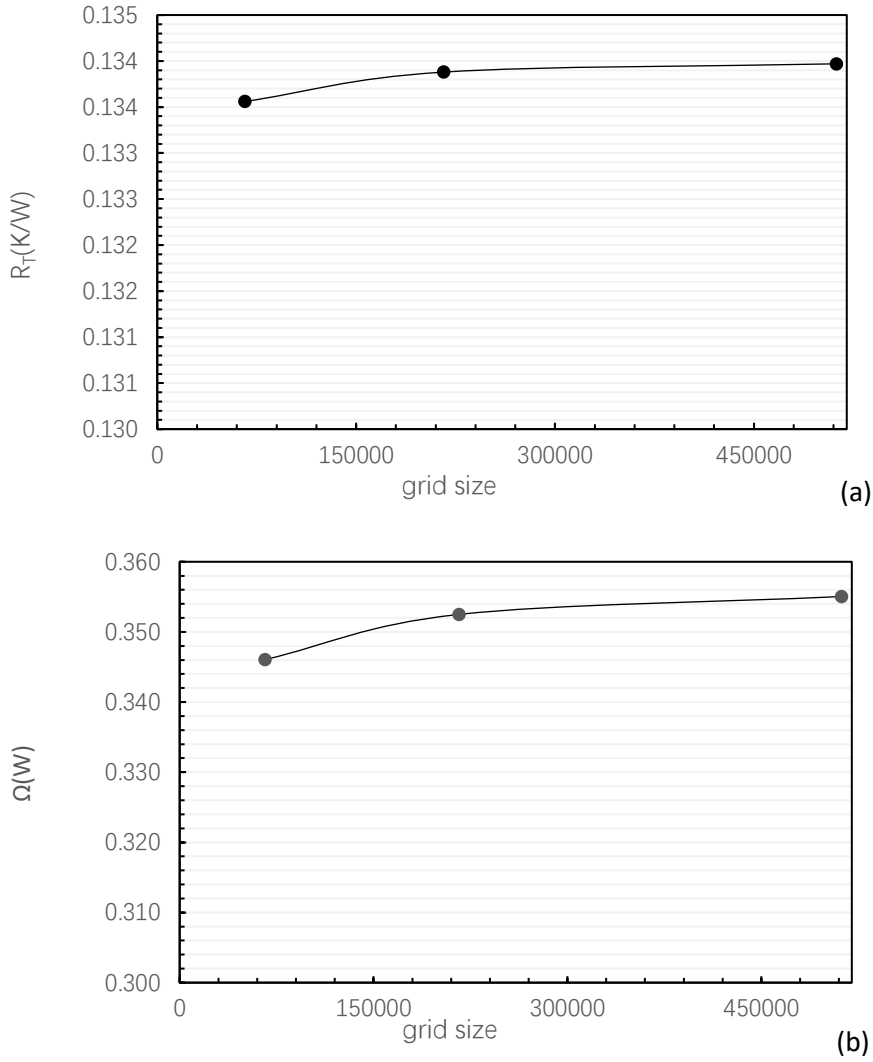


Figure 3-12 The results of (a) thermal resistance, R_t (b) pumping power, Ω for three grid sizes

Chapter 4 Numerical investigation of DL-MCHS with tapered channel profile

4.1 Introduction

In this chapter, the thermal and hydraulic performance for DL-MCHS with parallel and counter flow are firstly numerically studied for eight different designs at various Re. The thermal performance in terms of temperature distribution, thermal resistance, Nusselt number and hydraulic performance in terms of velocity distribution are presented. Then the parametric study is conducted to explore the effect of channel inlet width, channel outlet width and channel height on thermal and hydraulic performance for DL-MCHS with parallel and counter flow configuration at fixed volumetric flow rate of 200ml/min. At last, the thermal-hydraulic thermal performance in terms of Figure of Merit is presented.

4.2 The thermal performance for DL-MCHS with different designs at various Re

Figure 4-1 and Figure 4-2 illustrates the temperature distribution along flow direction on the bottom and symmetry plane for four designs (1,4,5 and 8) at Re=200 for DL-MCHS with parallel and counter flow configuration, respectively. For both parallel and counter flow configuration, Design 8 exhibits the highest maximum temperature and Design 1 shows the lowest maximum temperature. For both parallel flow and counter configuration, same trend can be found in Design 1,4 and 8 that the temperature gradually increases along the flow direction. While due to the flow direction difference in top and bottom channel, a pull back of heat can be found at the inlet of upper channel and makes temperature distribution more uniformity. For Design 5, same trend can be found for both flow configurations that the temperature increases and then decreases along the flow direction. This is due to the combine effect of coolant temperature increases and channel size decreases along the flow direction.

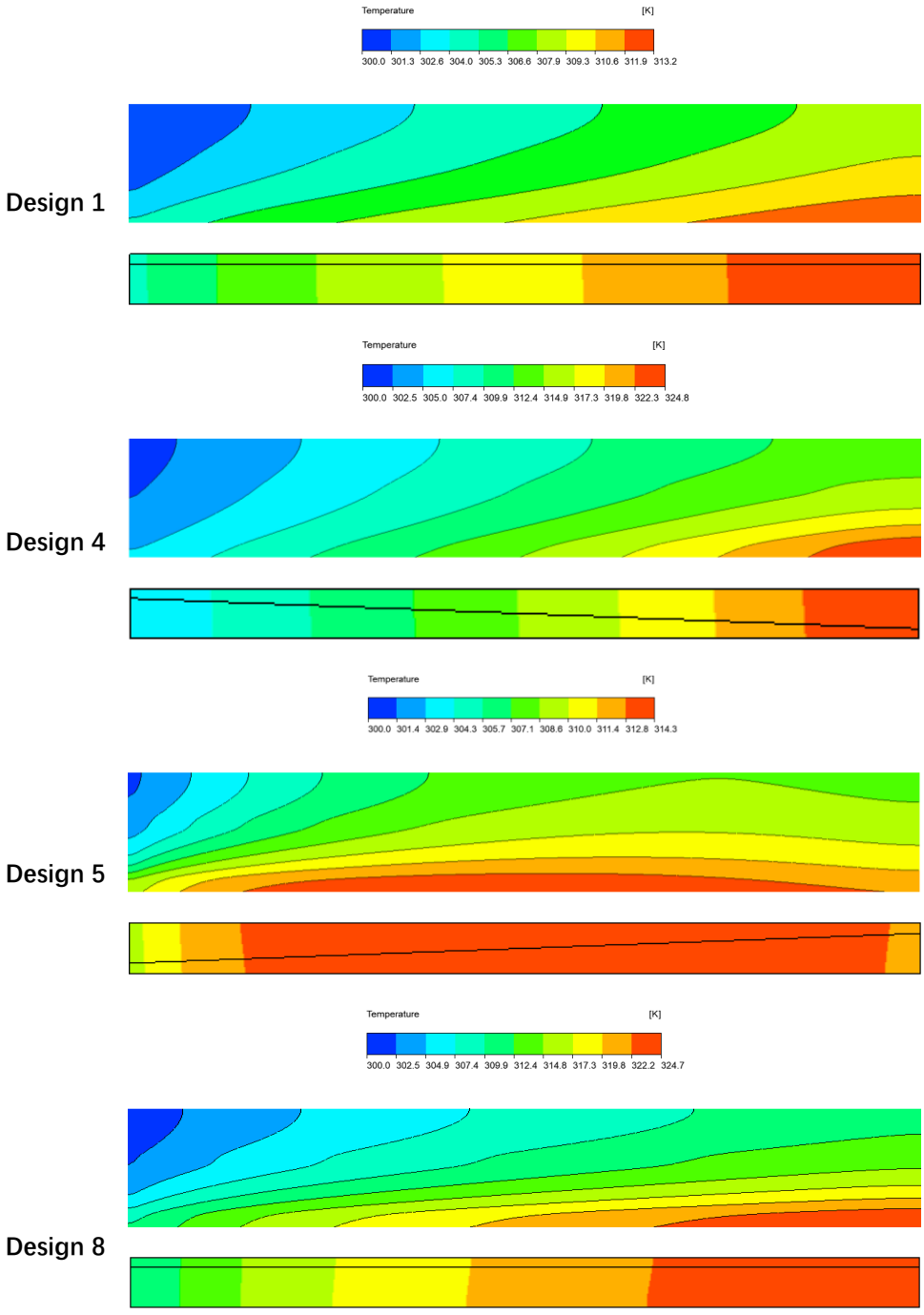


Figure 4-1 Temperature distributions along flow direction on the bottom and symmetry plane for four designs (1,4,5 and 8) at Re=200 for DL-MCHS with parallel flow configuration.

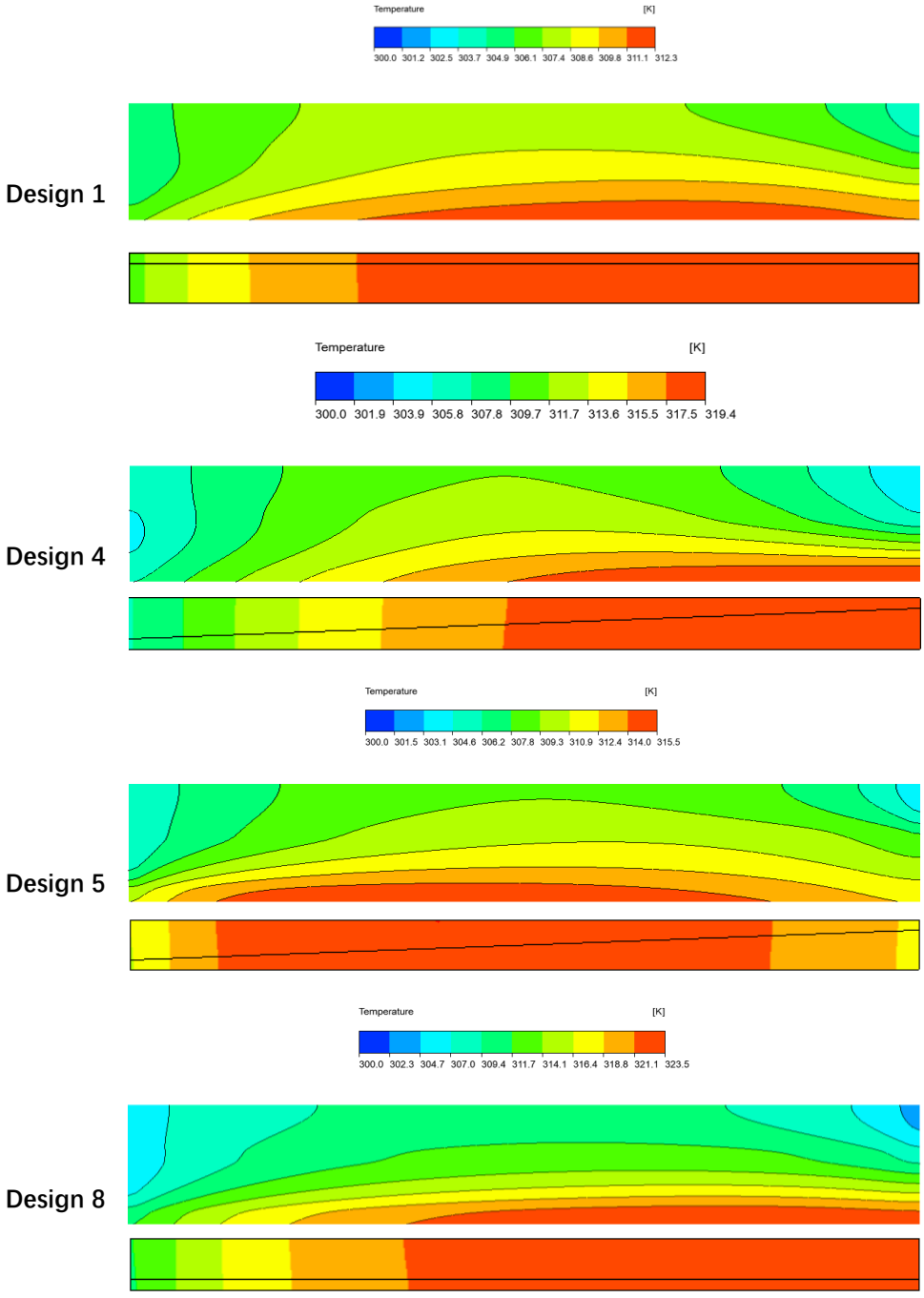


Figure 4-2 Temperature distributions along flow direction on the bottom and symmetry plane for four designs (1,4,5 and 8) at Re=200 for DL-MCHS with counter flow configuration.

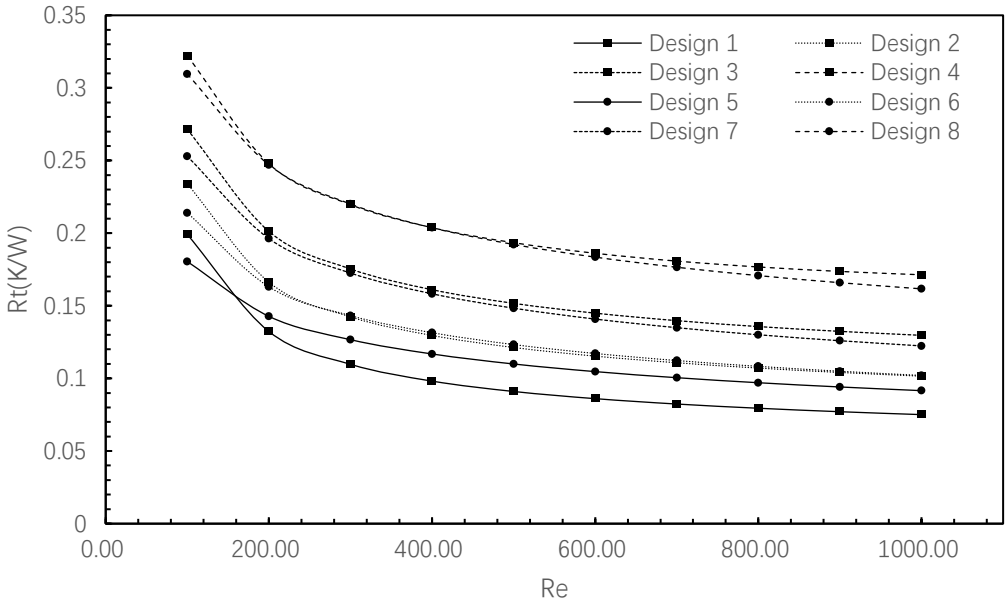


Figure 4-3 The R_t for DL-MCHS with parallel flow and with different designs at various Re.

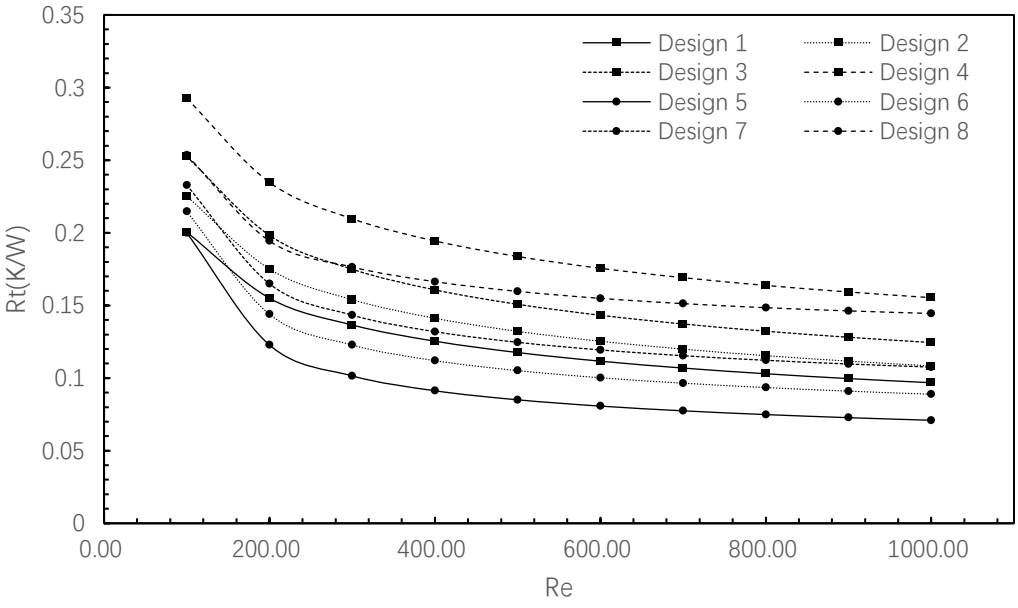


Figure 4-4 The R_t for DL-MCHS with counter flow and with different designs at various Re.

Figure 4-3 and Figure 4-4 presents the thermal resistance for DL-MCHS with parallel flow and counter flow at Re varying from 100 to 800, respectively. Same trend can be found for Design 1-8 for both flow configurations that the R_t decreases with the increase of Re and the increment becomes less significant. This is mainly due to the convective heat transfer in channels enhanced with the increase of Re [43]. For diverging channel designs with same value of W_i (design 2,3 and 4), the R_t decreases with the increase of W_o. While for converging channel designs with same value of W_o, (design 5,6 and7), opposite trend can be found that the R_t increases with the increase of W_o. For both converging and diverging channel designs, the design with smaller W_o exhibits lower value of R_t and the design with smallest W_i and W_o presents best thermal performance, this indicates that the channel size has great impact on heat transfer performance.

Figure 4-5 and Figure 4-6 presents the variation of Nu with Re for DL-MCHS with parallel and counter flow respectively. The diverging channel design with same W_i (Design 2-4) and converging with same W_o (Design 5-7) are plotted separately in each figure (a) and (b), respectively. For all design investigated, the Nu increases with the increase of Re as expected [68][125]. This indicates that the convective heat transfer enhanced with the increase of flow rate. Moreover, the converging channel designs show higher Nu as compared to straight channel design with same W_i and diverging channel designs show higher Nu as compared to straight channel design with same W_o. This indicates the converging channel and diverging channel design has better thermal performance as compared to the straight channel design with certain channel width. For converging designs in both flow configurations, Nu increases with the increase of W_o and the increment becomes less significant. The increment of Nu for design 2,3 and 4 compares to design 1 is 22.48%, 38.34% and 49.38% for parallel flow and 33.69%, 57.03% and 71.74% for counter flow when Re=100, respectively. For diverging designs in both flow configurations, the increment of Nu for design 5,6 and 7 compares to design 8 is 10.62%, 11.11% and 8.02% for parallel flow and 10.62%, 11.11, 7.72% for counter flow when Re=1000, respectively.

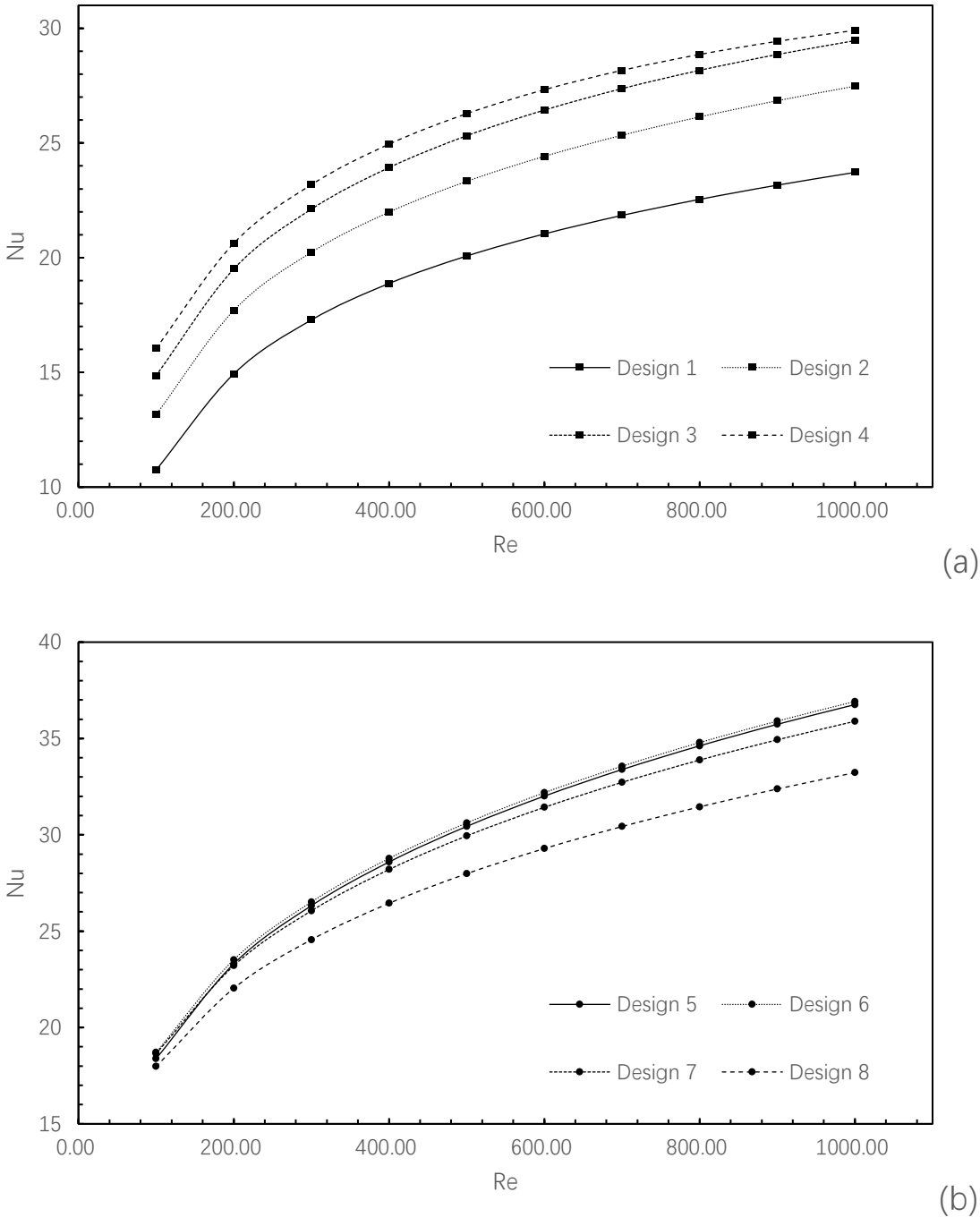


Figure 4-5 The Nu for Dl-MCHS with parallel flow at various Re for (a) Design 1-4 (b) Design 5-8.

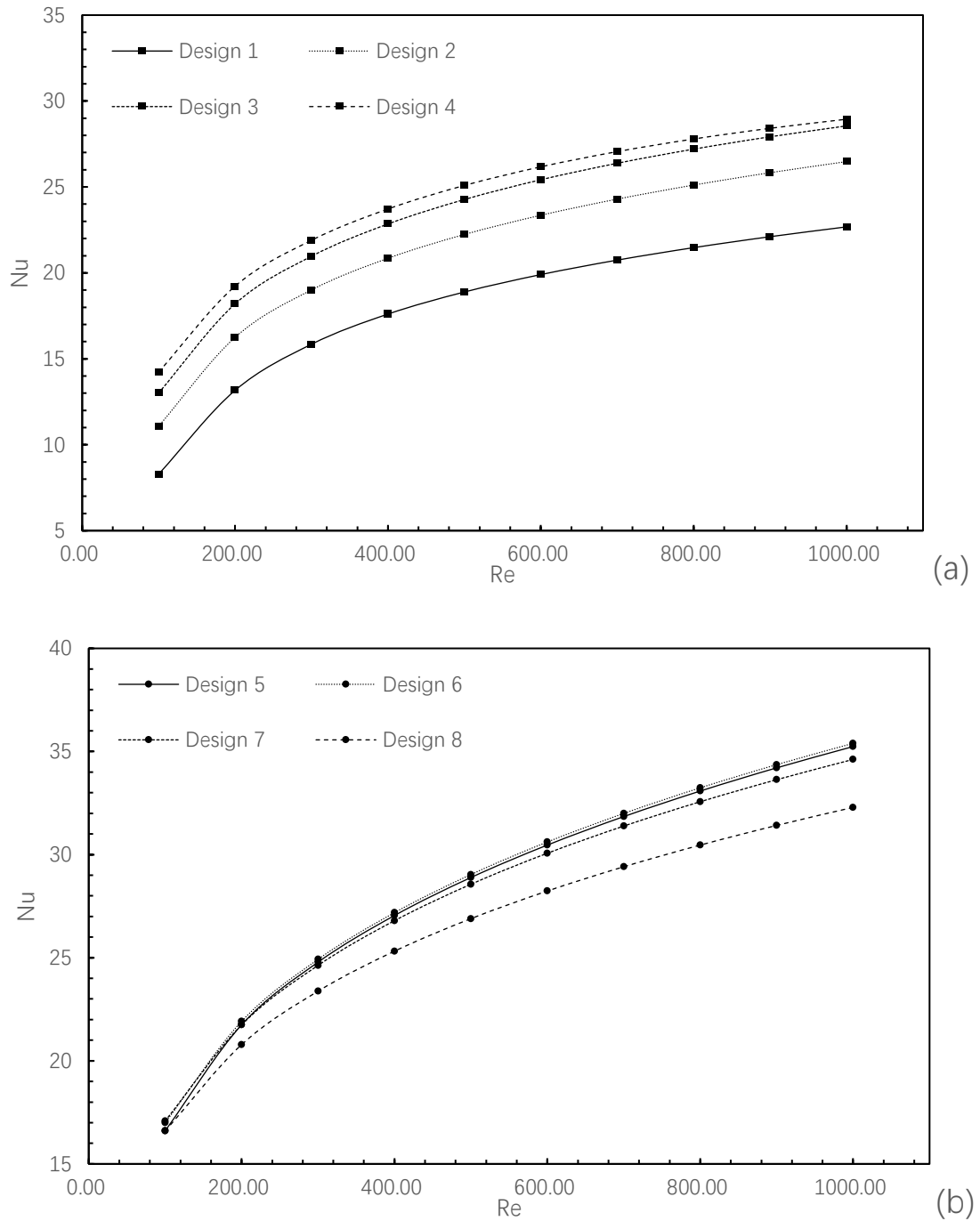


Figure 4-6 The Nu for Dl-MCHS with counter flow at various Re for (a) Design 1-4 (b) Design 5-8.

4.3 The hydraulic performance for DL-MCHS with different designs at various Re

The velocity distribution for DL-MCHS with different designs for Re=200 is shown in Figure 4-7. For all designs, due to the coolant's viscosity effect, the velocity is zero at the fluid-solid interface and gradually increases till channel [128]. For straight channel design (design 1and 8), the hydraulic boundary layer thickness thickens and becomes steady along flow direction due to the flow developing. While for diverging designs and converging designs, the hydraulic boundary layer thickness keeps varying along the flow direction due to the changes in channel width.

The pressure drop for DL-MCHS with different designs at various Re is presented in Figure 4-8. For all designs, the △P increases with the increase of Re as expected. When look into the designs with same W_i as shown in Figure 4-8(a), the design with larger W_o exhibits lower pressure drop at same Re and straight channel design of W_i=50μm and W_o=50μm presents largest △P. When look into the designs with same W_o as shown in Figure 4-8(b), the design with smaller W_i exhibits higher pressure drop at same Re and straight channel design of W_i=200μm and W_o=200μm presents lowest △P. This indicates that the diverging channel designs exhibit better hydraulic performance as compared to straight channel design with same W_i. and converging channel designs present worse hydraulic performance as compared to straight channel design with same W_o.

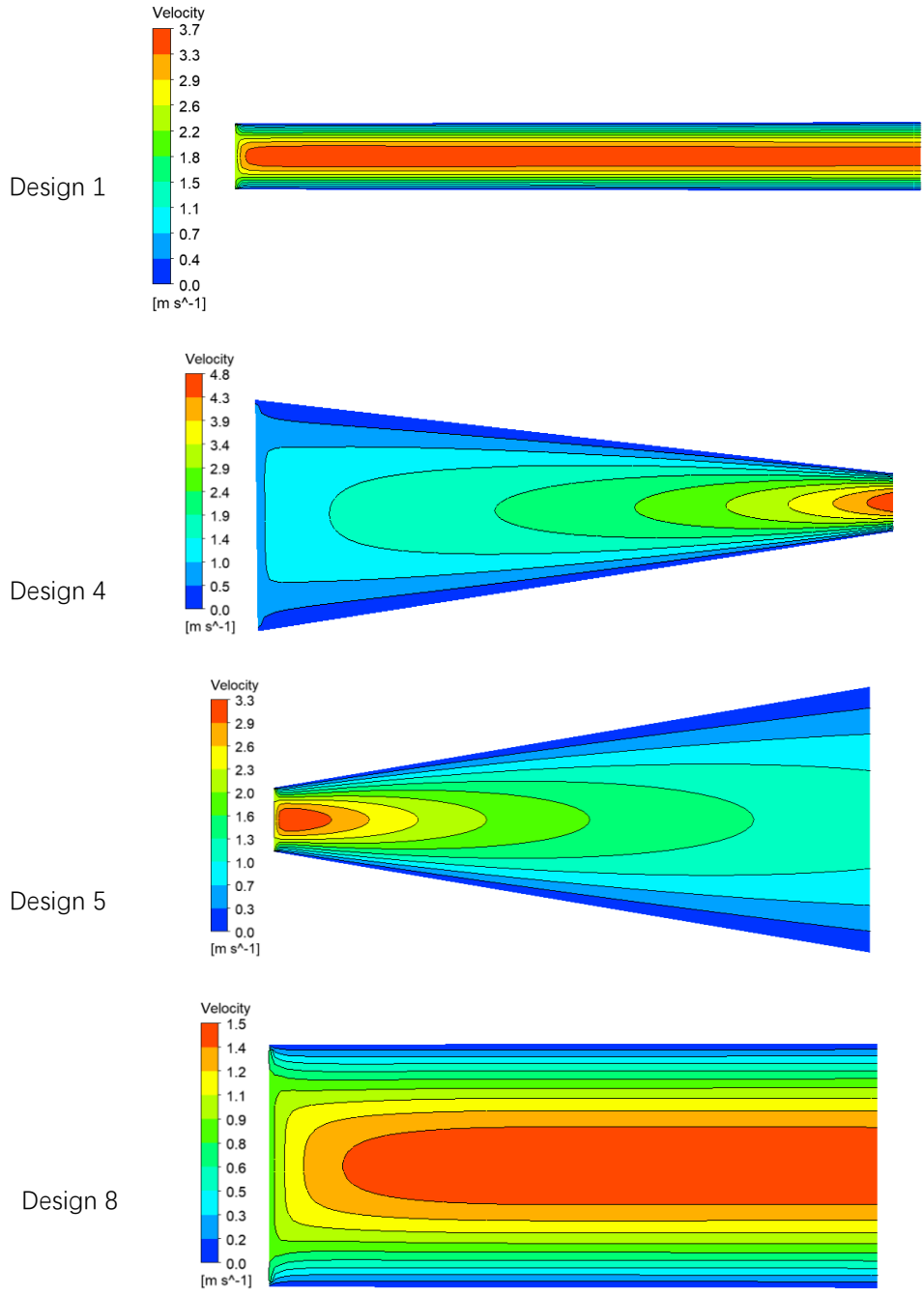


Figure 4-7 The velocity distribution for DL-MCHS with different designs for Re=200.

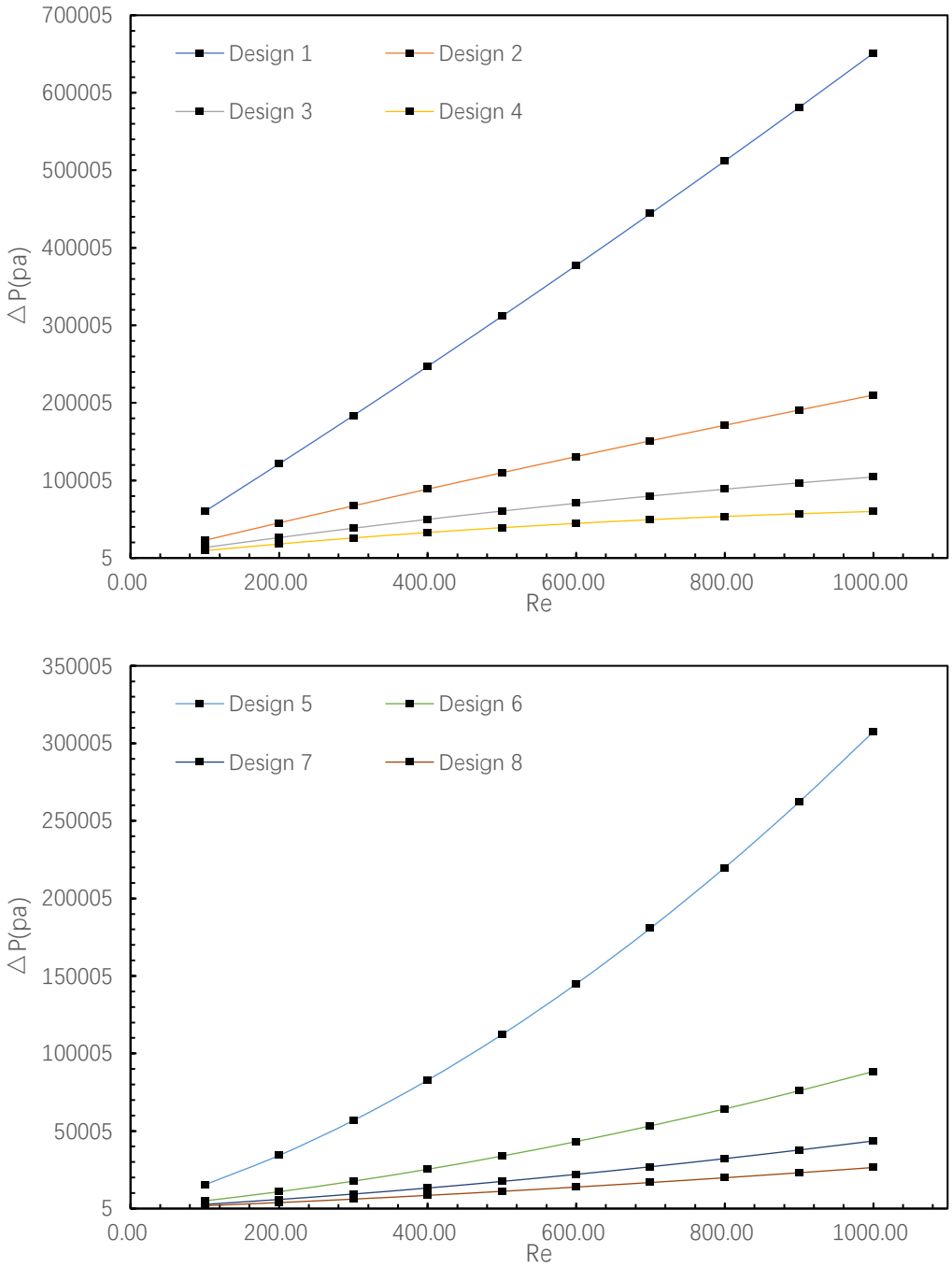


Figure 4-8 The pressure for DL-MCHS with different designs at various Re.

4.4 The overall thermal resistance for DL-MCHS with different W_o, W_i and H_{ch}

4.4.1 The thermal resistance for DL-MCHS operating in counter flow configuration

To study the effect of different design parameters on thermal and hydraulic performance for DL-MCHS with different flow configurations, the parametric study based on different design parameters at same volumetric flow rate is presented afterwards. Figure 4-10 shows the overall thermal resistance of different value of W_o, W_i and H_c for counter flow configuration. The Figure 4-9 (a), (b), (c) and (d) illustrate the overall thermal resistance for different channel height H_{ch} of 325μm, 350 μm, 375 μm and 400 μm, respectively. For all the cases, the flow rate for bottom layer and upper layer is the same. The results reveals that the value of R_T increases almost linearly with W_o for any value of W_i and H_{ch}.

For the data presented in Figure 4-10, the bars with bold border represents straight channel design with $W_o = W_i$. The bars that are on the left side of the bolded bar are of converging channel design whereas the bars on the right side of the bolded bar are of diverging channel design.

When looking into the effect of W_o , for any given value of W_i and H_{ch}, the overall thermal resistance R_T reduces with the decrease in W_o. For a fixed value of W_i, the decrease in W_o transforms the geometry from diverging channel design ($W_o > W_i$) to straight channel ($W_o = W_i$) and then to converging channel design ($W_o < W_i$). The results reflect that converging channel design gives lower thermal resistance R_T (better thermal performance) than the diverging channel design. For the case of converging channel, the flow path for coolant become narrower along the flow direction and this is expected to cause an increase in flow velocity. Literally, this means converging channel design gives better thermal performance, and smaller value of channel outlet width gives better thermal performance.

When looking into the effect of W_i, for any given value of W_o and H_{ch}, the overall thermal resistance reduces slightly with the decrease of W_i. Literally, this means smaller value of channel inlet width W_i gives better thermal performance.

When looking into the effect of H_{ch}, for any given value of W_o and W_i, the overall thermal resistance increases slightly with the increase of channel wall thickness. Literally, this means smaller value of channel wall thickness gives better thermal resistance but the effect is small.

4.4.2 The thermal resistance for DL-MCHS operating in parallel flow configuration

The results of thermal resistance for DL-MCHS of different W_o, W_i and H_{ch} for parallel flow configuration are presented in Figure 4-11. The results in Figure 4-11. (a), (b), (c) and (d) illustrate the thermal resistance for different channel height H_{ch} of 325μm, 350 μm, 375 μm and 400 μm, respectively. The results show the same trend as parallel flow only have slightly larger value of overall thermal resistance.

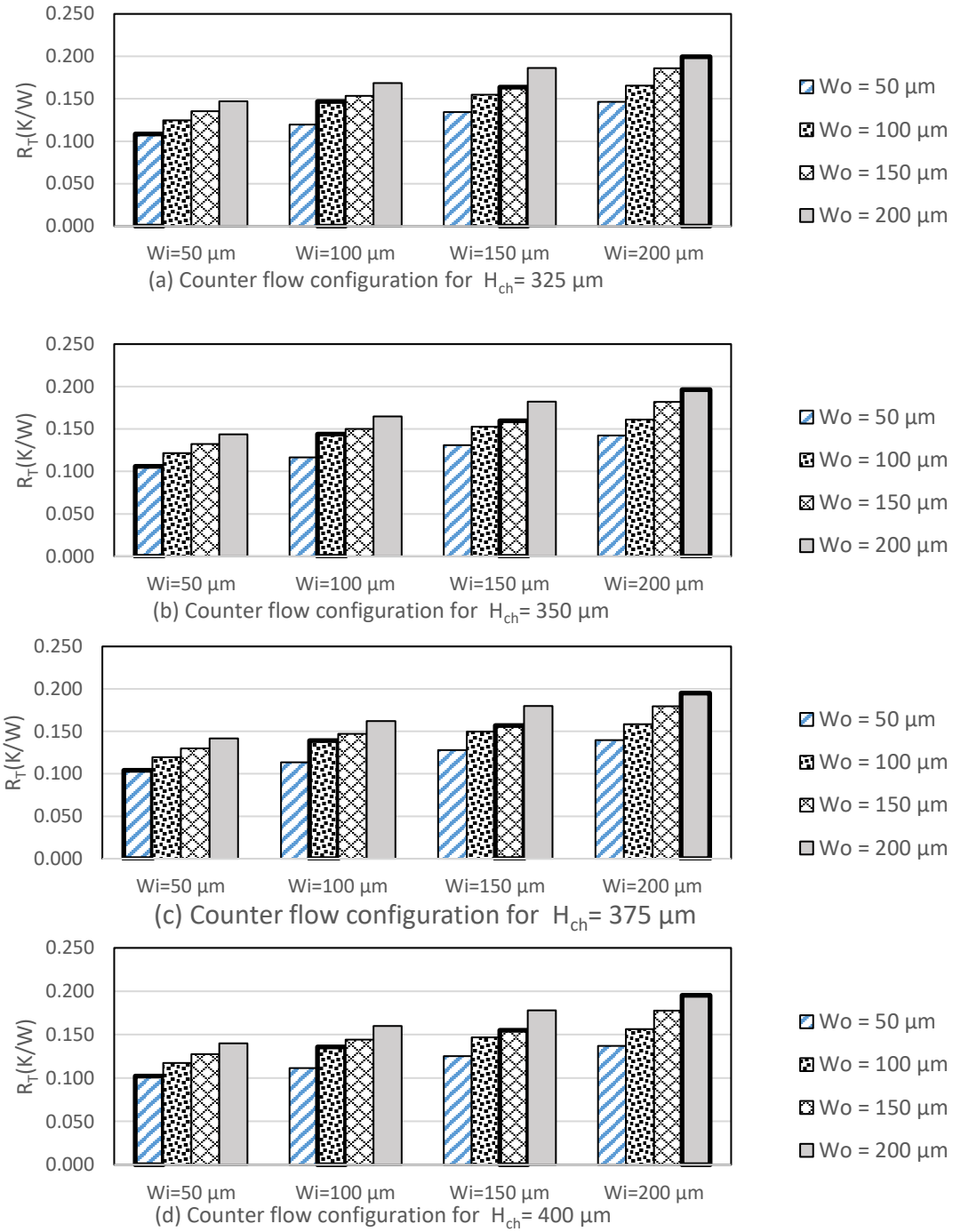
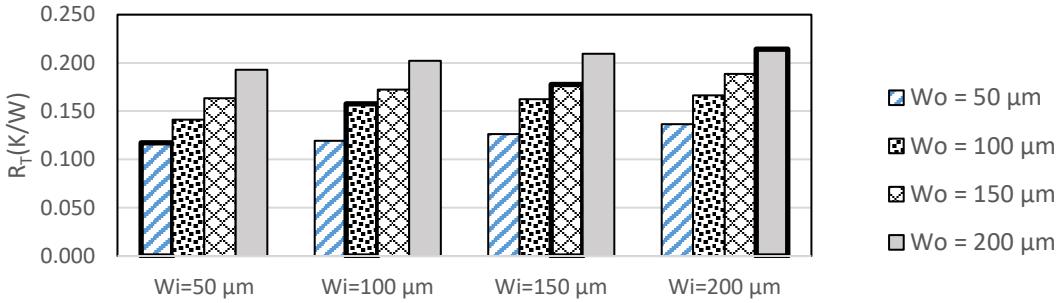


Figure 4-10 The thermal resistance for counter flow configuration in DL-MCHS with different W_o, Wi and H_{ch} (a) H_{ch} = 325 µm, (b) H_{ch} = 350 µm, (c) H_{ch} = 375 µm, and (d) H_{ch} = 400 µm.



(a) Parallel flow configuration for H_{ch}= 325 µm

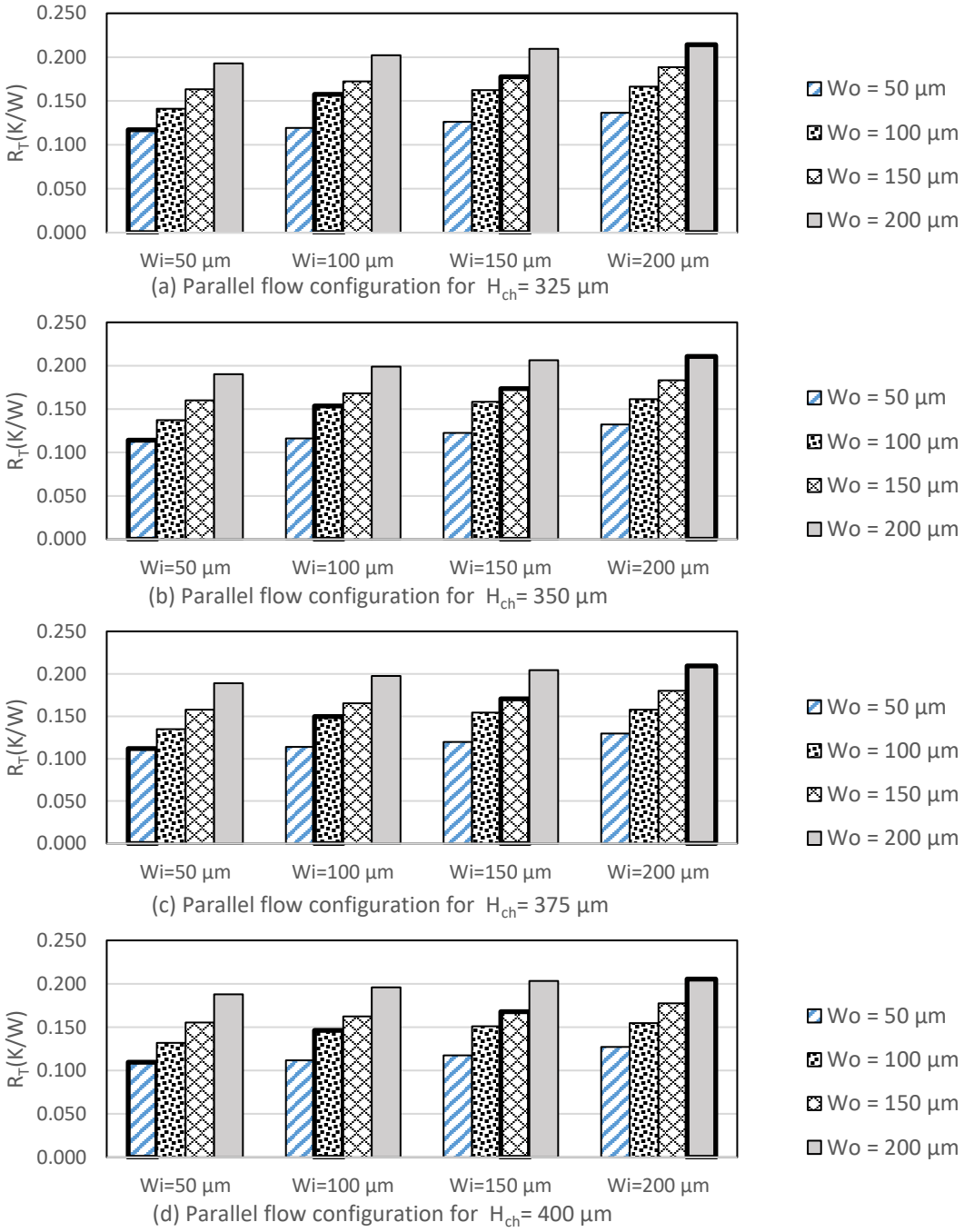


Figure 4-11 The thermal resistance for parallel flow configuration in DL-MCHS with different W_o, Wi and H_{ch} (a) H_{ch} = 325 µm, (b) H_{ch} = 350 µm, (c) H_{ch} = 375 µm, and (d) H_{ch} = 400 µm.

4.4.3 The comparison of thermal resistance between parallel and counter flow configuration.

Based on the simulation results of all 128 cases, the comparison between parallel and counter flow configuration of overall thermal resistance versus W_i is plotted in Figure 4-12，Figure 4-13，Figure 4-14 and Figure 4-15 for different channel height of 325μm, 350 μm, 375μm and 400 μm, respectively. The results in each figure (a), (b), (c) and (d) illustrate the thermal resistance for outlet width, W_o of 50μm, 100 μm, 150 μm and 200 μm, respectively. Figure 4-12 (a) shows parallel flow configuration has lower overall thermal resistance than counter flow configuration when W_i is large and counter flow configuration shows its advantage when W_i is small. Figure 4-12 (b), (c) and (d) shows counter flow configuration has lower overall thermal resistance compared to the parallel configuration. Figure 4-13，Figure 4-14 and Figure 4-15 show the same trend that the counter flow configuration have lower thermal resistance than parallel flow configuration except the first two points of W_o=50 μm at fixed volume flow rate of 200/min and the difference between parallel flow and counter flow configuration become more significant with the decrease of W_o. As a result, the counter flow configuration always has better thermal performance than parallel flow configuration when the W_i is small and the difference become more significant with the decrease of W_i.

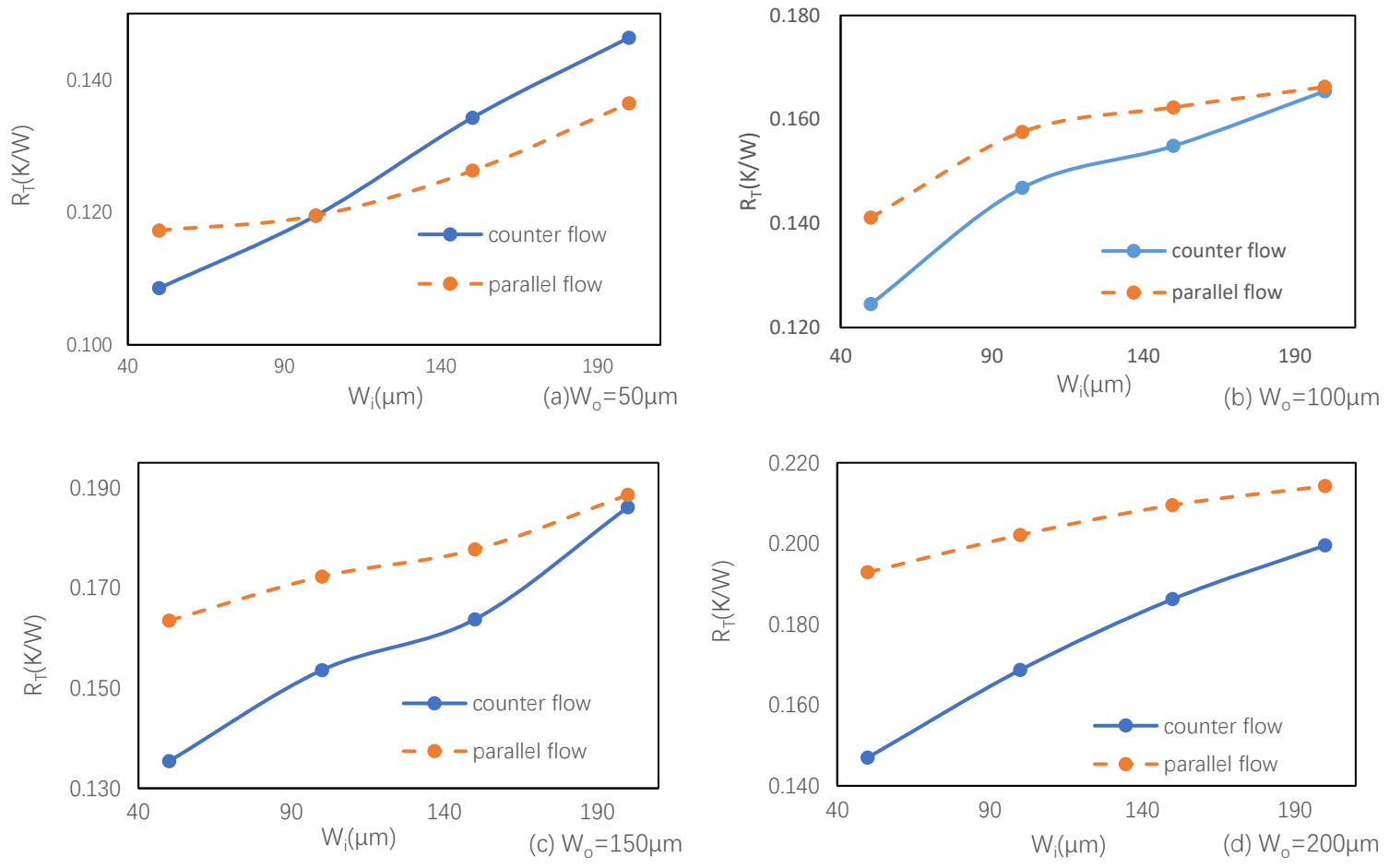


Figure 4-12 Comparison of thermal resistance between parallel and counter flow configuration for H_{ch} =325μm and (a) W_o =50μm, (b) W_o =100μm, (c) W_o =150μm (d) W_o =200μm

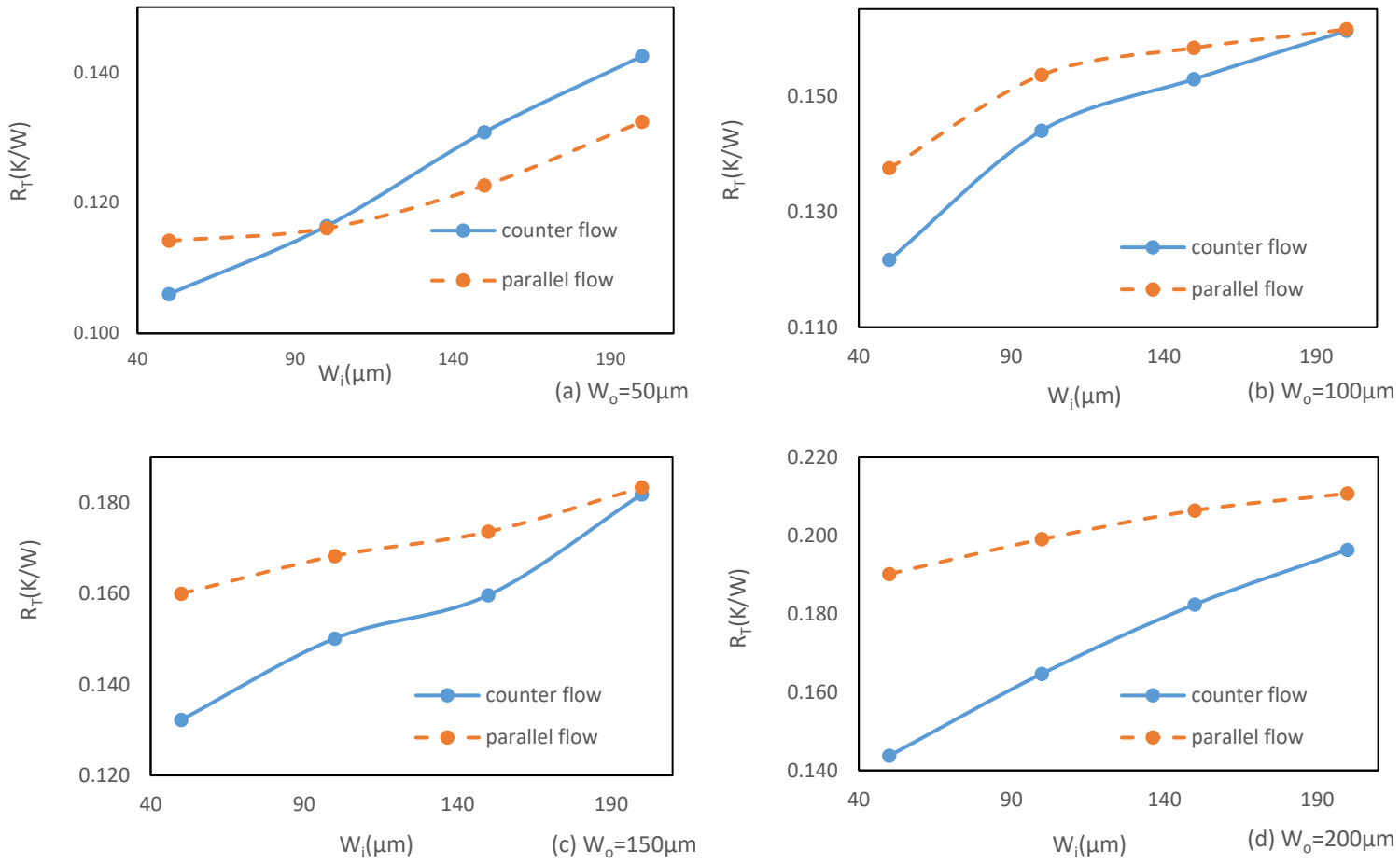


Figure 4-13 Comparison of thermal resistance between parallel and counter flow configuration for H_{ch} =350μm and (a) W_o=50μm, (b) W_o =100μm, (c) W_o =150μm (d) W_o =200μm

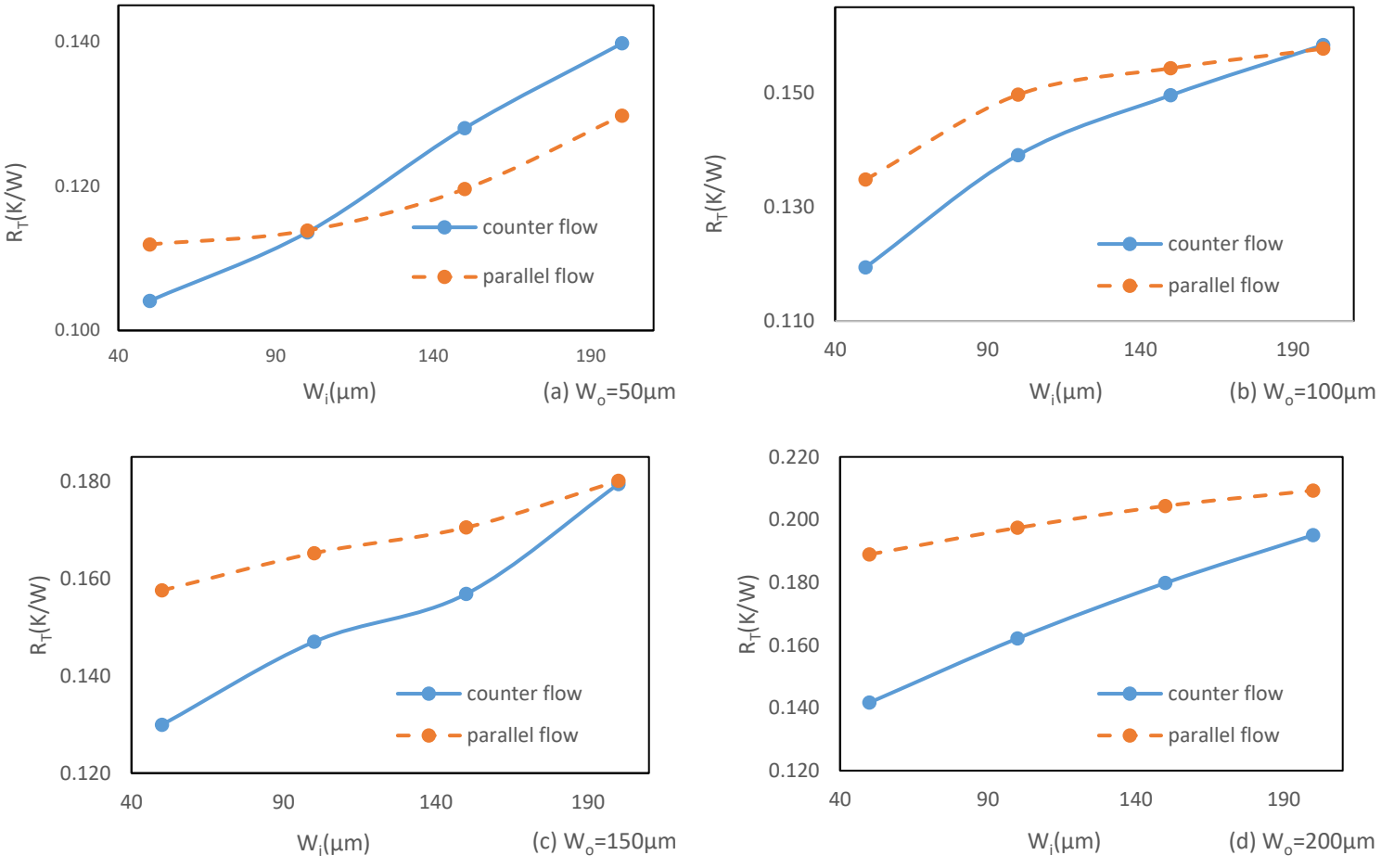


Figure 4-14 Comparison of thermal resistance between parallel and counter flow configuration for H_{ch} =375μm and (a) W_o=50μm, (b) W_o =100μm, (c) W_o =150μm (d) W_o =200μm

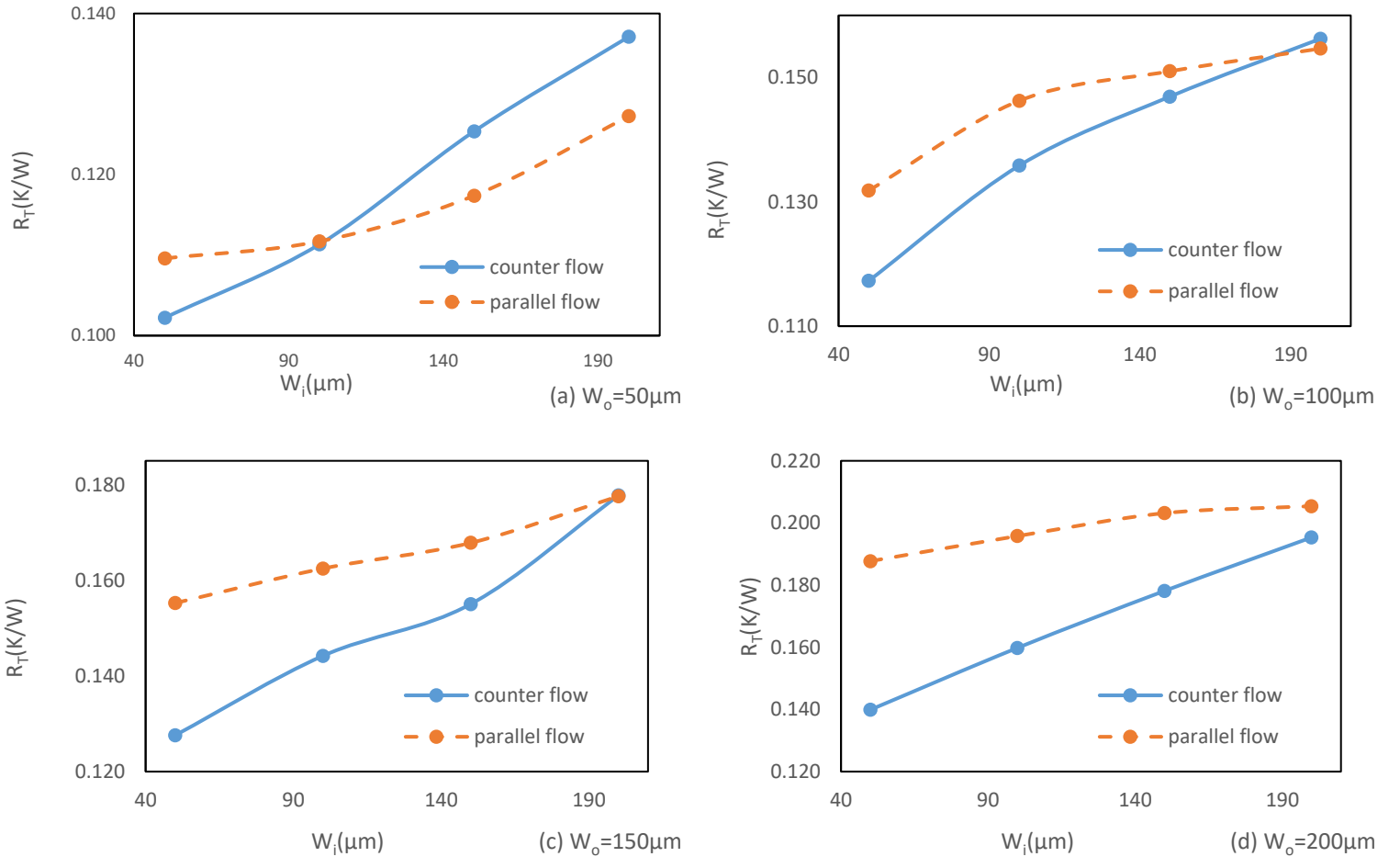


Figure 4-15 Comparison of thermal resistance between parallel and counter flow configuration for H_{ch} =400μm and (a) W_o =50μm, (b) W_o =100μm, (c) W_o =150μm (d) W_o =200μm

The temperature distribution along the flow direction at the bottom surface of the DL-MCHS for parallel flow and counter flow configuration for $W_o = 50\mu m$, $W_i = 50\mu m$ is shown in Figure 4-16. The lines from top to bottom represent $H_{ch} = 325\mu m, 350\mu m, 375\mu m$ and $400\mu m$, respectively. For parallel flow configuration, temperature increase from inlet till outlet as a result of the uniform heating. The maximum temperature appears at the outlet of the heat sink. For counter flow configuration, temperature increase till the middle and then decrease as a result of cold coolant coming from the backside of the heat sink for upper layer. The maximum temperature appears at the middle of the heat sink. This reveals that the counter flow configuration has better temperature uniformity than the parallel flow configuration due to the similarity of the maximum temperature.

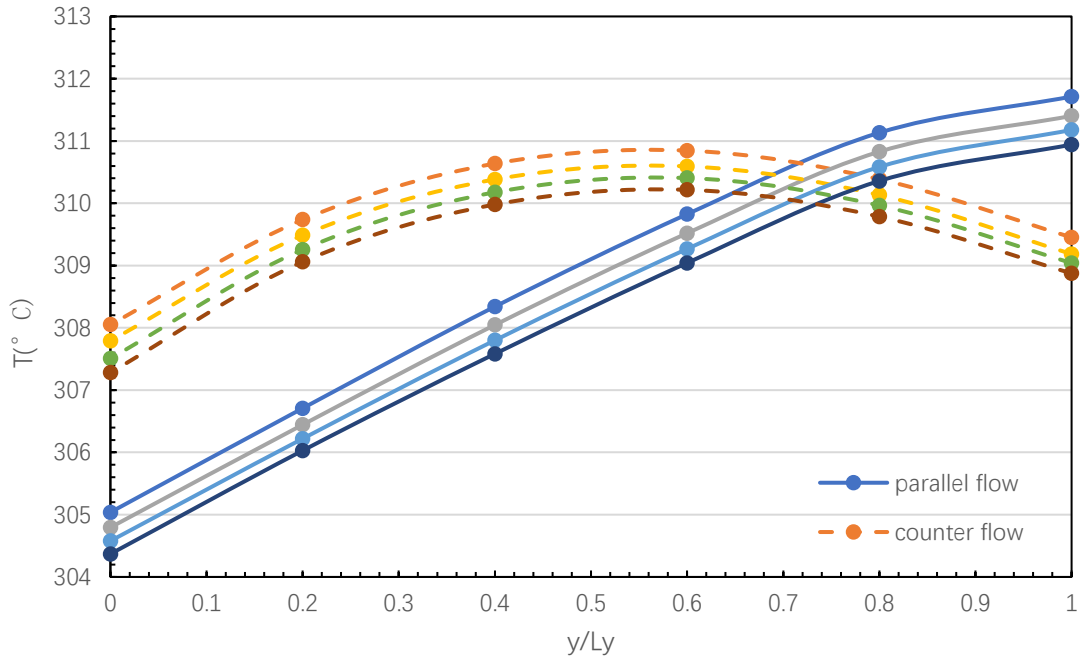


Figure 4-16 Temperature distribution along the bottom surface of the DL-MCHS for parallel flow and counter flow configuration.

To understand the trend shown in Figure 4-12-Figure 4-15, the maximum temperature along the flow axial direction $T_{y,max}$ is presented in Figure 4-17 for the cases of Wi = 50 µm and Wi = 200 µm. The trend observed in Figure 4-12 (a) can be analysed based on the results in Figure 4-17 which illustrate the changes in base temperature along the flow axial direction. Physically, the DL-MCHS with Wo = 50 µm

and Wi = 50 μm has straight channel profile, while the DL-MCHS with Wo = 200 μm and Wi = 50 μm. In Figure 4-17, when comparing the temperature variation patterns, the counter flow for W_i = 50 μm and W_i = 200 μm shows similar variation pattern with the peak temperature lies at the vicinity of mid-section. However, the temperature variation patterns for parallel flow among W_i = 50 μm and W_i = 200 μm show significant difference. For W_i = 50 μm of parallel flow (straight channel profile), the peak temperature is near the channel outlet. For W_i = 200 μm of parallel (converging channel profile), the peak temperature is located at about y/L = 0.6, which is not located at the channel outlet; this is due to the increase in velocity towards the channel outlet owing to the highly tapered channel, giving better heat removal near the outlet. This means, the converging geometry has significantly changed the temperature variation pattern for parallel flow configuration, and converging channel profile results in a better uniformity of temperature from the location of mid-channel to channel outlet which can be observed in Figure 4-17. Referring to equation (10), the thermal resistance R_T is evaluated based on the maximum base temperature T_{max}. From Figure 4-17, for W_i = 50 μm, T_{max} is higher for the counter flow whereas for W_i = 200 μm, T_{max} is higher for the parallel flow. This results in the opposite trend found in Figure 4-12(a).

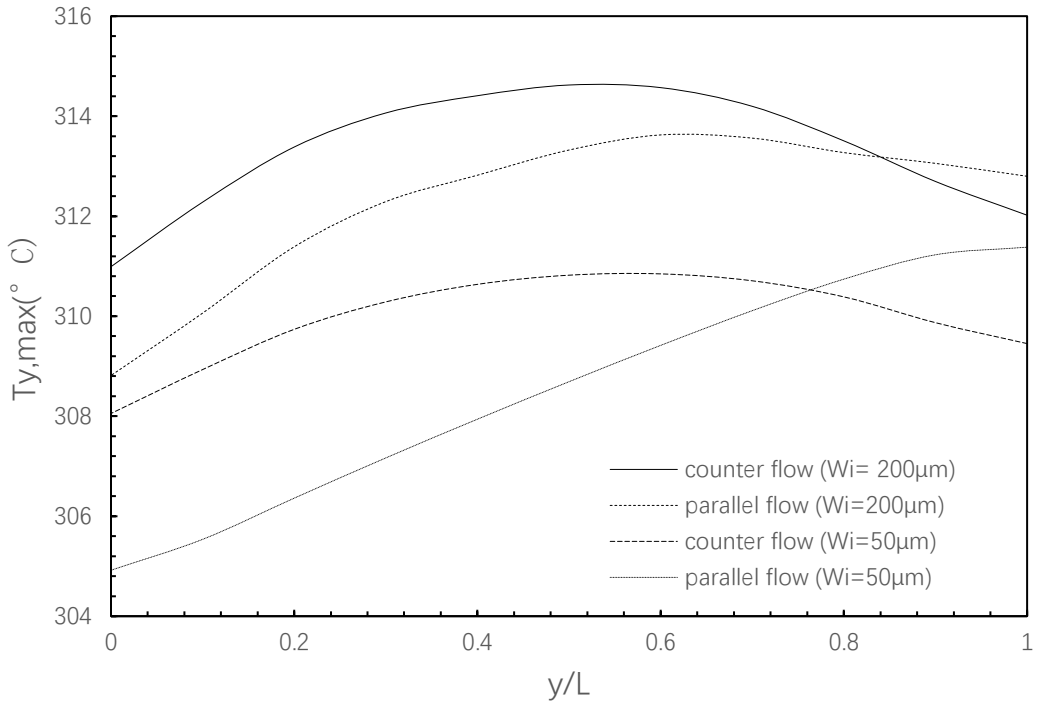


Figure 4-17 Temperature distribution along the bottom surface of the DL-MCHS for parallel flow and counter flow configuration for H_{ch} =325μm and Wo=50μm

4.4.4 DL-MCHS design with high thermal performance

By looking through the thermal performance for all 128 cases based on overall thermal resistance alone, the design with smallest value of W_i, W_o always give better performance. The increase of H_{ch} decreases the maximum temperature, but the effect is not significant compared with other two parameters. This trend happens for both counter flow and parallel flow configuration.

With all the parameters investigated, the DL-MCHS design of $W_o = W_i = 50\mu m$ and $H_{ch} = 400\mu m$ operated in counter flow is identified as the best thermal performance since it has lowest value of thermal resistance.

4.5 The overall pumping power for DL-MCHS with different W_o, W_i and H_c for counter flow configuration

4.5.1 The overall pumping power for DL-MCHS operating in counter flow configuration

The results of overall pumping power for DL-MCHS of different W_o, W_i and H_c for counter flow configuration are presented in Figure 4-18. The results in Figure 4-18 (a), (b), (c) and (d) illustrate the overall pumping power for channel height H_{ch} of 325μm, 350 μm, 375 μm and 400 μm, respectively. The results for overall pumping powers are presented in the same way as the results of overall thermal resistance in Fig. 4.6. However, the trend obtained for pumping power is contrary to that of overall thermal resistance. Which means to achieve better thermal performance, it always needs more power to pump the coolant.

When looking into the effect of W_o, for any given value of $W_i$and H_{ch}, the overall pumping power Ω decreases drastically with the increase in W_o. The increase in W_o from small value to large value transform the geometry from converging channel design to straight channel and then to diverging channel design. This also reflects that converging channel design gives higher pumping power than the diverging channel design. Literally, this means diverging channel design is cost more than the diverging channel.

When looking into the effect of W_i, for any given value of W_o and H_{ch}, the pumping power Ω decreases fast with the increase in W_i. Literally, this means smaller value of channel inlet width is less cost effective.

When looking into the effect of H_{ch}, for any given value of W_o and W_i, the pumping power Ω decreases less with the increase in H_{ch}. This means larger channel height is more cost effective.

4.5.2 The overall pumping power for DL-MCHS operating in parallel flow configuration

The results of overall pumping power for parallel flow configuration are presented in Figure 4-18. The results in Figure 4-18 (a), (b), (c) and (d) illustrate the overall pumping power for channel height H_{ch} of 325μm, 350 μm, 375 μm and 400 μm, respectively. The results in Figure 4-19 for parallel flow configuration shows generally the same trend as in counter flow. The value of pressure drop for each case is almost the same for parallel/counter flow configuration with negotiable difference. This reflect the flow direction does not affect the pressure drop, the pressure drop for both flow configuration is the same.

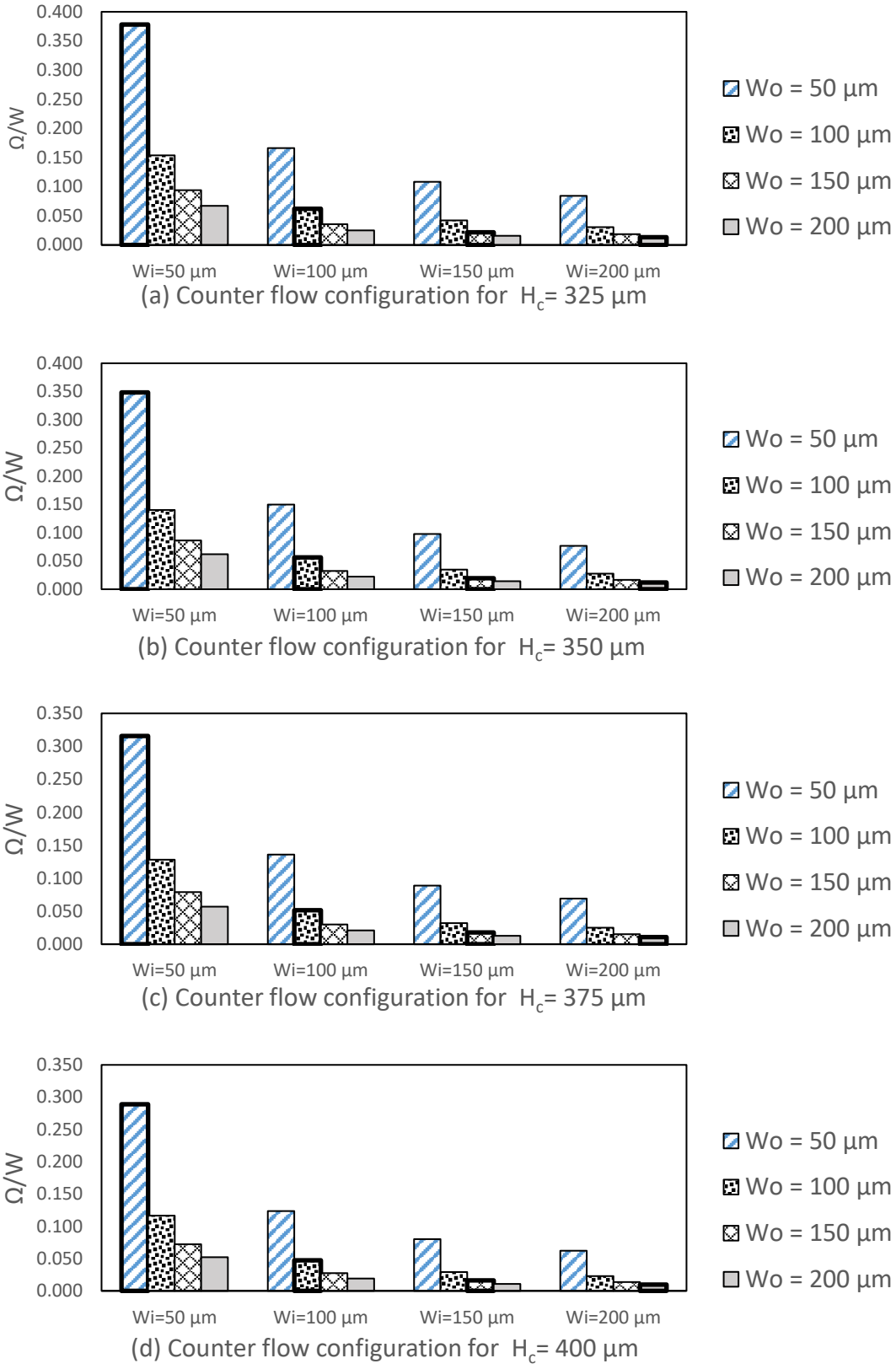
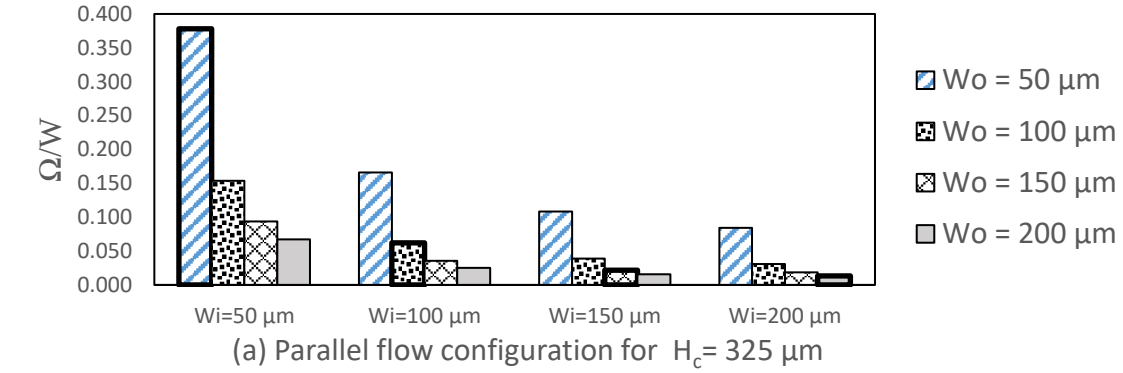
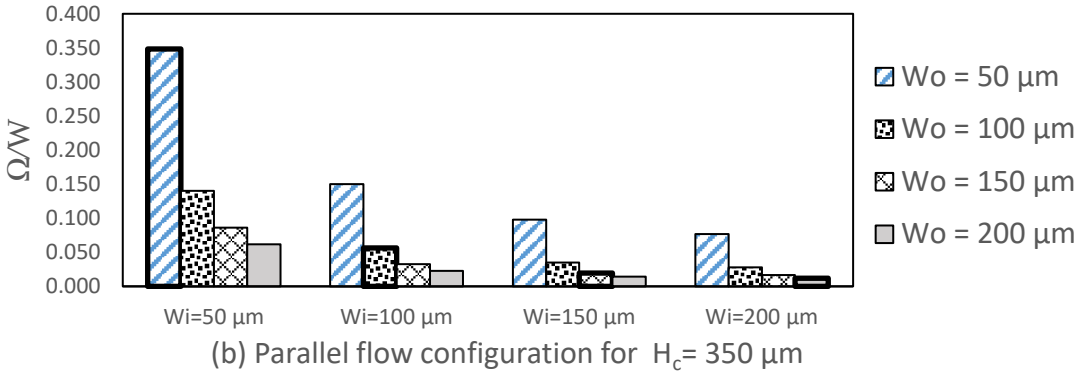


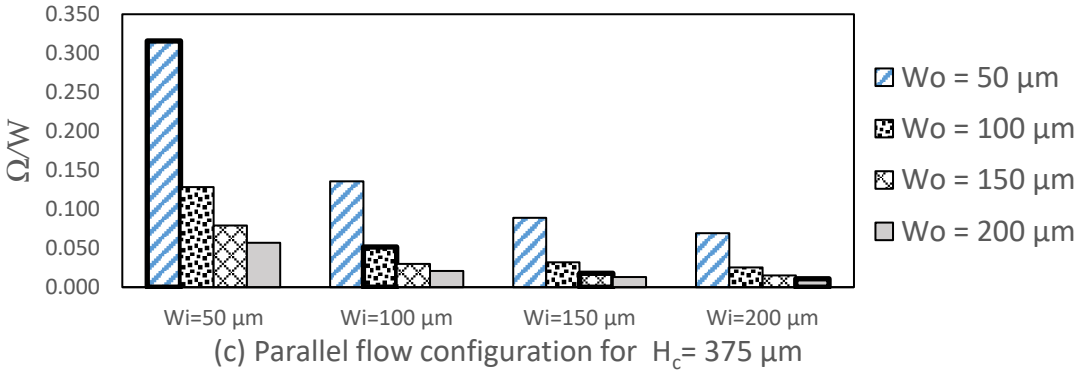
Figure 4-18 The overall pumping power for counter flow configuration in DL-MCHS with different Wo, Wi and H_c (a) H_c = 325 µm, (b) H_c = 350 µm, (c) H_c = 375 µm, and (d) H_c = 400 µm



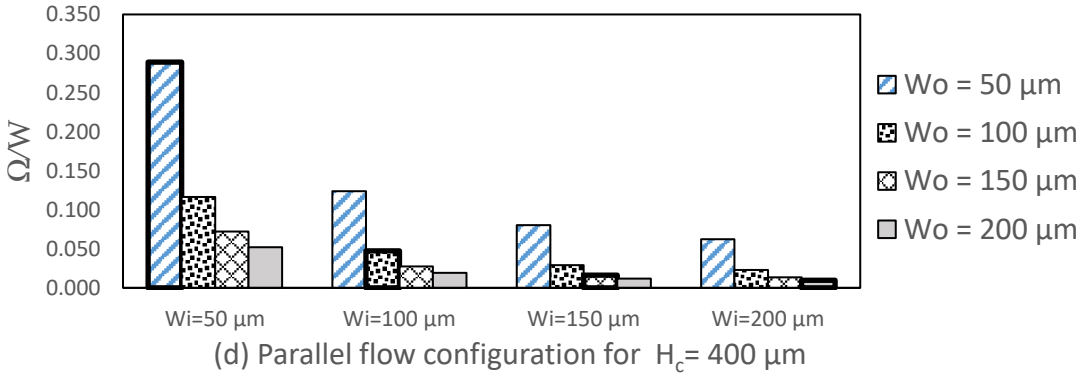
(a) Parallel flow configuration for H_c= 325 µm



(b) Parallel flow configuration for H_c= 350 µm



(c) Parallel flow configuration for H_c= 375 µm



(d) Parallel flow configuration for H_c= 400 µm

Figure 4-19 The overall pumping power for parallel flow configuration in DL-MCHS with different Wo, Wi and H_{ch} (a) H_{ch} = 325 µm, (b) H_{ch} = 350 µm, (c) H_{ch} = 375 µm, and (d) H_{ch} = 400 µm.

4.6 The thermal-hydraulic performance for DL-MCHS with different flow configurations

To evaluate the thermal hydraulic performance, the FOM for DL-MCHS with parallel and counter flow configuration is shown in Figure 4-20 and Figure 4-21, respectively. In Figure 4-20 and Figure 4-21, the design with W_i =50um and W_o =50um in each flow configuration is used as base case. When W_i is fixed, the FOM increases with the increase of Wo and the increment becomes less significant for all cases investigated. When W_o is fixed, the FOM increases and then decreases with the increase of W_i and the peak point occurred at W_i=150μm. For both flow configurations, design with W_i=150μm and W_o=200μm presents the highest value of FOM (1.68 for PF and 1.55 for CF) and design with W_i=50μm and W_o=50μm presents the lowest value (1 for PF and 0.88 for CF). The comparison of FOM between DL-MCHS with parallel and counter flow configuration is shown in Figure 4-22. In Figure 4-22, the design with W_i =50um and W_o =50um for DL-MCHS with parallel flow is used as base case for both flow configurations. It can be observed that the DL-MCHS designs with parallel flow configuration always shows better thermal-hydraulic performance as compared with counter flow configuration for all cases investigated. The difference between two flow configurations becomes smaller with the increase of either Wi or Wo. Maximum difference of 0.12 (12.13%) is found between parallel and counter flow configuration for design with W_i=50μm W_o=50μm.

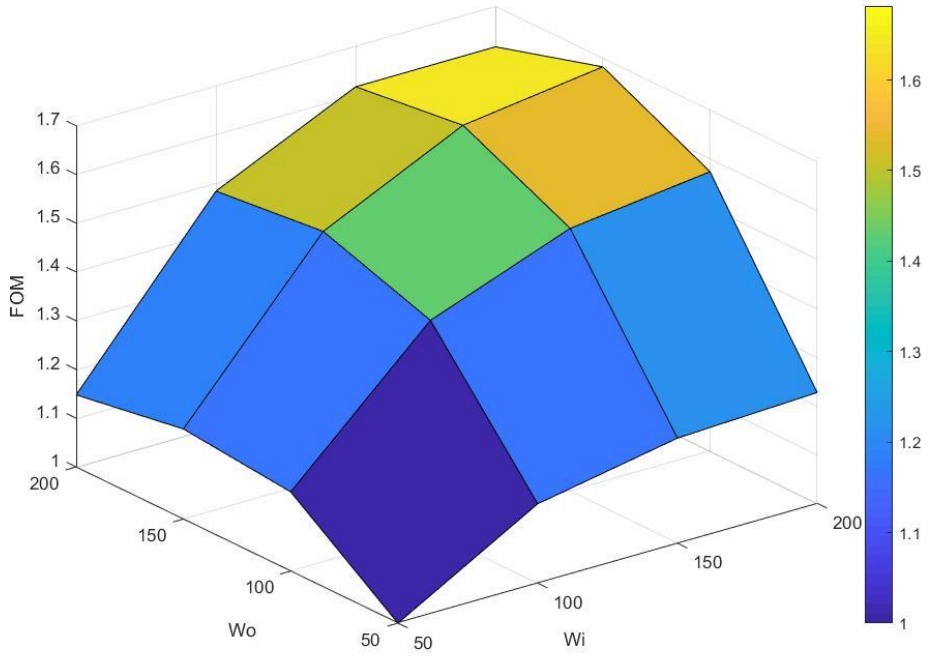


Figure 4-20 The FOM for DL-MCHS with parallel flow configuration.

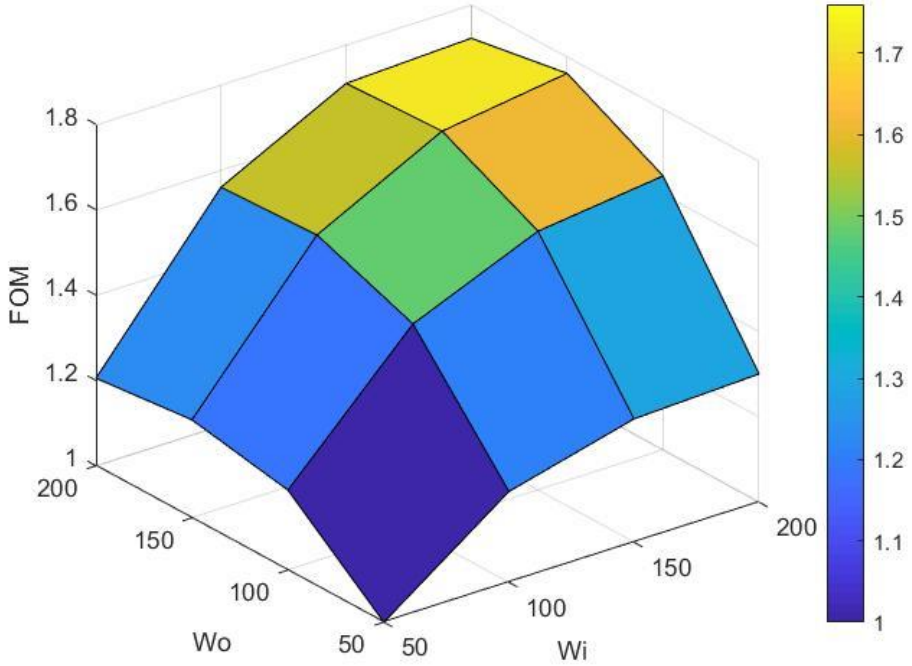


Figure 4-21 The FOM for DL-MCHS with counter flow configuration.

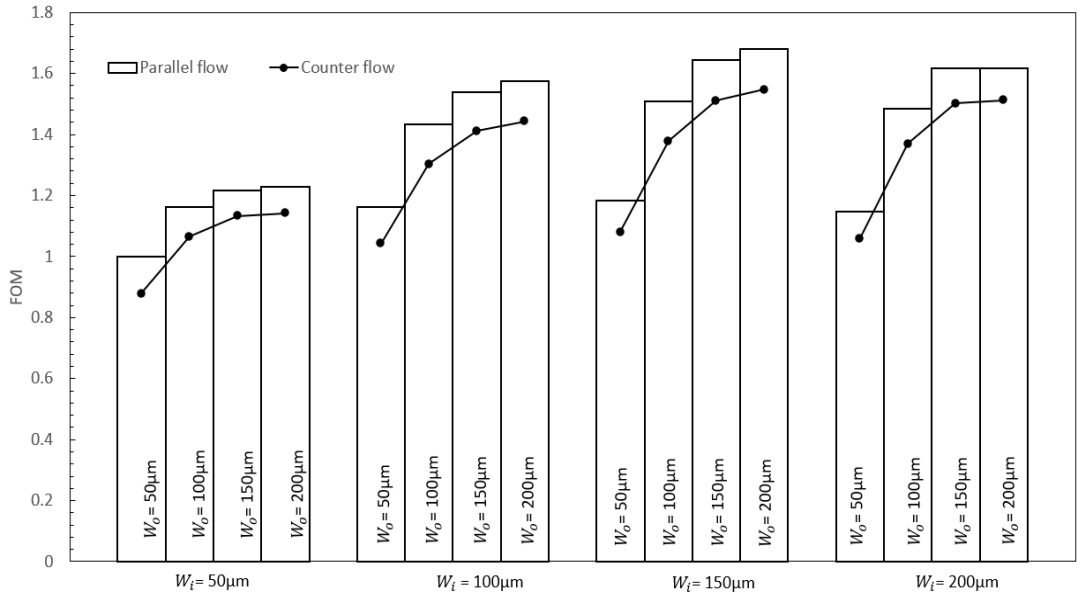


Figure 4-22 The comparison of FOM between Dl-MCHS with parallel and counter flow configuration.

4.6 Conclusions

The thermal performance and hydraulic performance of width-tapered DL-MCHS for parallel/counter flow configuration of three parameters (inlet width W_i, outlet width W_o and channel height H_c) have been investigated by simulation. The optimum design has been chosen based on FOM. The conclusion can be drawn as below:

- The DL-MCHS with converging channel design presents higher Nu as compared with straight channel design with same W_o, the increment of Nu for design 2,3 and 4 compares to design 1 is 22.48%, 38.34% and 49.38% for parallel flow and 33.69%, 57.03% and 71.74% for counter flow when Re=100, respectively.
- The DL-MCHS with diverging channel design presents higher Nu as compared with straight channel design with same W_i. For diverging designs in both flow configurations, the increment of Nu for design 5,6 and 7 compares to design 8 is 10.62%, 11.11% and 8.02% for parallel flow and 10.62%, 11.11, 7.72% for counter flow when Re=1000, respectively.

- Based on the performance of overall thermal resistance alone, the optimal geometrical design of DL-MCHS has lowest value of W_o and W_i and highest value of H_c i.e., $W_i = W_o = 400\mu m$, $H_{ch} = 400\mu m$.
- The designs with counter flow configuration always have better thermal performance than the designs with parallel flow configuration when Q is large and the difference become more significant with the decrease of W_i, the maximum difference of 0.05K/W (21.67%) can be found at design with $W_i = 50\mu m$ $W_o = 200\mu m$ at $H_{ch} = 375\mu m$.
- The design with counter flow configuration has better temperature uniformity compare to the design with parallel flow configuration based on the temperature along the base surface.
- The most critical parameters that contribute to the thermal performance is W_o, followed by W_i, the effect of H_{ch} is small.
- The DL-MCHS with parallel flow always shows better thermal-hydraulic performance as compared with counter flow with exact channel dimensions, maximum difference of 0.12 (12.13%) is found between parallel and counter flow configuration for design with W_i=50μm W_o=50μm.
- For the optimization of thermal-hydraulic performance (considering both thermal resistance and pumping power), the design with W_i=150μm and W_o=200μm presents the highest value of FOM (1.68 for PF and 1.55 for CF) and design with W_i=50μm and W_o=50μm presents the lowest value (1 for PF and 0.88 for CF).

Chapter 5 Numerical Investigation of Tapered DL-MCHS with Alternating Flow Configuration

5.1 Introduction

In previous chapter, the performance for DL-MCHS with counter flow is compared with DL-MCHS with parallel flow. The flow direction difference in top and bottom channel greatly affected the thermal and hydraulic performance. In this chapter, the novel flow configuration, which the flow direction different in left and right channels for every two microchannels is proposed and numerically investigated. The thermal and hydraulic performance at various Re is firstly investigated. Then the parametric study is conducted to explore the effect of W_i and W_o on MCHS performances. At last, the thermal hydraulic performance based on FOM is presented.

5.2 Thermal performance for Dl-MCHS with alternating flow at various Re

The temperature distribution for DL-MCHS with alternating flow and with different designs at Re=200 is presented in

Figure 5-1. It can be observed that temperature gradually increase and then decreases. This is mainly due to the flow direction different in channels leads to the heat accumulated in middle. Moreover, the maximum temperature increases with either W_i or W_o increases. The maximum temperature increases 2.8K and 4.9K when W_o changes from 50μm to 200μm for design with W_i =50μm and design with W_i =200μm, respectively. This is due to the increase in W_i or W_o leads to the decrease of flow velocity inside channel and hence weakens the thermal performance.

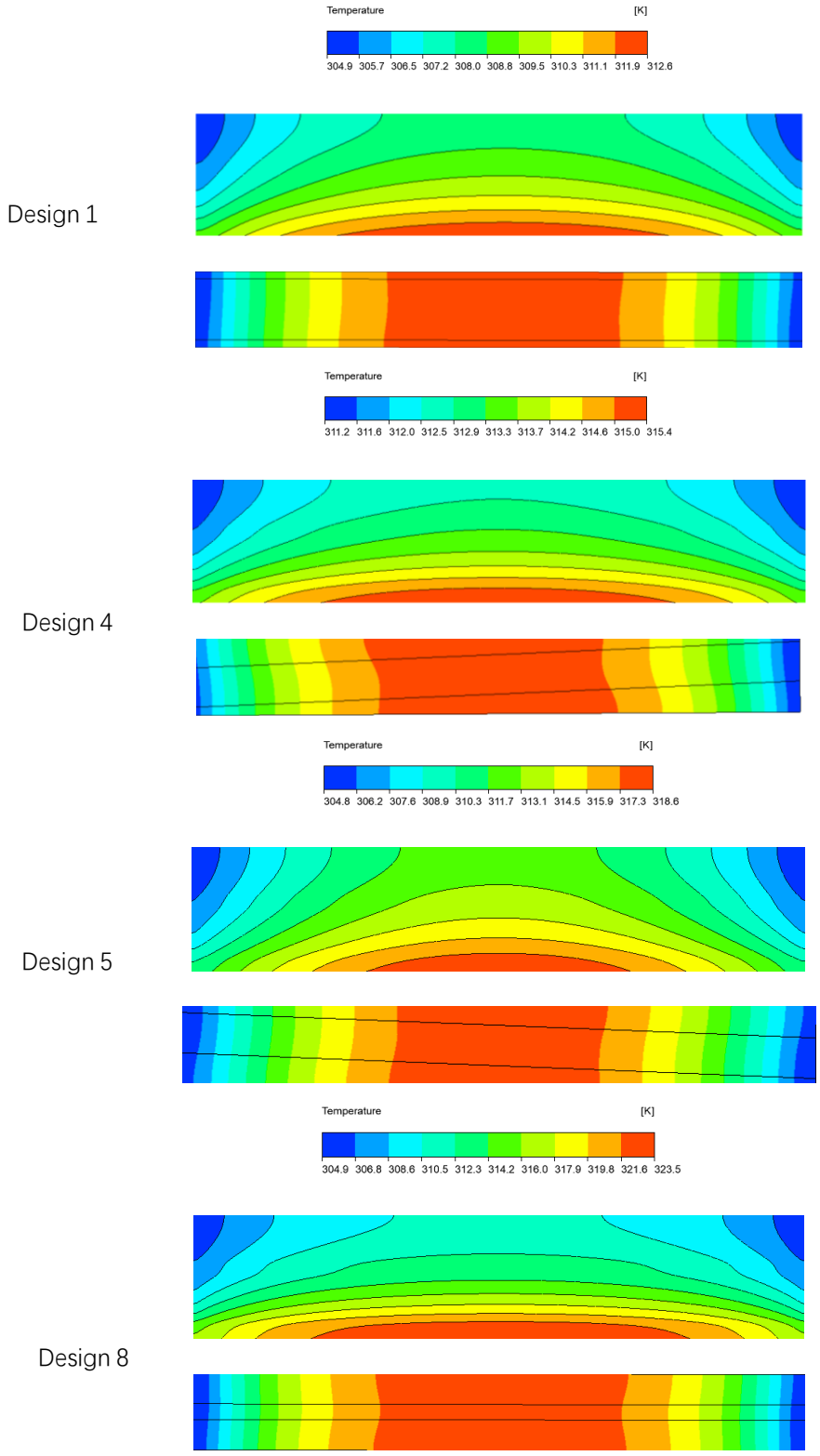


Figure 5-1 Temperature distribution for four designs at Re=200.

Figure 5-2 presents the R_t for DL-MCHS with alternating flow and with different Re ranging from 100 to 1000. It can be observed that for all designs investigated, R_t decreases with the increase of Re and the decrement becomes less significant, which indicates that the thermal performance enhanced with the increase of flow velocity and the enhancement reduced with the further increase of flow velocity. For both converging and diverging designs, R_t increases with the increase of W_o for all Re.

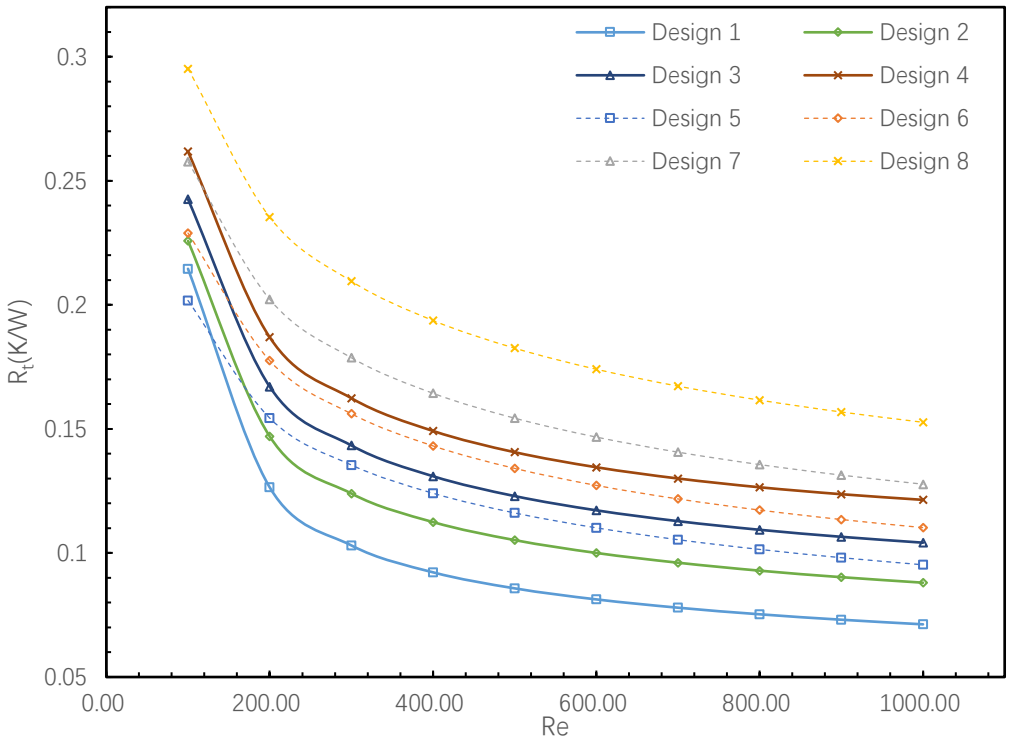


Figure 5-2 R_t for DL-MCHS with alternating flow and with different Re ranging from 100-1000.

The Nu for DL-MCHS with alternating flow and with different Re ranging from 100-1000 is illustrated in Figure 5-3. For all designs, Nu increases with the increase of Re. Moreover, the converging channel designs show higher Nu as compared to straight channel design with same W_i and diverging channel designs show higher Nu as compared to straight channel design with same W_o. For diverging designs, the Nu increases up to 37.45%, 63.71% and 81.56% for design 5,6 and 7 as compared to straight channel design with same W_i of 50μm for Re=100, respectively. And for converging design, the Nu increase up to 13.94%, 12.6% and 8.78% for design 2,3,4 as compared to the straight channel design with same W_o of 50μm for Re=1000.

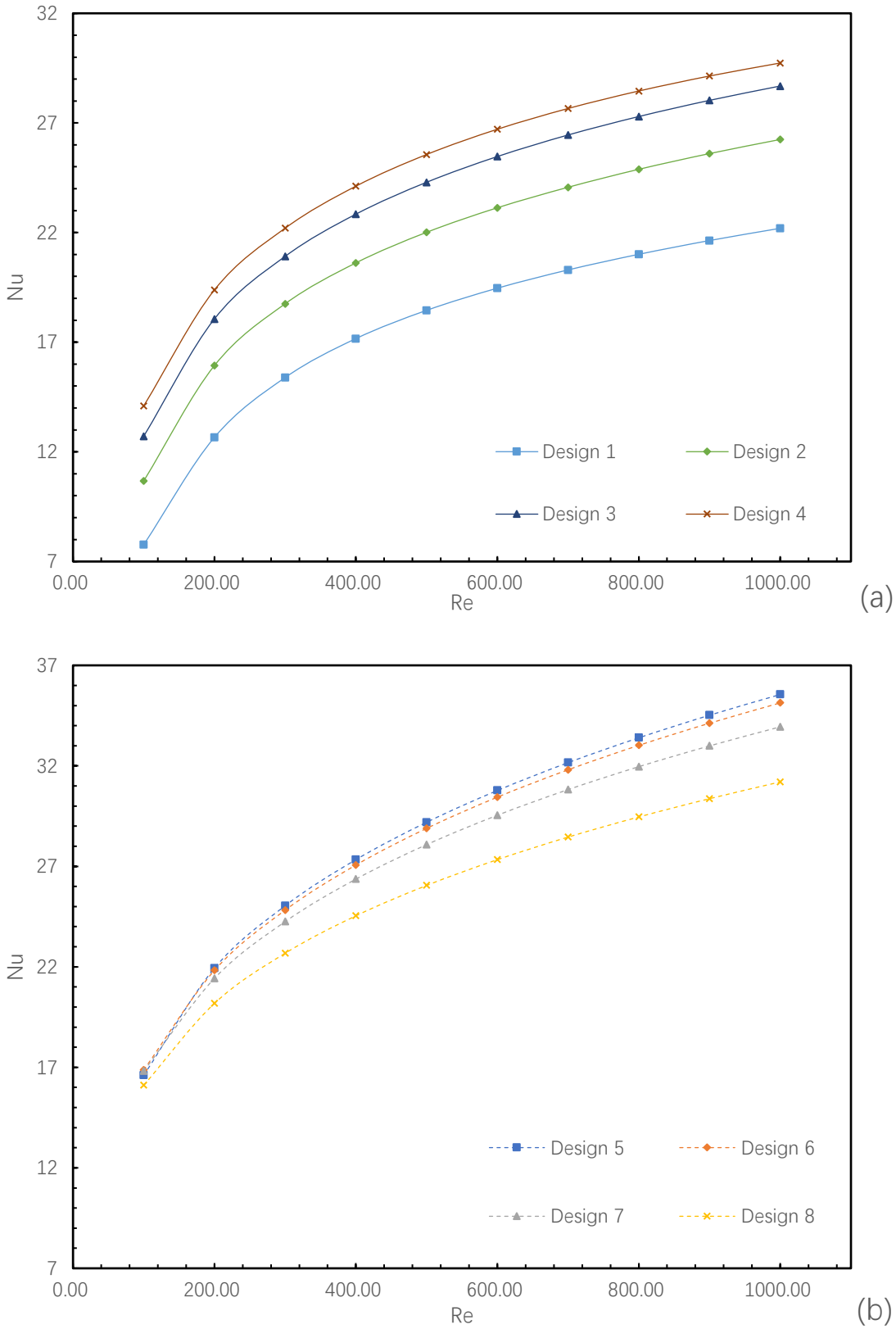


Figure 5-3 Nu for DL-MCHS with alternating flow and with different Re r for (a) Design 1-4 (b) Design 5-8

5.3 The thermal and hydraulic performance for DL-MCHS with alternating flow at fixed volumetric flow rate

To investigate the effect of W_i and W_o on thermal and hydraulic performance for DL-MCHS with alternating flow, thermal performance in terms of thermal resistance, R_t and hydraulic performance in terms of pressure drop,ΔP plotted in $\log_{10}$ scale for DL-MCHS with different value of W_i and W_o under alternating flow is shown in Figure 5-4 and Figure 5-5, respectively. As can be seen from the Figure 5-4 that, the design with small W_i or W_o gives lower R_t and R_t increases with either W_i or W_o increases, where the lowest value of R_t appears at design with $W_i = 50\mu m$ $W_o = 50\mu m$ and highest value of R_t appears at design with $W_i = 200\mu m$ $W_o = 200\mu m$. As for hydraulic performance as shown in Figure 5-5, opposite trend can be found from R_t that, the design with small W_i or W_o gives higherΔP and ΔP decreases with the increase of either W_i or W_o increase. When the W_i or W_o is small, the decrement of ΔP is dramatic and the decrement becomes less significant with increase of either W_i or W_o. The lowest value of ΔP appears at design with $W_i = 200\mu m$ $W_o = 200\mu m$ and highest value of ΔP appears at design with $W_i = 50\mu m$ $W_o = 50\mu m$. This is as expected, since small channel width gives better thermal performance but in sacrifice of hydraulic performance [77].

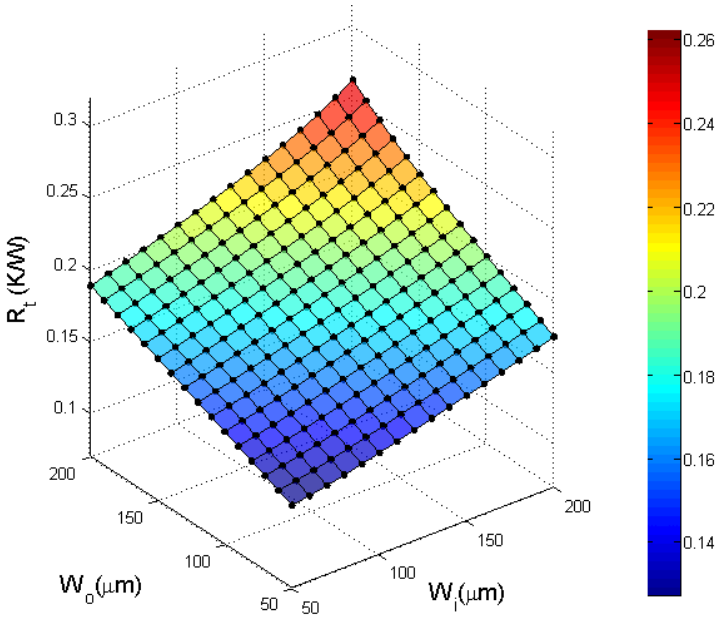


Figure 5-4 The thermal resistance for DL-MCHS with alternating flow configuration.

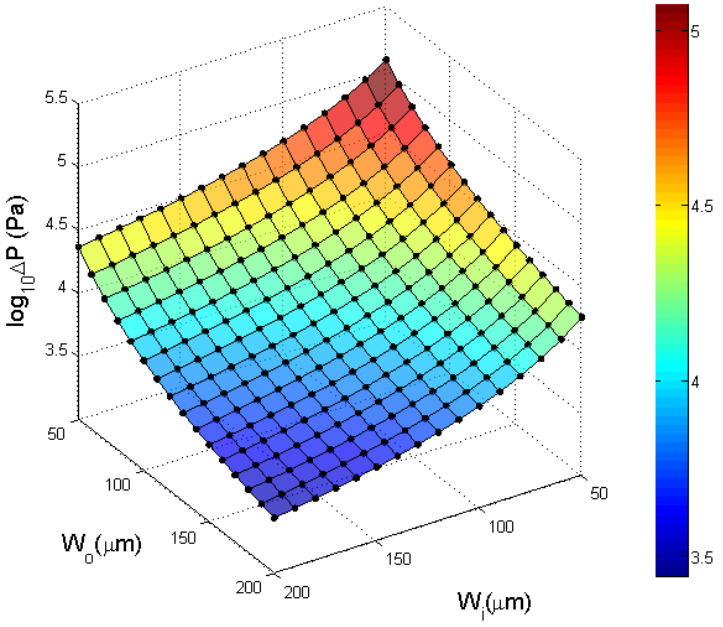


Figure 5-5 The pressure drop for DL-MCHS with alternating flow configuration

To see the effect of different flow configurations on thermal performance, the results of R_t for DL-MCHS with alternating flow configuration is compared to our previous study's results [65]. Totally 32 designs with 4 different values of W_i of and 4 different values of W_o for DL-MCHS with parallel and counter flow configuration is used for comparison as shown in Figure 5-6 and Figure 5-7, respectively. As can be seen from Figure 5-6 that, the DL-MCHS with alternating flow configuration shows lower value of R_t when W_i at high values or W_o at small values as compared to the DL-MCHS with parallel flow configuration. For all designs investigated, the alternating flow configuration with design of $W_i = 50\mu m$ $W_o = 200\mu m$ shows 0.065K/W lower values of R_t as compared to the DL-MCHS with parallel flow configuration. As for DL-MCHS with counter flow configuration shown in Figure 5-7, the DL-MCHS with alternating flow configuration shows largely similar results as compared to the DL-MCHS with counter flow configuration.

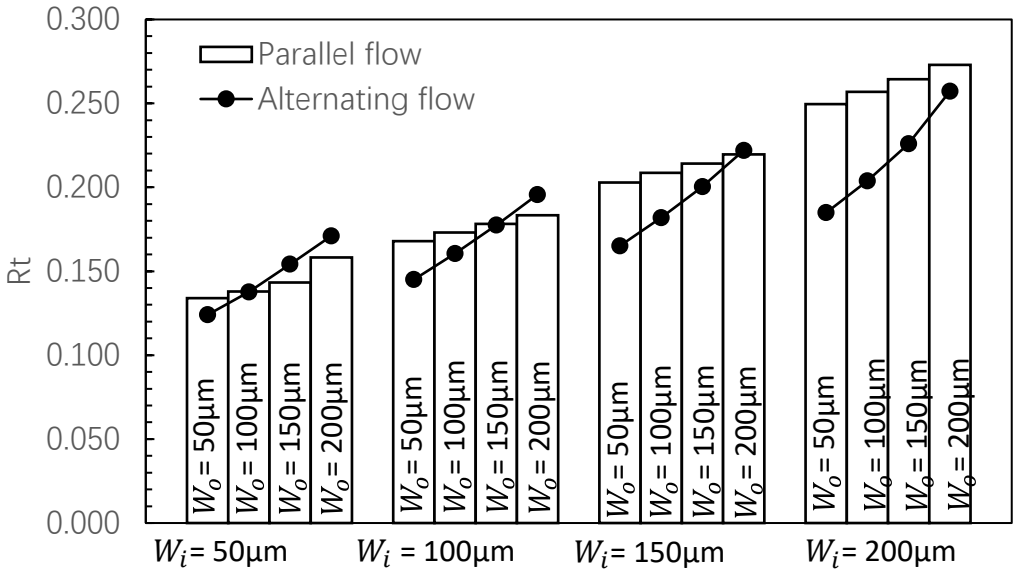


Figure 5-6 The comparison of R_t between DL-MCHS with alternating and parallel flow configuration.

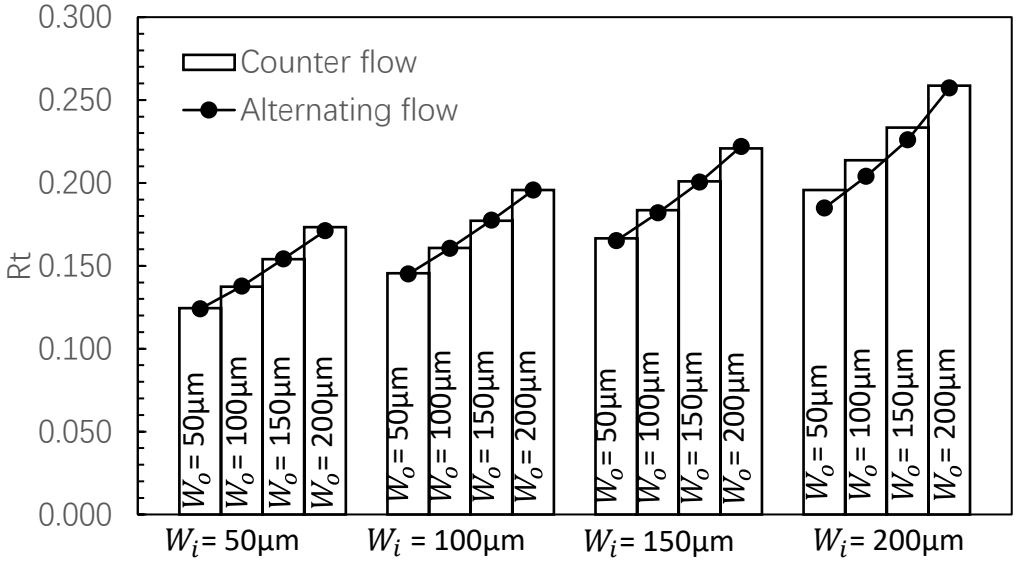


Figure 5-7 The comparison of R_t between DL-MCHS with alternating and counter flow configuration.

Besides of thermal resistance, ΔT_b is another parameter to evaluate the thermal performance in terms of temperature uniformity. Figure 5-8 shows the ΔT_b for DL-MCHS with alternating flow configuration and with different value of W_i and W_o. First looking into the effect of W_o, for any given value of W_i, ΔT_b

increases with the increase of W_o, which $W_o = 50\mu m$ has the lowest value of ΔT_b and $W_o = 200\mu m$ has the highest value of ΔT_b for all values of W_i investigated. This indicates that the smaller W_o gives better temperature uniformity. Then looking into the effect of W_i, for any given value of W_o, ΔT_b decreases with the increase of W_i until it reaches the lowest value of ΔT_b and then increases. The lowest value of ΔT_b for different W_o varies from $W_i = 80\mu m$ to $W_i = 100\mu m$. This indicate that the design with small channel inlet size has better temperature uniformity. For all cases investigated, the DL-MCHS design with $W_i = 80\mu m$ $W_o = 50\mu m$ under alternating flow has the lowest ΔT_b of 3.297°C.

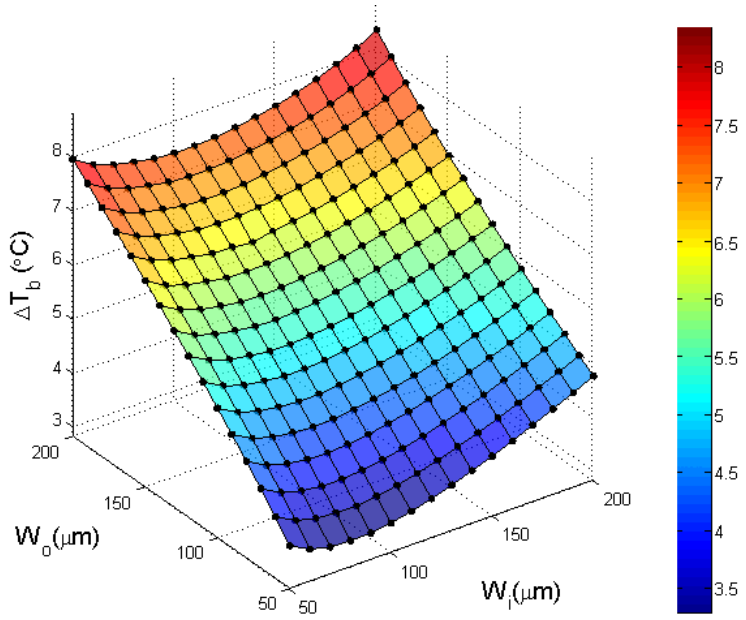


Figure 5-8 The ΔT_b for DL-MCHS with alternating flow configuration

To explain the above results, the temperature distribution on the bottom surface of the heat sink along the flow direction, $T_{y,max}$ for DL-MCHS with alternating flow and different W_i and W_o is shown in Fig 5.9. As can be seen from Fig 5.9 that, for all designs investigated, the $T_{y,max}$ increases with the increase of y/L until $T_{y,max}$ reaches the symmetry position at y/L=0.5 and then decreases. This is as expected, since each DL-MCHS with alternating flow design has exact channel profile but different flow direction in each section's left and right part of the computational domain as mentioned in Fig. 5.1. For DL-MCHS with alternating flow configuration and straight channel design($W_i = W_o$) as shown in Fig 5.9(a), the

ΔT_b increases with the increase of W_{ch}. The reason is that the increase of temperature at y/L=0.5($T_{b,max}$) is larger than the increase of temperature at y/L=0($T_{b,min}$) with the increase of W_{ch}, which indicated that $T_{b,max}$ is more sensitive to the changes of W_{ch} as compared to $T_{b,min}$. Comparing the DL-MCHS designs with alternating flow configuration and same W_i of $50\mu m$ for different W_o of $50\mu m, 100\mu m, 150\mu m, 200\mu m$ as shown in Fig 5.7(b), ΔT_b increases with the increase of W_o. This happens because coolant's velocity decreases with the increase of W_o along the flow direction, which weakens the heat removal ability, greatly increases the $T_{b,max}$ and increases the ΔT_b. While comparing the DL-MCHS with alternating flow configuration and with same W_o for different W_i of $50\mu m, 100\mu m, 150\mu m, 200\mu m$ as shown in Fig 7(c), ΔT_b first decreases and then increases with the increase of W_i. The reason is that, with the increase of W_i, the channel width changes at y/L=0.5 is only half as compared to y/L=0, which gives lower temperature increase at y/L=0.5. However, $T_{b,max}$ is more sensitive to the channel width change as compared to $T_{b,min}$. As a combination of these two effects, ΔT_b shows a decrease with the increase of W_i when W_i is small and shows an increase with the increase of W_i after W_i reaches a certain value.

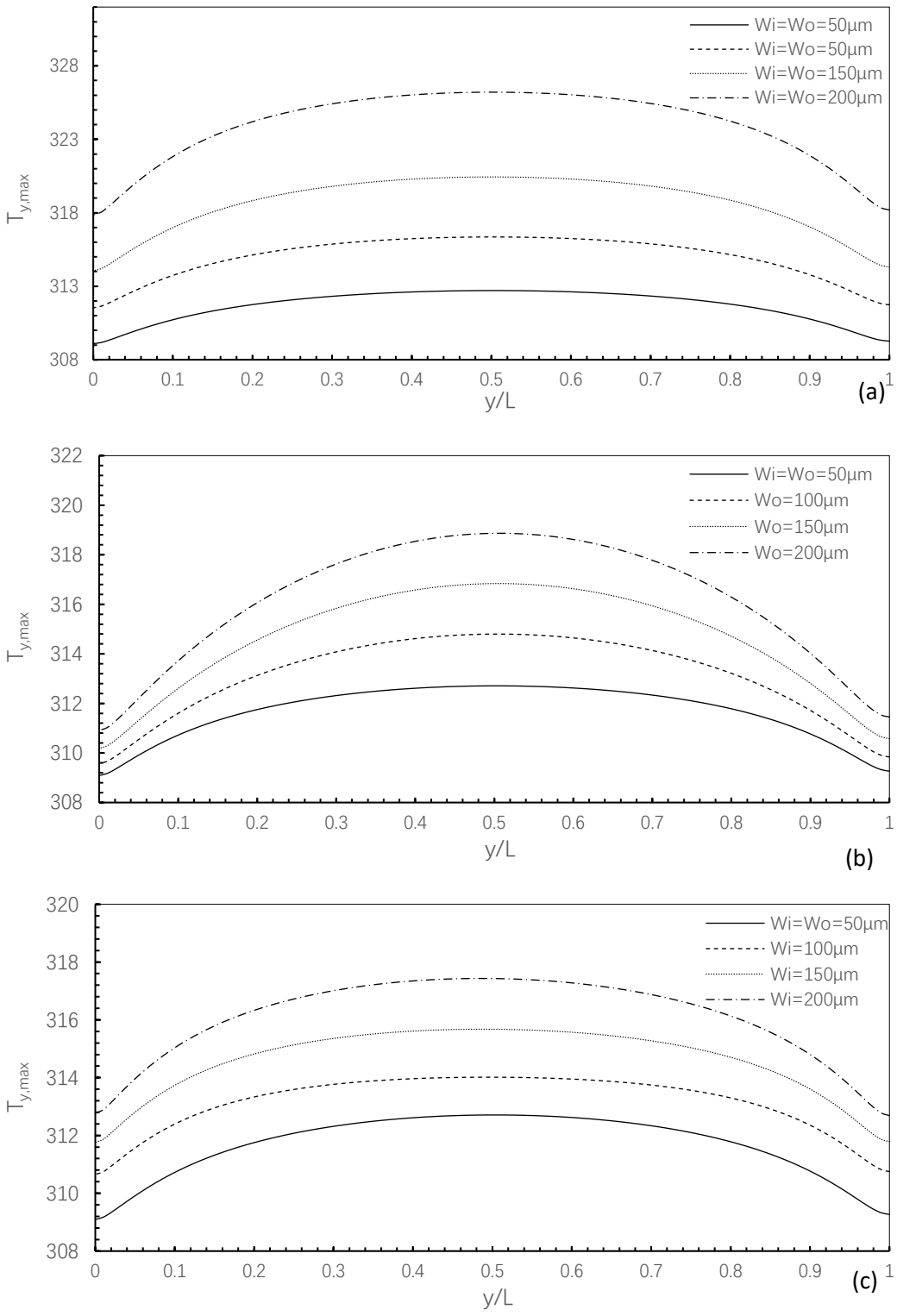


Figure 5-9 Temperature distribution for DL-MCHS with alternating flow configuration with (a) Straight channel design (b) tapered channel design with fixed W_i of 50μm (c) tapered channel design with fixed W_o of 50μm

5.4 Thermo-hydraulic performance for DL-MCHS with alternating flow configuration

To take into account of both thermal and hydraulic performance at the same time, Fig 5.8 shows the FOM for DL-MCHS with alternating flow configuration and different channel profile. For all designs investigated, the DL-MCHS with alternating flow and straight channel design of $W_i = 50\mu m$ $W_o = 50\mu m$ is used for comparison. First looking into the effect of W_i, for any given value of W_o, increasing the W_i will increase the FOM until an optimum point is reached. After this point, increasing W_i results in a decrease of FOM. Then looking into the effect of W_o, at low value of $W_i (W_i < 140\mu m)$, The FOM increases with the increase of W_o. For higher value of W_i $(W_i \geq 140\mu m)$, the FOM of the design with $W_o = 180\mu m, 190\mu m,$ and $200\mu m$ decrease rapidly with the increase of W_i. This indicated that the DL-MCHS with alternating flow configuration with designs of larger W_o have better thermos-hydraulic performance when W_i is small. This happens is because when W_i and W_o is small, increase W_i or W_o only slightly increases the R_t, but dramatically decreases the ΔP as shown in Fig 5.2 and 5.3. While keep increasing W_i or W_o, the decrements of ΔP becomes less significant as shown in Fig. 5.2. When W_i / W_o increased till a certain value, the increment of hydraulic performance can't cover the decrement of the thermal performance, which results in a decrease in the thermo-hydraulic performance. For all cases investigated, the value of FOM is larger than 1 and the design of $W_i = 160\mu m$ $W_o = 190\mu m$ gives the highest value of FOM of 1.7605 when compared to the design of $W_i = 50\mu m$ $W_o = 50\mu m$, which means that the design with $W_i = 160\mu m$ $W_o = 190\mu m$ has the best thermo-hydraulic performance among all cases investigated.

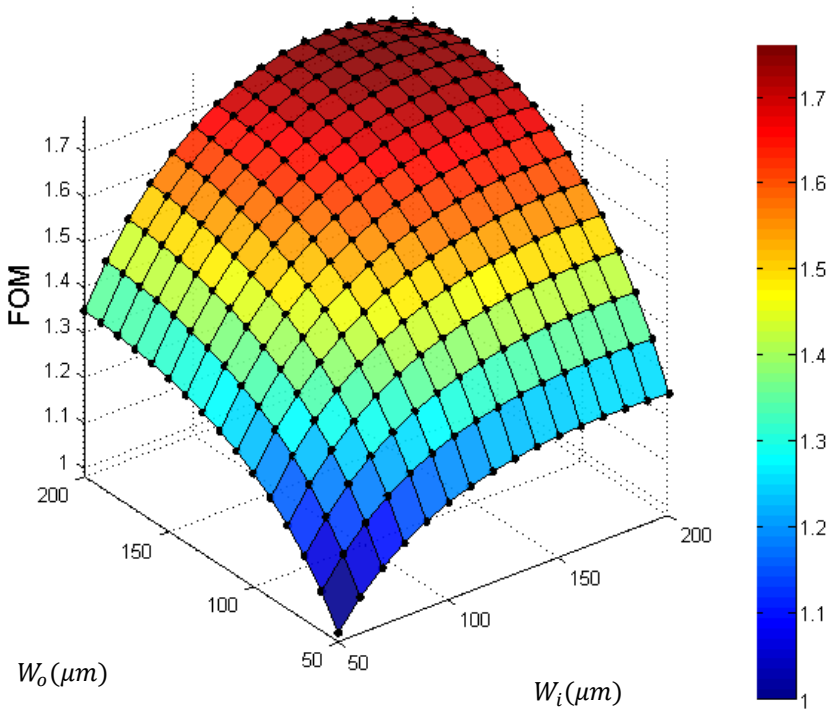


Figure 5-10 FOM for DL-MCHS with alternating flow configuration

5.5 The thermal performance for Dl-MCHS with different substrate material

Figure 5-11 (a)-(d) presents the R_t for DL-MCHS with alternating flow and with different W_i for W_o of 50μm, 100μm,150μm and 200μm, respectively. Three substrate materials of silicon, copper and aluminium are considered and their physical properties used in simulation are listed in Table 5-1. It can be found that for all cases investigated, silicon-based MCHSs show highest value of R_t, followed by aluminium-based MCHSs and then the copper based MCHSs. This indicates that the substrate material with higher value of thermal conductivity always performs better performance. From literature review, the experimental study on DL-MCHS is rare. Wei et al.[29] successfully conducted experimental study on silicon-based stacked DL-MCHS and shows a good example to be referenced to. Hence, the silicon-based MCHS is chosen to be used in present study due to the manufacturability.

Table 5-1 The material properties of Aluminum, copper and silicon[29]..

	Density, ρ (kg/m^3)	Specific heat, c_p ($J/(kg \cdot ^oC)$)	thermal conductivity, K ($W/(m \cdot K)$)
Aluminium	2719	871	202.4
Copper	8978	381	387.6
Silicon	2330	710	148

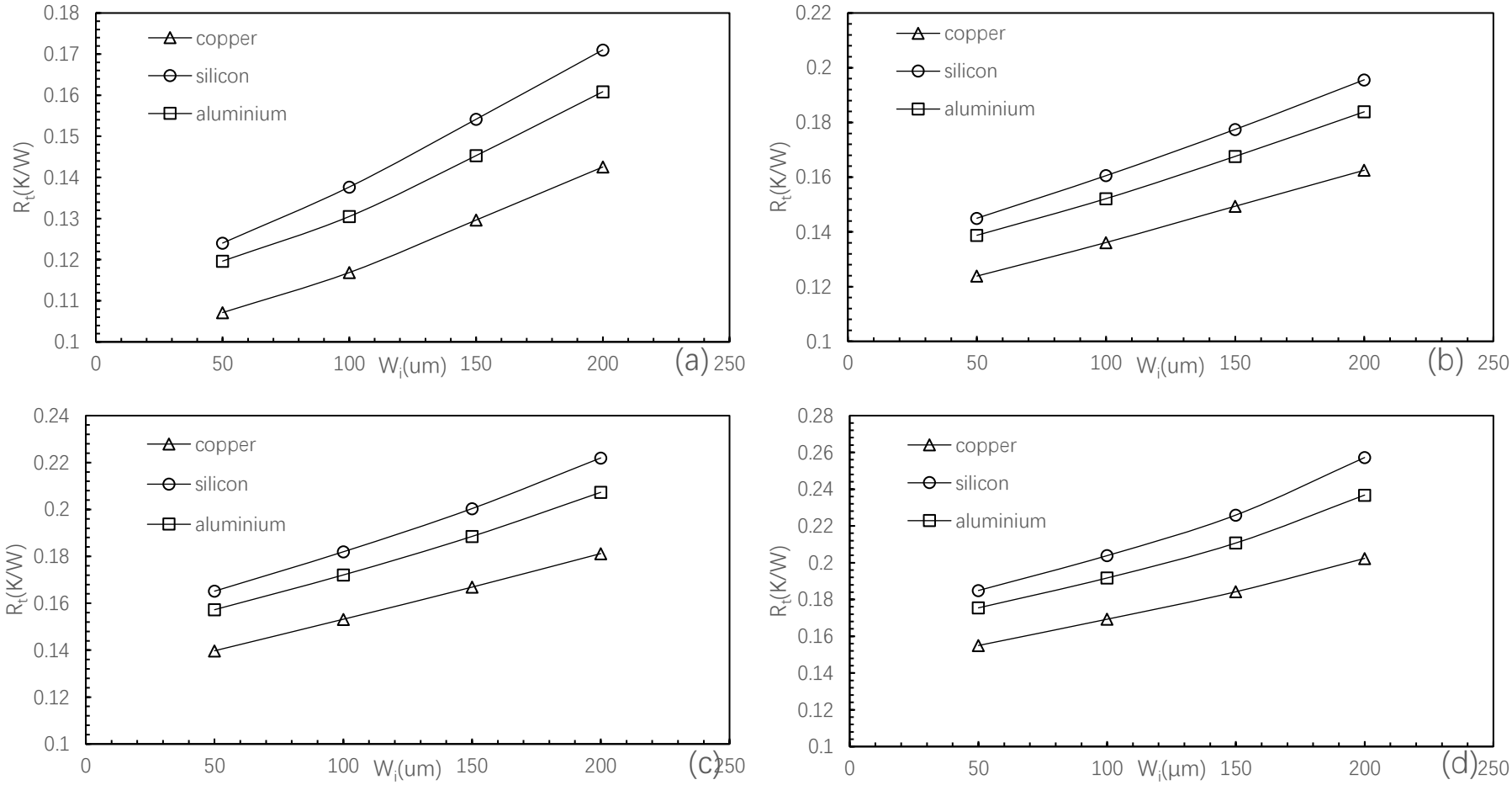


Figure 5-11 The R_t for DL-MCHS with alternating flow and different substrate materials for W_o of (a)50μm, (b)100μm, (c)150μm and (d)200μm.

5.6 Conclusion

The thermal and hydraulic performance have been investigated for DL-MCHS with alternating flow and different inlet width W_i, outlet width W_o through simulation. The thermal resistance, pressure drop, temperature uniformity and FOM have been analyzed. The conclusions can be drawn as follows

- The R_t decreases and $\triangle P$ increases with the increase of Re.
- For diverging designs, the Nu increases up to 37.45%, 63.71% and 81.56% for design 5,6 and 7 as compared to straight channel design with same W_i of 50μm for Re=100, respectively.
- For converging design, the Nu increase up to 13.94%, 12.6% and 8.78% for design 2,3,4 as compared to the straight channel design with same W_o of 50μm for Re=1000.
- The design with small inlet channel width or outlet channel width gives lower thermal resistance but results in high pressure drop.
- The DL-MCHS with alternating flow configuration shows better thermal performance (lower thermal resistance) for the case of higher channel inlet size or smaller channel outlet size as compared to the DL-MCHS with parallel flow configuration.
- The DL-MCHS with alternating flow configuration shows largely similar results of thermal resistance as compared to the DL-MCHS with counter flow configuration
- The DL-MCHS with alternating flow design with small inlet channel width or small outlet channel width gives better temperature uniformity. The optimum DL-MCHS with alternating flow with channel design has the lowest temperature difference of 3.297°C.
- The optimum DL-MCHS with alternating flow and tapered channel show about 76% better in thermo-hydraulic performance as compared with benchmark of DL-MCHS with straight channel design with inlet and outlet channel size of 50μm.

Chapter 6. Numerical investigation on Three-Layered Microchannel Heat Sink with Tapered Channel Profile

6.1 Introduction

In this chapter, the thermal and hydraulic performance for three-layered MCHS with parallel and counter flow1(CF1), counter flow 2(CF2) and counter flow 3 (CF3) are firstly numerically studied for eight different designs at various Re. The thermal performance in terms of temperature distribution, thermal resistance and hydraulic performance in terms of pressure drop are presented. Then the parametric study is conducted to explore the effect of channel inlet width and channel outlet width a on thermal and hydraulic performance for three-layered MCHS with different flow configurations at fixed volumetric flow rate of 200ml/min. At last, the thermal hydraulic thermal performance in terms of Figure of Merit is presented.

6.2 The thermal performance for three-layered MCHS with different flow configurations at various Re.

Figure 6-1to Figure 6-4 presents the temperature distribution for three-layered MCHS with different flow configurations at Re=200 for design 1,4,5 and 8, respectively. For all designs, the temperature gradually increases along the flow direction for PF, while for CF, CF2 and CF3, there is an obvious pull back of heat due to the flow direction difference. With the increase of W_i/W_o, the maximum temperature increases for all flow configurations. For all designs investigated, among three counter flow configurations, the CF1 always show best thermal performance, followed by CF2 and CF3. This is because CF1 has shorter distance between the channel with opposite flow direction and the heat source. For Design 1,4 and 8, three-layered MCHS with CF1 presents lowest maximum temperature, while for design 5, PF exhibits the best thermal performance.

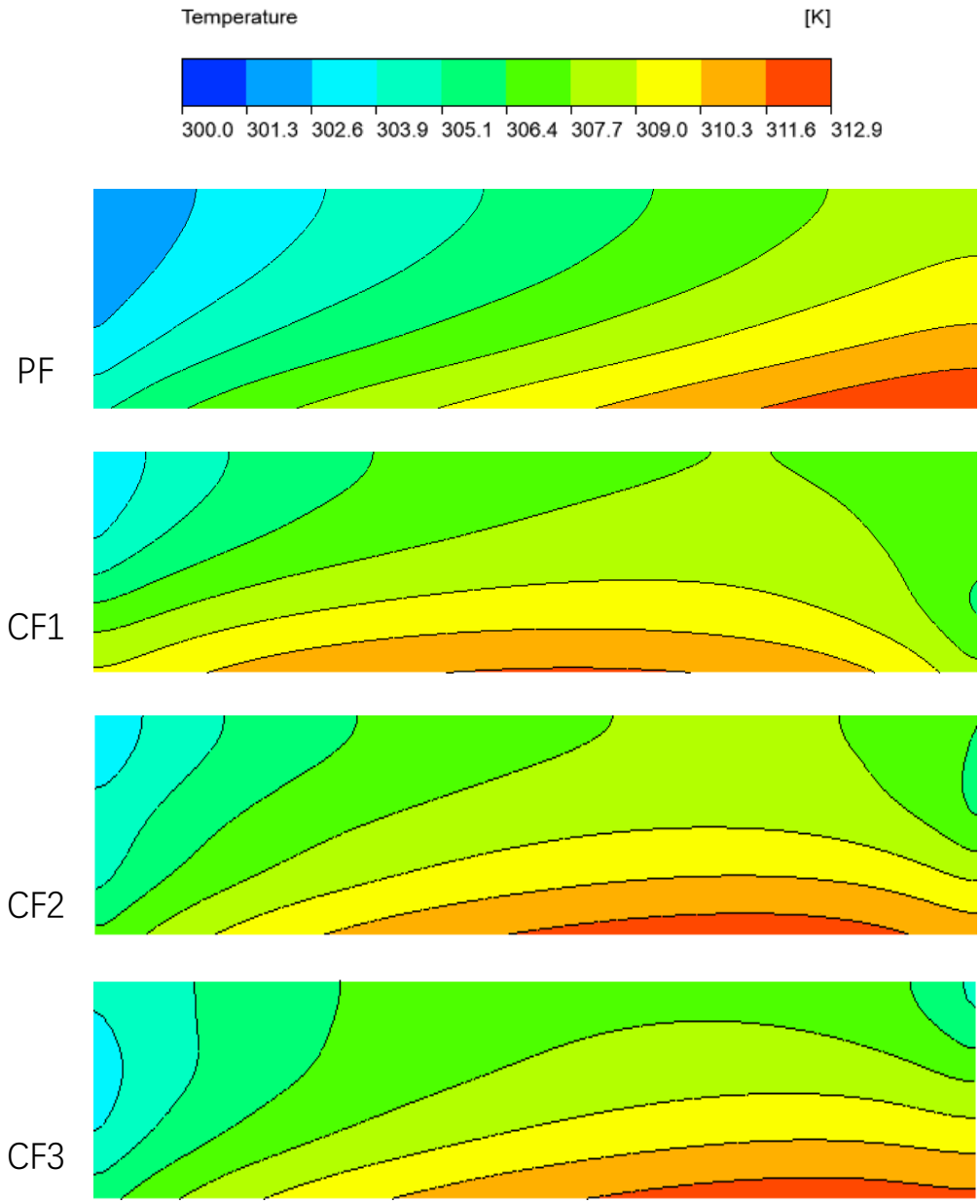


Figure 6-1 Temperature distribution for three-layered MCHS with different flow configurations for Design 1

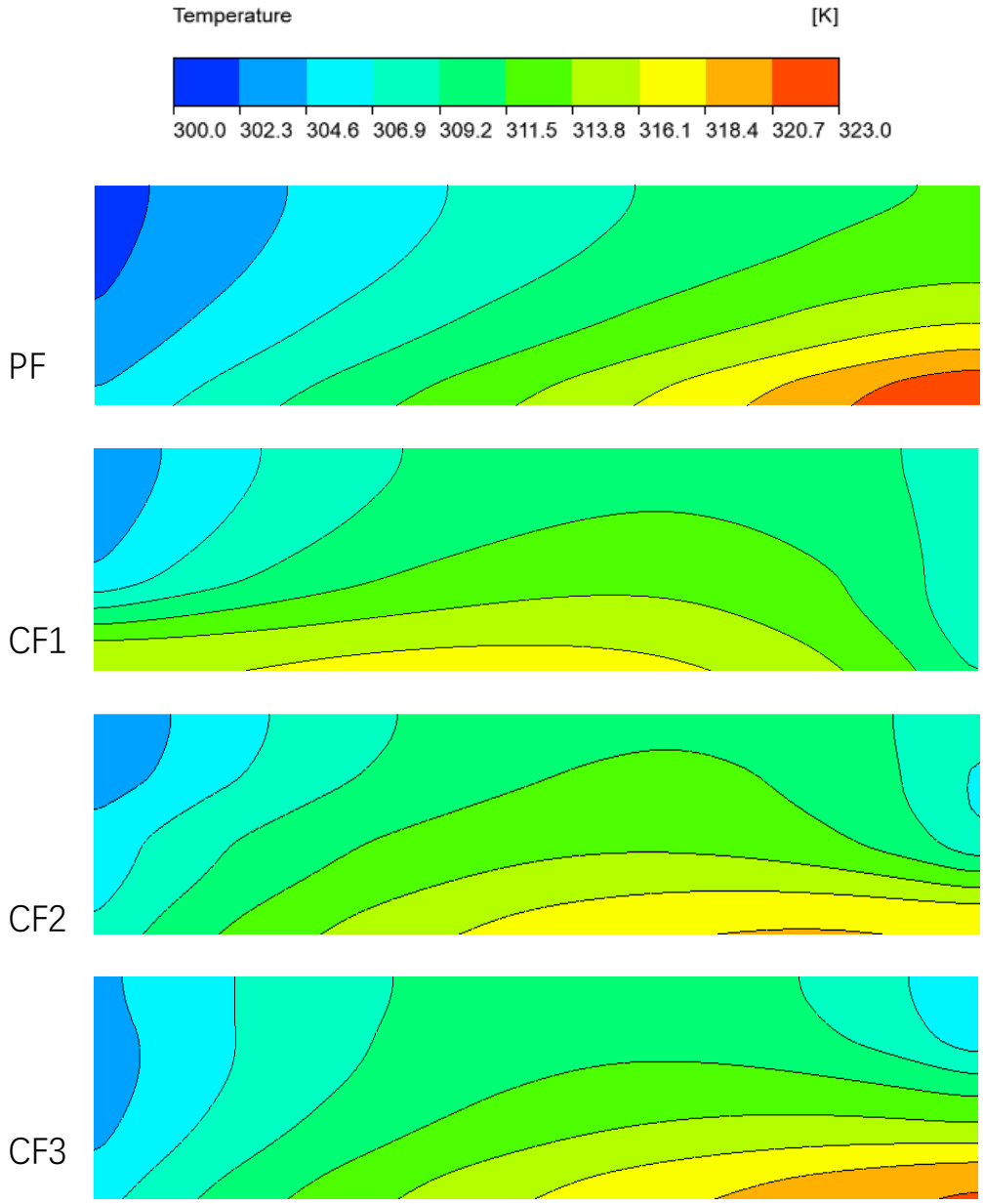


Figure 6-2 Temperature distribution for three-layered MCHS with different flow configurations for Design 4

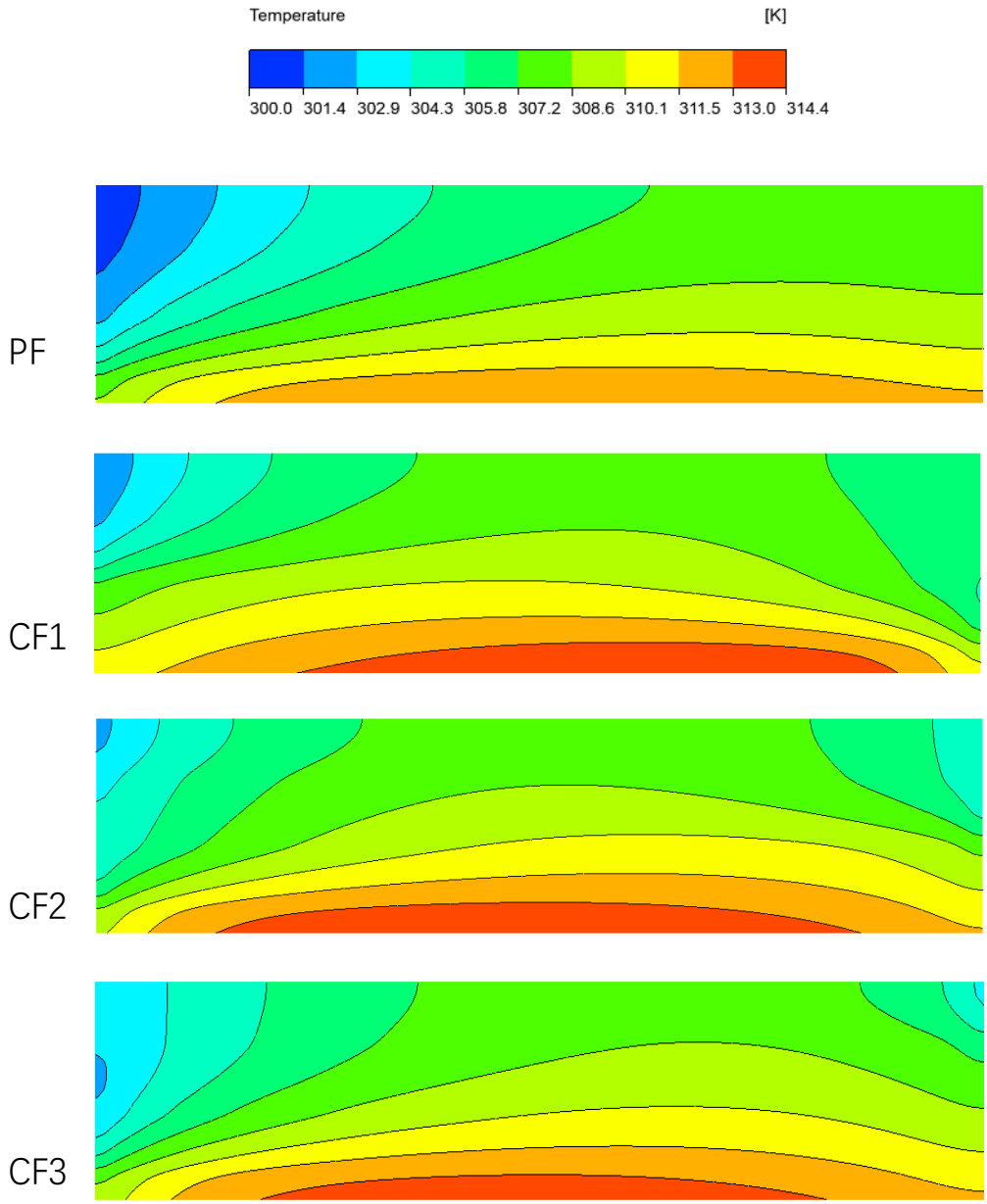


Figure 6-3 Temperature distribution for three-layered MCHS with different flow configurations for Design 5

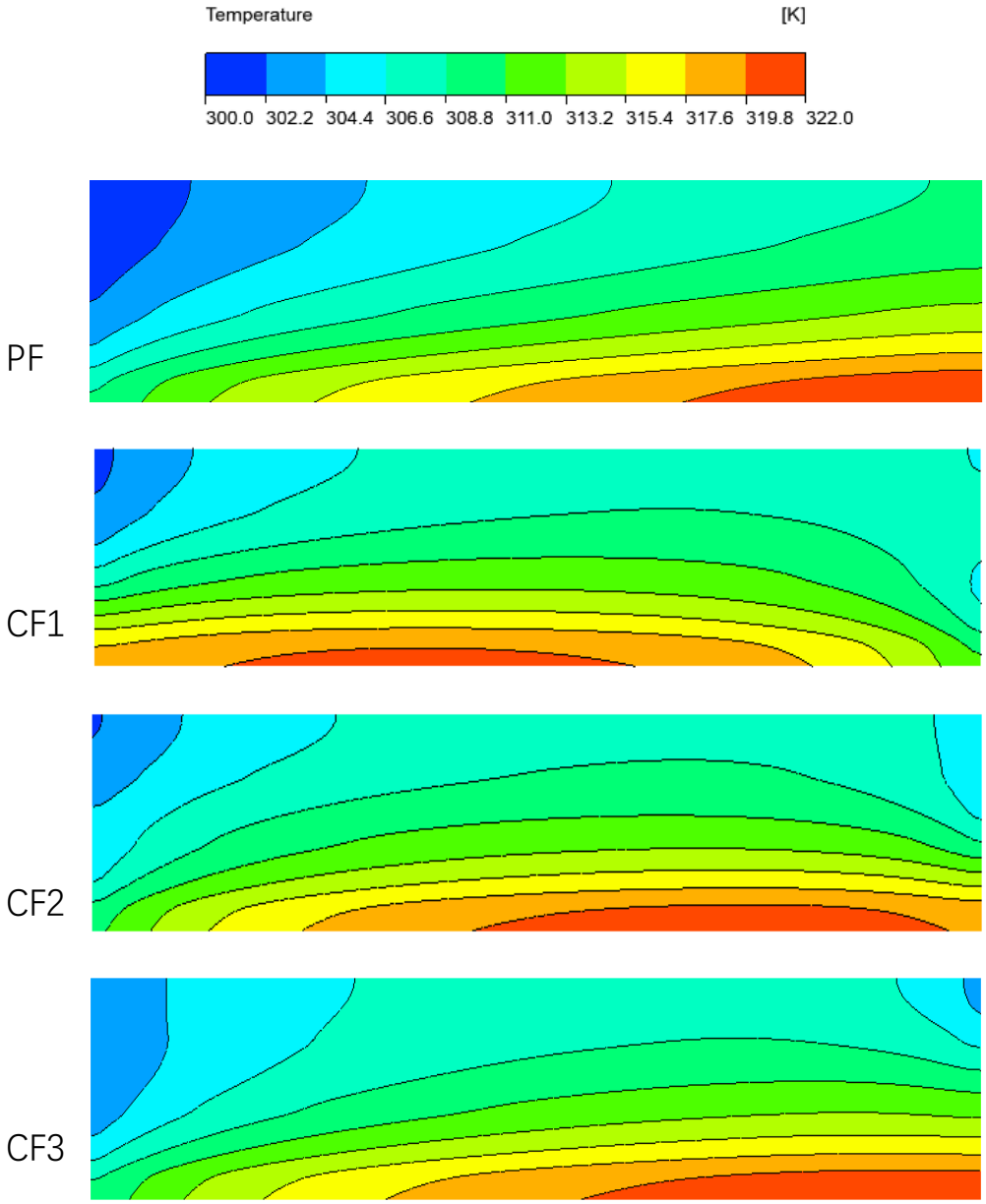


Figure 6-4 Temperature distribution for three-layered MCHS with different flow configurations for Design 8

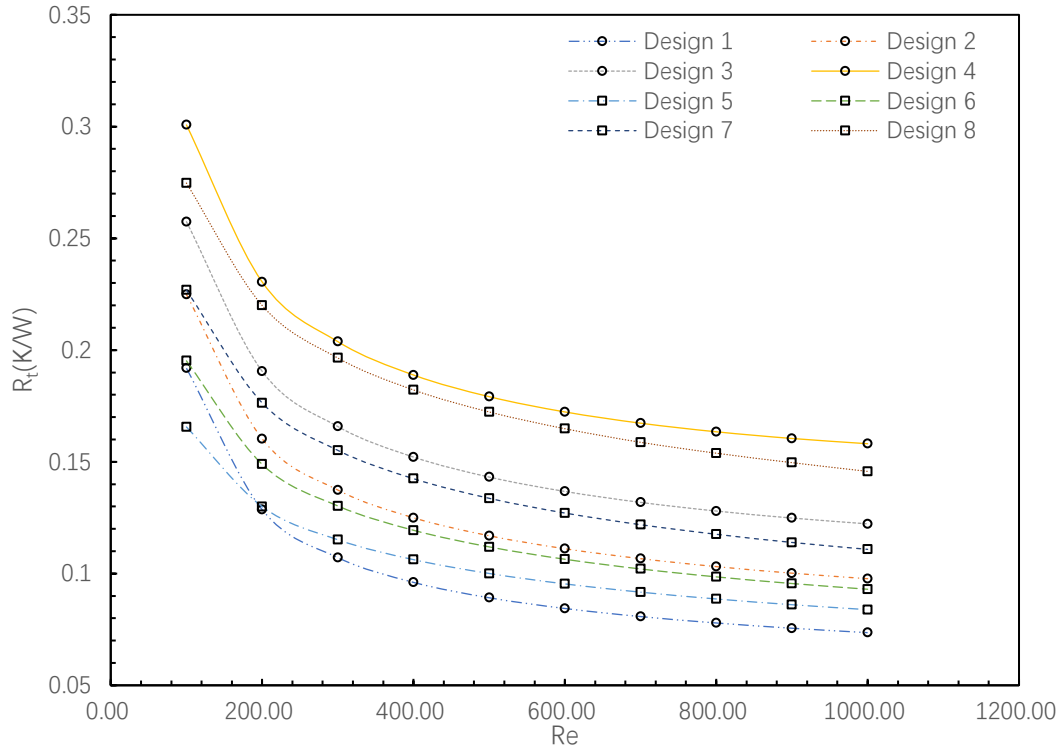


Figure 6-5 The R_t for three-layered MCHS with PF at various Re.

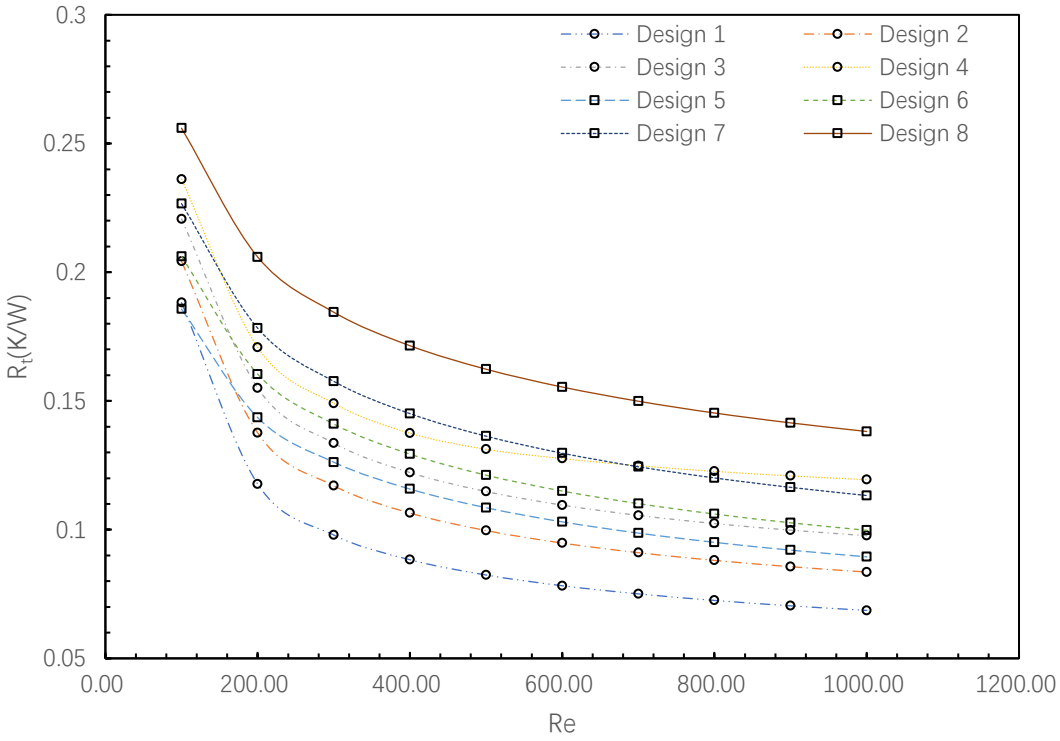


Figure 6-6 The R_t for three-layered MCHS with CF1 at various Re.

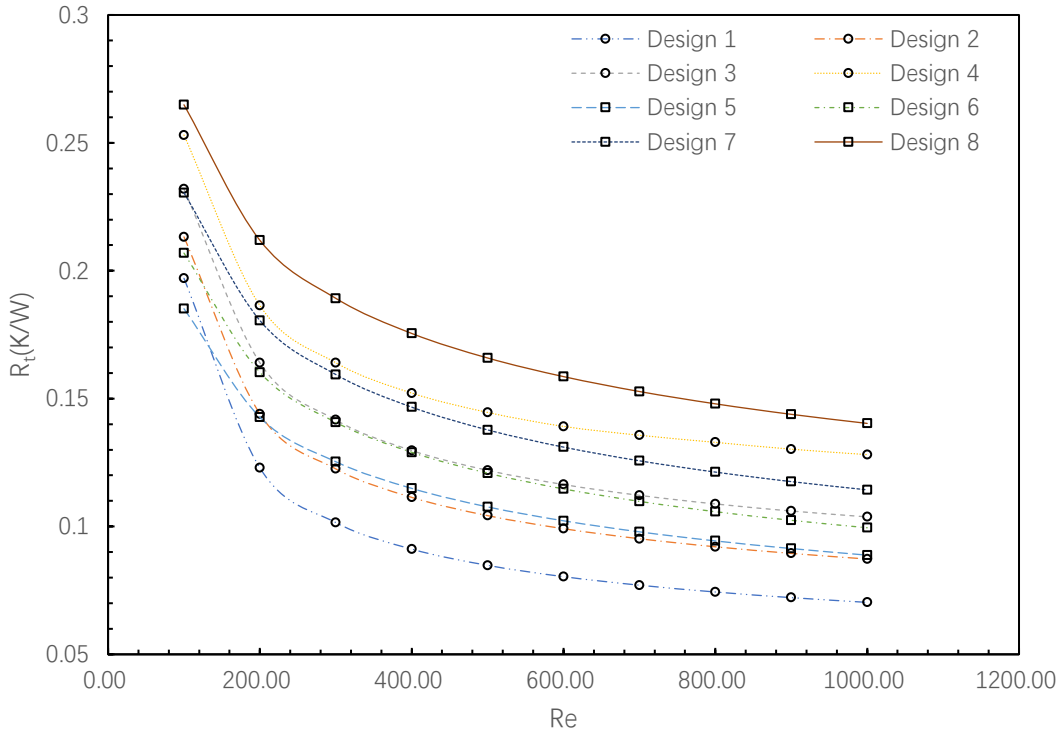


Figure 6-7 The R_t for three-layered MCHS with CF2 at various Re.

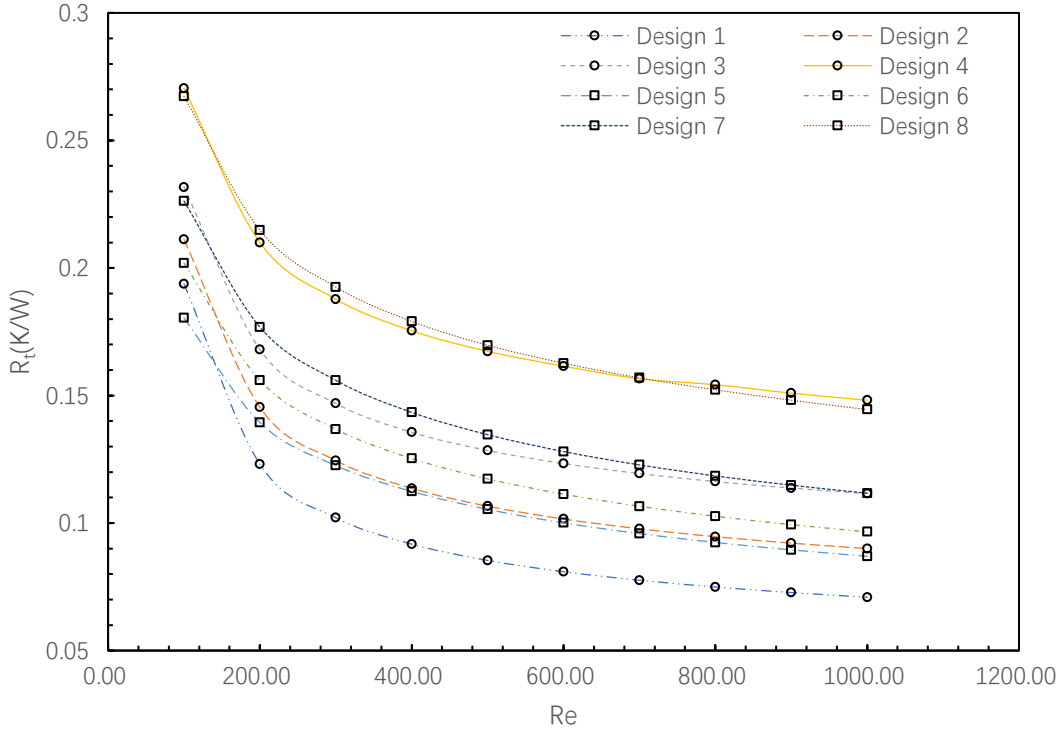


Figure 6-8 The R_t for three-layered MCHS with CF3 at various Re.

The R_t for three-layered MCHS with PF, CF1, CF2 and CF3 at various Re is shown inFigure 6-5 to Figure 6-8. For all cases investigated, the R_t decreases with the increase of Re and tends to be stable. It can be found that Design 5 presents lowest R_t for all flow configurations and most of Re except for Re=100. This is due to the thermal performance enhances with the increase of flow velocity as expected.

6.3 The hydraulic performance for three-layered MCHS at various Re.

Figure 6-9 presents the △P versus Re for three-layered MCHS with different designs. It can be observed that for all designs investigated, the △P increases with the increase of Re. When look into the designs with same W_i as shown in Figure 6-9 (a), the design with larger W_o exhibits lower △P and the difference increases with the increase of W_o and Re. Maximum difference of 89.87% can be found between design 1 and design 4 at Re=1000. When look into the designs with same W_o as shown in Figure 6-9 (b), the design with larger W_i presents lower △P while the difference decreases with the increase of the W_i. Maximum difference of 90.18% can be found between design 5 and design 8 at Re=1000. This indicates that the design with smaller W_i / W_o always displays larger △P, which is mainly due to the flow velocity varies with the varying of the channel size.

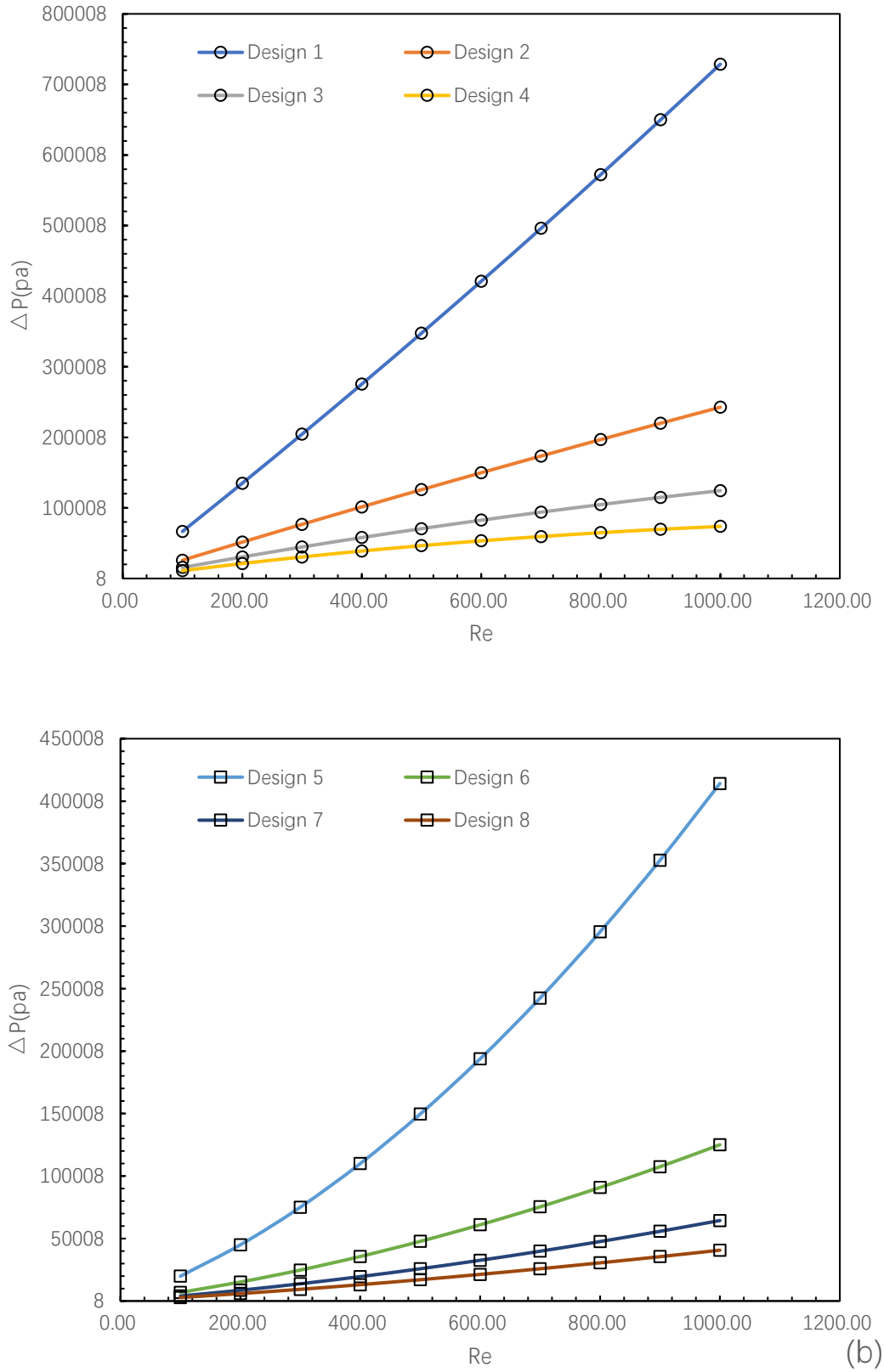


Figure 6-9 The △P for three-layered MCHS for (a) design 1-4 (b) design 5-8.

6.4 The thermal performance for three-layered MCHS with different flow configurations.

To study the effect of W_i at fixed value of W_o for three-layered MCHS with different flow configurations, the results of R_t for W_o of 50μm, 100 μm, 150μm and 200μm are plotted in Figure 6-10(a)-(d), respectively. It can be observed that, generally the increase of W_i increases the value of R_t for all the flow configurations investigated. This would mean the increase in channel inlet width leads to poorer heat transfer. The increase in channel inlet width will change the channel geometry from diverging channel to converging channel if the channel outlet width is unchanged. It is evident in Fig. 6.3(a) that, the geometry with smallest value of Wo and Wi gives the lowest value of R . The CF1 flow configuration provide the best thermal performance among the 4 flow configurations when Wi is small as observed in Figure 6-10 (a). However, the PF flow configuration gives the lowest value of R_t when Wi increases to high value, which can be observed in Figure 6-10 (a) and Figure 6-10(b).

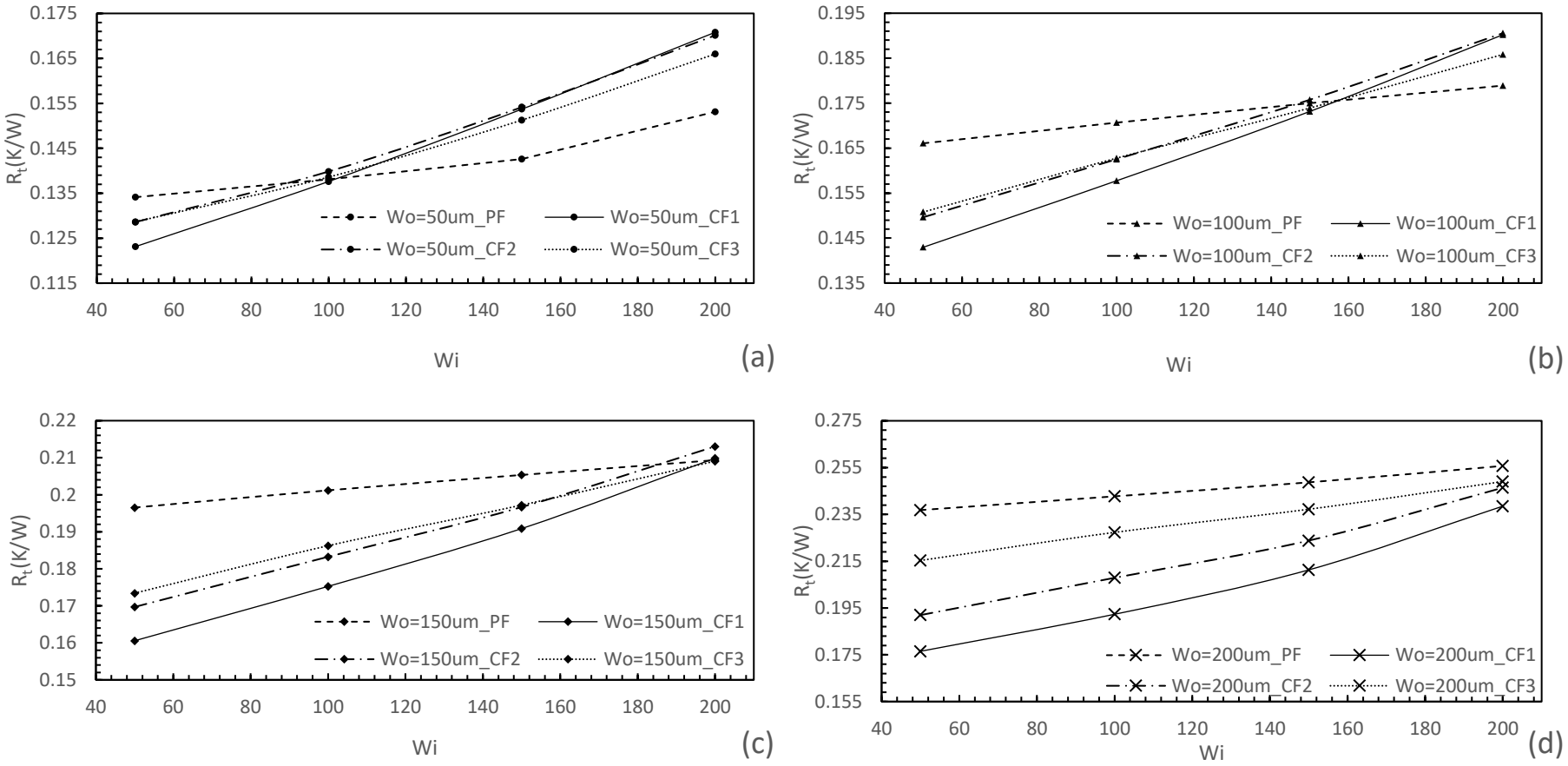


Figure 6-10 Comparison of thermal resistance among PF, CF1, CF2 and CF3 flow configurations for (a)$W_o = 50\mu m$, (b)$W_o = 100\mu m$, (c)$W_o = 150\mu m$ and (d)$W_o = 200\mu m$

6.5 Temperature distribution for three-layered MCHS

To understand how tapered channel profile has affected the thermal performance, Figure 6-11(a),(b) and (c) are plotted to show the local variation of temperature , $T_{y,max}$ at the bottom surface of the heat sink along the flow direction for (i) converging channel geometry of $W_i = 200\mu m$ $W_o = 50\mu m$, (ii) straight channel geometries of $W_i = 50\mu m$ $W_o = 50\mu m$ and (iii) diverging channel geometry of $W_i = 50\mu m$ $W_o = 200\mu m$. $T_{y,max}$ here is the local maximum temperature at the bottom wall along the flow direction.

The trend of the temperature variation along the y direction for the 4 flow configurations are analysed. It is found that, the temperature $T_{y,max}$ for parallel flow configuration increases from the inlet towards the outlet until it attains the peak temperature at the outlet as shown in Figure 6-11(b) and Figure 6-11 (c). The trend for PF shown in Figure 6-11(a) is similar as $T_{y,max}$ increases from inlet, with the peak close the channel exit, but not exactly at the exit. There is lightly difference for PF in Figure 6-11(a) as the curve becomes nearly horizontal from the middle towards the end of the channel.

When the counter flows (CF1, CF2 and CF3) are compared to the parallel flow (PF), it is found that, the counter flows have the location of peak temperature near the centre of the channel rather than near the channel exit. This means the counter flows are able to moderate the heat transfer patterns to attain more balance heat transfer between both end of the channels. With such moderation, the counter flows are able to reduce the peak temperature as compared to the parallel flow as observed in Figure 6-11 (b) (straight channel profile) and Figure 6-11(c) (converging channel profile), and improves the temperature non-uniformity.

When compared among the counter flows of CF1, CF2 and CF3, CF1 gives the lowest peak temperature for the case of straight channel (Figure 6-11(b)) and for the case of diverging channel (Figure 6-11(c)), which directly improves the thermal resistance. In Figure 6-11(c), CF3 gives the lowest peak temperature among counter flows.

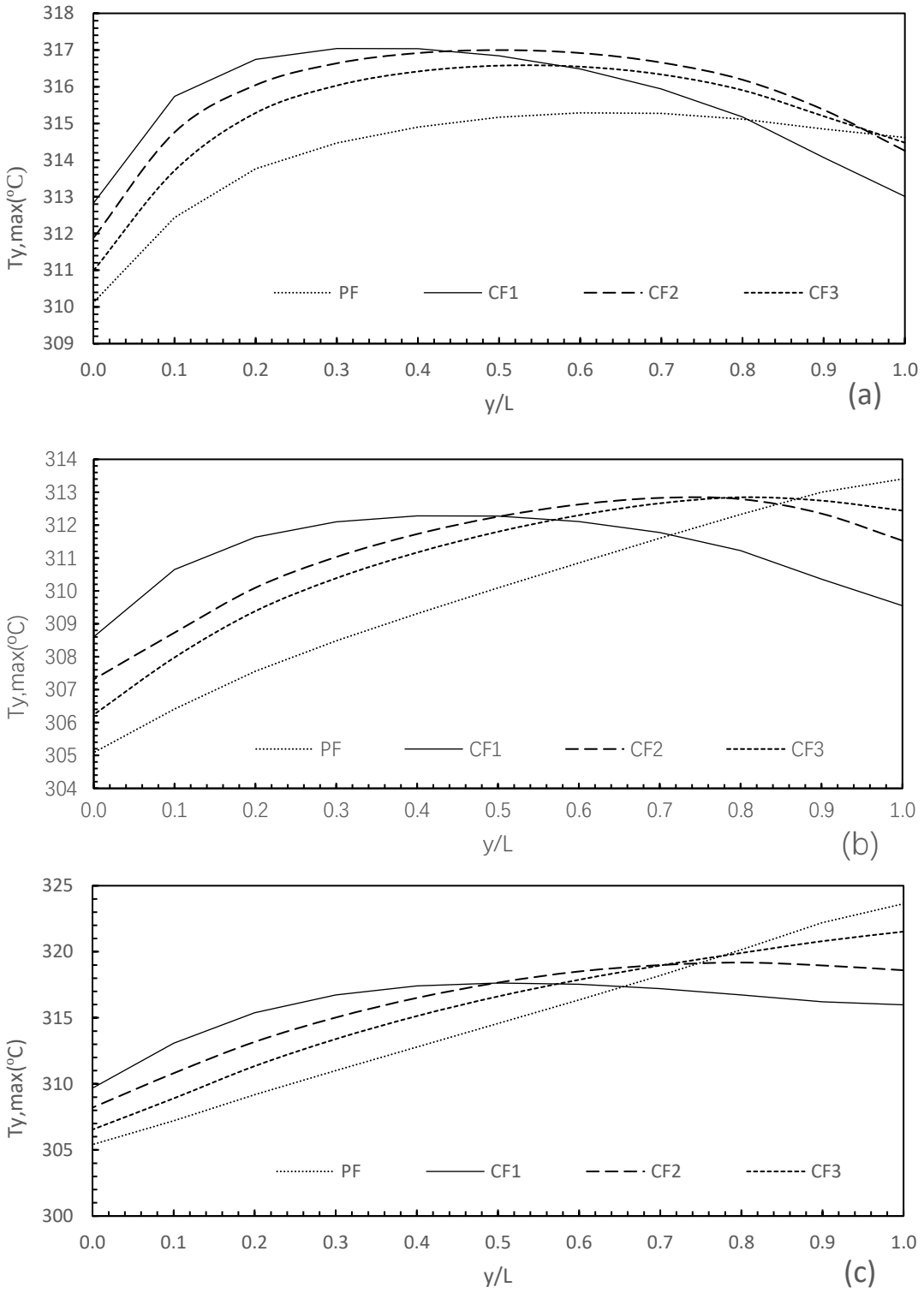


Figure 6-11 Comparison of $T_{y,max}$ among 4 flow configurations for case of (a) converging channel with $W_i = 200\mu m$ $W_o = 50\mu m$, (b) straight channel with $W_i = 50\mu m$ $W_o = 50\mu m$ and (c) diverging channel with $W_i = 50\mu m$ $W_o = 200\mu m$

6.6 Thermal-hydraulic performance for three-layered MCHS with different flow configurations.

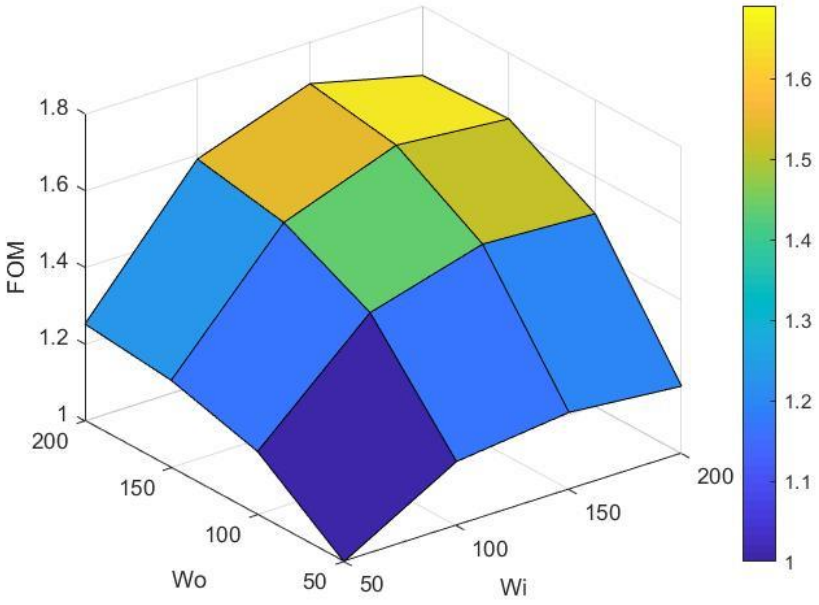


Figure 6-12 FOM for three-layered MCHS with PF.

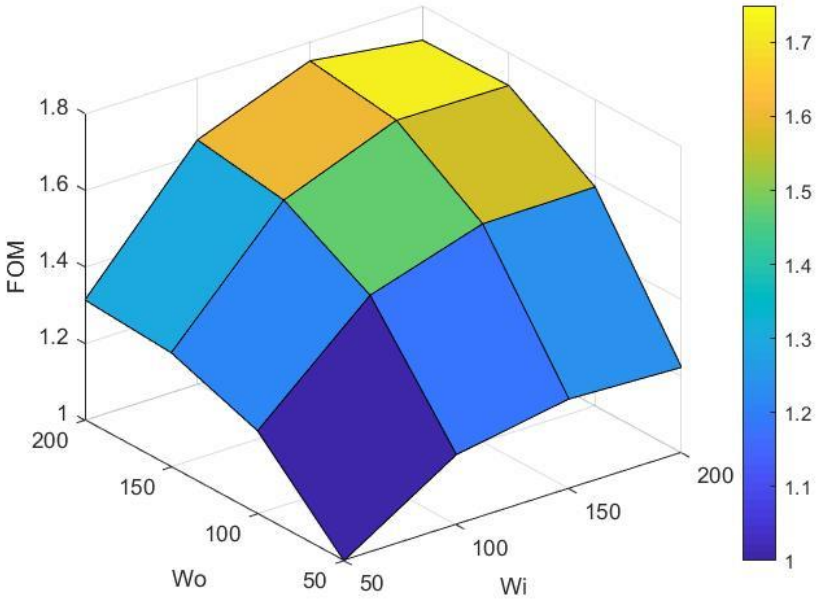


Figure 6-13 FOM for three-layered MCHS with CF1.

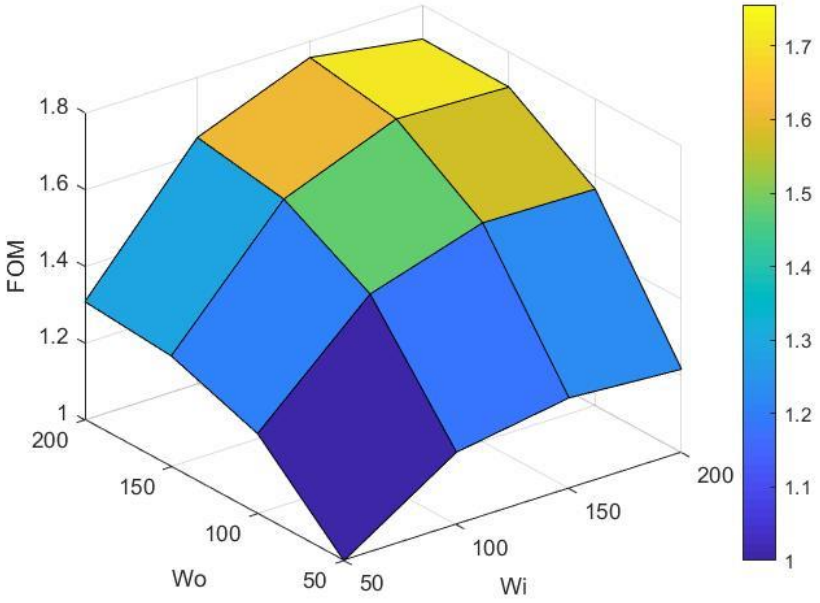


Figure 6-14 FOM for three-layered MCHS with CF2.

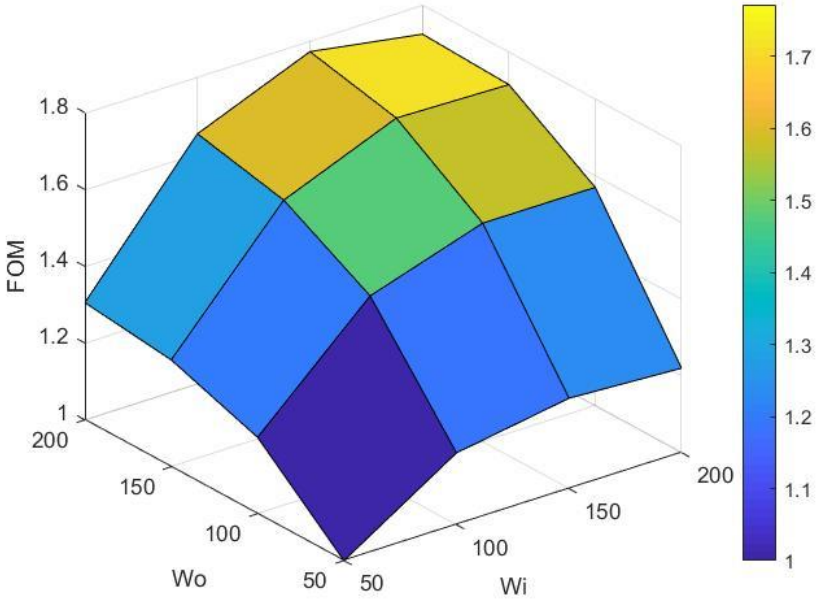


Figure 6-15 FOM for three-layered MCHS with CF3.

Figure 6-12 to Figure 6-15 presents the FOM for three-layered MCHS with PF, CF1, CF2 and CF3, respectively. For each flow configuration, the design with W_i=50μm and W_o=50μm is used as base case.

Same trend can be found for all four different flow configurations that the FOM increases and then decreases with the increase of W_i/W_o. For all flow configurations, the design with W_i=50μm and W_o=50μm has lowest ROM of 1 and the design with W_i=150μm and W_o=200μm shows highest FOM and it has value of 1.69, 1.75, 1.76 and 1.77 for PF, CF1, CF2 and CF3, respectively. This means that for all flow configurations, the design with W_i=150μm and W_o=200μm has highest and design with W_i=50μm and W_o=50μm has the lowest thermal-hydraulic performance. To compare the thermal-hydraulic performance between different flow configurations, Figure 6-16 is plotted. For all cases investigated, the three-layered MCHS with parallel flow and with W_i=50μm and W_o=50μm is used as base case. It can be found that for all designs studied, the PF always shows higher FOM as compared with CF1, CF2 and CF3. which indicated that the three-layered with PF exhibits better thermal hydraulic performance as compared with CF1, CF2 and CF3. For PF, Maximum enhancement of 14.41%,14.81% and 11.72% in terms of thermal hydraulic performance can be found when compared with CF1, CF2 and CF3, respectively.

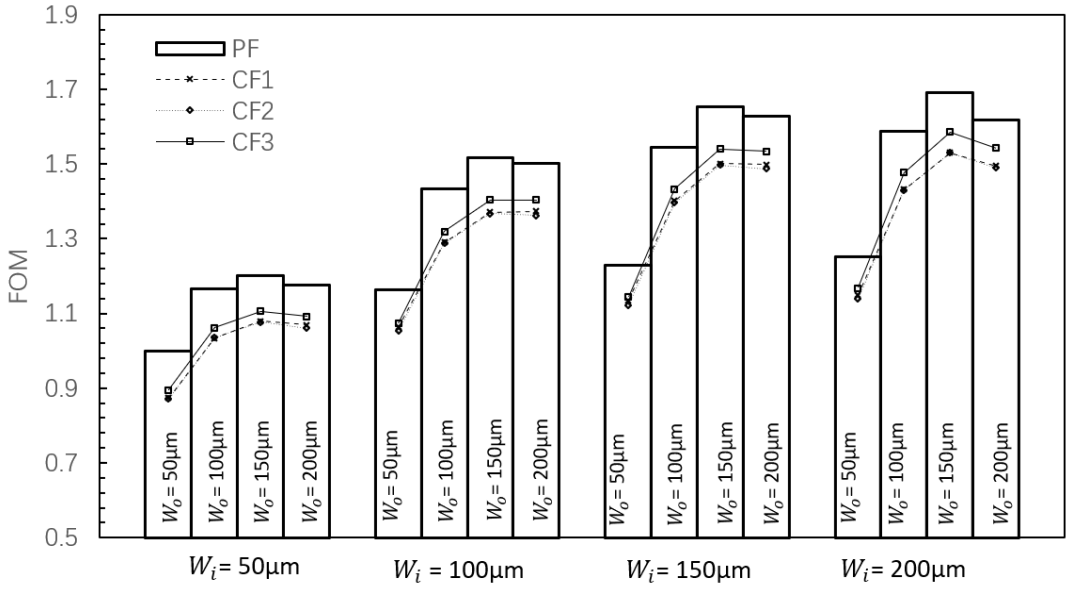


Figure 6-16 The comparison of FOM between three-layered MCHS with PF, CF1, CF2 and CF3.

6.7 Conclusions

The thermal performance of three-layered MCHS with horizontally tapered channels have been investigated for PF, CF1, CF2 and CF3 flow configurations for different inlet width W_i at dfferent outlet width $W_o$through simulation. The thermal resistance and base temperature for counter and parallel flow has been analysed. The conclusion can be drawn as follows:

- For low value of channel inlet size (converging channel profile) in three-layered MCHS, CF1 flow configuration gives the lowest value of R_t
- For high value of channel inlet size (converging channel profile), parallel flow configuration gives the lowest value of R_t
- The counter flow configuration alters the temperature variation pattern of the parallel flow by moving the peak temperature location toward the center of the channel, giving better temperature uniformity.
- The three-layered MCHS with CF1 flow configuration demonstrate best temperature uniformity with lowest peak temperature for the case of straight and converging channel profile.
- The three-layered MCHS design with W_i=150μm and W_o=200μm has best thermal-hydraulic performance and optimum design shows about 69%,75%,76% and 77% better in thermal-hydraulic performance for PF, CF1, CF2 and CF3 as compared with base case, respectively.
- The PF shows better thermal-hydraulic performance and the enhancement can up to 14.41%,14.81% and 11.72% as compared with CF1, CF2 and CF3, respectively.

Chapter 7. Heat Transfer Network and Correlation for a Double-Layered Microchannel Heat Sink

7.1 Introduction

In previous chapters, the thermal and hydraulic performance for double- and three- layered MCHS has been numerically investigated. Although counter flow/alternating flow /CF1/CF2/CF3 shows better thermal performance for certain cases, the MCHS with parallel flow configuration always shows the best the thermal-hydraulic performance. According to this, a thermal resistance network is proposed in this chapter to provide a more convenient tools to predict the thermal resistance for MCHS with parallel flow. Moreover, local Nusselt number in terms of axial distance channel outlet width is proposed for different channel inlet width.

7.2 Thermal resistance correlation

Figure 7-1 shows the heat flow within a half of a repeated section of the DL-MCHS at location $y(0 \leq y \leq L)$, where x and y are geometrical lengths as shown in Figure 3-2. Uniform heat flux is applied at the bottom surface of the heat sink and consider total amount of heat $Q_{1,y}$ is first conducted through the horizontal rib of the bottom layer, which can be written as:

$$Q_{1,y} = \frac{k_s A_y}{t}\left(T_{1,y} - T_{2,y}\right) = \frac{T_{1,y} - T_{2,y}}{\frac{t}{k_s A_y}} \tag{7.1}$$

where $A_y = N \cdot W \cdot y$ is the based area of heat sink from $y = 0$ till the location y.

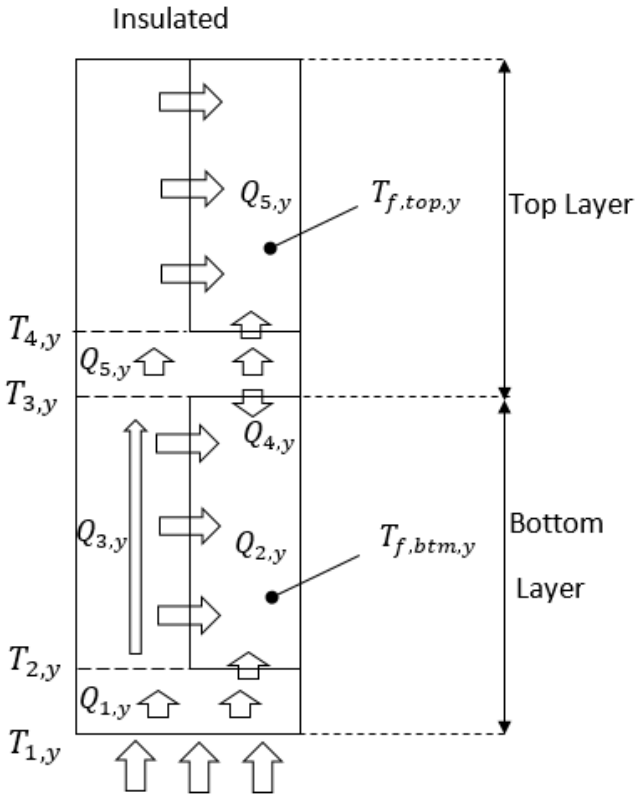


Figure 7-1.The heat transfer flow within DL-MCHS.

The heat is then transferred from the horizontal rib to the second section consist of vertical fin and fluid passage. Part of the heat of amount $Q_{2,y}$ is transferred into the fluid through the solid-fluid interface while the remaining heat $Q_{3,y}$ is transferred to top of the vertical fin of bottom layer.

Using the fin theory, convection can be presented in terms of $T_{2,y}$ and $T_{3,y}$. With that, $Q_{2,y}$ transferred through the fluid-solid interface can be obtained as follows:

$$Q_{2,y} = N\left(T_{2,y} - T_{f,btm,y}\right)\delta_{btm,y} + N\left(T_{3,y} - T_{f,btm,y}\right)\delta_{btm,y} + h_{btm,y}A_y\left(T_{2,y} - T_{f,btm,y}\right)$$

$$= \frac{T_{2,y} - T_{f,btm,y}}{\frac{1}{N\delta_{btm,y}}} + \frac{T_{3,y} - T_{f,btm,y}}{\frac{1}{N\delta_{btm,y}}} + \frac{T_{2,y} - T_{f,btm,y}}{\frac{1}{h_{btm,y}A_y}} \tag{7.2}$$

Where $T_{f,btm,y}$ is the averaged fluid temperature in the bottom channel at location y.

$\Delta_{btm,y} = \sqrt{h_{btm,y} \cdot P_{fin} \cdot k_s \cdot A_{c,y}} \cdot \cos\left(h_{btm,y} \cdot m_{btm,y} \cdot H_{ch} - 1\right)/\sin(h_{btm,y} \cdot m_{btm,y} \cdot H_{ch})$ is the heat transfer rate along the bottom fin area. $P_{fin,y} = 2(y + W_r)$ is the perimeter of a single fin, $A_{c,y} = yW_r$ is the cross-section area of a single fin and $W_r = W - W_{ch}$ is the rib width for a single channel.

$Q_{3,y}$ can be expressed as follows:

$$Q_{3,y} = \frac{k_s A_{rib,y}}{H_{ch}}\left(T_{2,y} - T_{3,y}\right) = \frac{T_{2,y} - T_{3,y}}{\frac{H_{ch}}{k_s A_{rib,y}}} \tag{7.3}$$

Where $A_{rib,y} = W_r \cdot y \cdot N$ is total vertical rib area.

The heat amount of $Q_{3,y}$ that is transferred into the top layer horizontal rib is split into $Q_{4,y}$ and $Q_{5,y}$. $Q_{4,y}$ is transferred into the fluid from the bottom surface of top layer horizontal rib, and it is expressed as:

$$Q_{4,y} = N h_{btm,y} A_y \left(T_{3,y} - T_{f,btm,y}\right) = \frac{T_{3,y} - T_{f,btm,y}}{h_{btm,y} A_y} \tag{7.4}$$

The remaining heat $Q_{5,y}$ is first conducted through the horizontal rib of the top layer and then transferred to the fluid in the top layer through convection. The convection thorough the top channel can be solved to obtain $T_{4,y}$ by fin theory with the following boundary conditions:

- insulated surface at the top of top layer
- constant temperature at top surface of the horizontal rib at the top layer.

With that, $Q_{5,y}$ is expressed as:

$$Q_{5,y} = \frac{k_s A_y}{t}\left(T_{3,y} - T_{4,y}\right) = \left(N\delta_{top,y} + h_{top,y} A_y\right)\left(T_{4,y} - T_{f,top,y}\right)$$

$$= \frac{T_{3,y} - T_{4,y}}{\frac{t}{k_s A_y}} = \frac{T_{4,y} - T_{f,top,y}}{\frac{1}{N\delta_{top,y} + h_{top,y} A_y}} \tag{7.5}$$

Where $\delta_{top,y} = \sqrt{h_{top,y} \cdot P_{fin,y} \cdot k_s \cdot A_{c,y}} \cdot \sinh\left(m_{top,y}\right) \cdot H_{ch} / \left(\cosh\left(m_{top,y}\right) \cdot H_{ch}\right)$ is the heat transfer rate at the top fin area, $T_{f,top,y}$ is the averaged fluid temperature in the top channel at location y.

Note that based on the energy balance of the fluid, the amount of heat transferred into the fluid will be stored in the fluid and result in fluid temperature increase. The amount of heat has been transferred to the fluid at top channel $Q_{top,y}$ and at bottom channel $Q_{btm,y}$ can be obtained as follows:

$$Q_{top,y} = \dot{m} c_{p,f}\left(T_{f,top,y} - T_{f,top,in}\right) = \frac{T_{f,top,y} - T_{f,top,in}}{\dot{m} c_{p,f}} \tag{7.6a}$$

$$Q_{btm,y} = \dot{m}c_{p,f}\left(T_{f,btm,y} - T_{f,btm,in}\right) = \frac{T_{f,btm,y} - T_{f,btm,in}}{\dot{m}c_{p,f}} Q_{top,y} = \dot{m}c_{p,f}\left(T_{f,top,y} - T_{f,top,in}\right) = \frac{T_{f,top,y} - T_{f,top,in}}{\dot{m}c_{p,f}} \quad \text{(b)}$$

The overall energy balance is presented by:

$$Q_y = Q_{1,y} = Q_{2,y} + Q_{3,y} = Q_{2,y} + Q_{4,y} + Q_{5,y} = Q_{top,y} + Q_{btm,y} \quad (7.7)$$

Substituting Eq. (7.6) into Eq. (7.7), the following can be obtained:

$$Q_y = \frac{T_{1,y} - T_{2,y}}{\frac{t}{k_s A_y}}$$

$$= \frac{T_{2,y} - T_{f,btm,y}}{\frac{1}{N\delta_{btm,y}}} + \frac{T_{3,y} - T_{f,btm,y}}{\frac{1}{N\delta_{btm,y}}} + \frac{T_{2,y} - T_{f,btm,y}}{\frac{1}{h_{btm,y}A_y}} + \frac{T_{2,y} - T_{3,y}}{\frac{H_{ch}}{k_s A_{rib}}}$$

$$= \frac{T_{2,y} - T_{f,btm,y}}{\frac{1}{N\delta_{btm,y}}} + \frac{T_{3,y} - T_{f,btm,y}}{\frac{1}{N\delta_{btm,y}}} + \frac{T_{2,y} - T_{f,btm,y}}{\frac{1}{h_{btm,y}A_y}} + \frac{T_{3,y} - T_{f,btm,y}}{\frac{1}{h_{btm,y}A_y}} + \frac{T_{3,y} - T_{4,y}}{\frac{t}{k_s A_y}}$$

$$= \frac{T_{2,y} - T_{f,btm}}{\frac{1}{N\delta_{btm,y}}} + \frac{T_{3,y} - T_{f,btm}}{\frac{1}{N\delta_{btm,y}}} + \frac{T_{2,y} - T_{f,btm}}{\frac{1}{h_{btm,y}A_y}} + \frac{T_{3,y} - T_{f,btm}}{\frac{1}{h_{btm,y}A_y}} + \frac{T_{4,y} - T_{f,top,y}}{\frac{1}{N\delta_{top,y} + h_{top,y}A_y}}$$

$$= \frac{T_{f,top,y} - T_{f,top,in}}{\dot{m}c_{p,f}} + \frac{T_{f,btm,y} - T_{f,btm,in}}{\dot{m}c_{p,f}} \quad (7.8)$$

The Eq. (7.8) can be converted into the thermal resistance network presented in Figure 7-2(a). However, Wei et al.[124]used an iterative method to solve the network to obtain thermal resistance, which is not efficient to predict the thermal performance. The present study simplified the network by imposing a modification of delta-wye to the network, which enable it to solve thermal resistance directly without iteration. The delta circuit and wye circuit are shown in rectangular box in Figure 7-2(a) and (b), respectively.

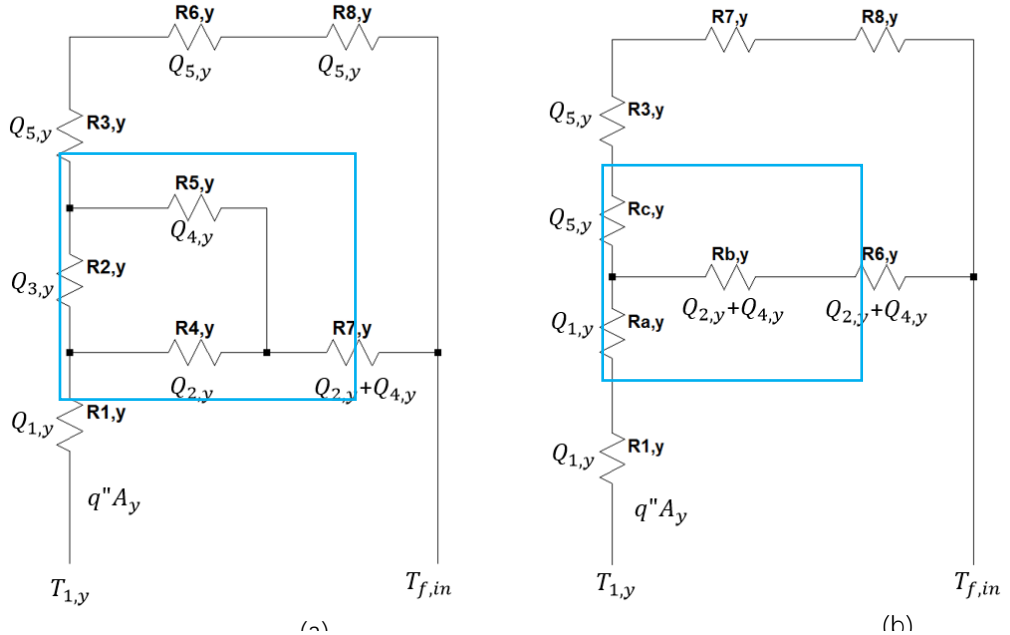


Figure 7-2 (a) shows the thermal resistance network proposed by Wei et al. [16] and (b) The thermal resistance after delta-wye conversion for DL-MCHS

$R_{1,y}$ and $R_{3,y}$ represent the conductive thermal resistance of the horizontal ribs for bottom layer and top layer of the MCHS, respectively. $R_{2,y}$ represent the conductive thermal resistance along the vertical fin of bottom layer. $R_{4,y}$, $R_{5,y}$ and $R_{6,y}$ represent the convective thermal resistance between walls and coolant. $R_{7,y}$ and $R_{8,y}$ represent the capacitive thermal resistance due to the temperature increase of the coolant. The delta-wye conversion is applied and the converted thermal resistance is shown in Fig 3(b). With the modified thermal resistance network in Fig. 3(b), correlation for local thermal resistance, R_y was obtained as:

$$R_y = R_{1,y} + R_{a,y} + \frac{1}{\frac{1}{R_{b,y}+R_{7,y}}+\frac{1}{R_{c,y}+R_{3,y}+R_{6,y}+R_{8,y}}} \tag{7.9}$$

Where

$$R_{a,y} = \frac{R_{2,y}R_{4,y}}{R_{2,y}+R_{4,y}+R_{5,y}} \tag{7.10a}$$

$$R_{b,y} = \frac{R_{4,y}R_{5,y}}{R_{2,y}+R_{4,y}+R_{5,y}} \tag{7.10b}$$

$$R_{c,y} = \frac{R_{2,y}R_{5,y}}{R_{2,y}+R_{4,y}+R_{5,y}} \quad (7.10c)$$

$$R_{1,y} = R_{3,y} = \frac{t}{k_s A_y} \quad (7.10d)$$

$$R_{2,y} = \frac{H_{ch}}{k_s A_{rib}} \quad (7.10e)$$

$$\mathrm{R_{a,y}} = \frac{\mathrm{R_{2,y}R_{4,y}}}{\mathrm{R_{2,y}+R_{4,y}+R_{5,y}}} \quad (7.10f)$$

$$R_{a,y} = \frac{R_{2,y}R_{4,y}}{R_{2,y}+R_{4,y}+R_{5,y}} \quad (7.10a)$$

$$R_{b,y} = \frac{R_{4,y}R_{5,y}}{R_{2,y}+R_{4,y}+R_{5,y}} \quad (7.10b)$$

$$R_{c,y} = \frac{R_{2,y}R_{5,y}}{R_{2,y}+R_{4,y}+R_{5,y}} \quad (7.10g)$$

$$\mathrm{R_{c,y}} = \frac{\mathrm{R_{2,y}R_{5,y}}}{\mathrm{R_{2,y}+R_{4,y}+R_{5,y}}} \quad (7.10h)$$

$$\mathrm{R_{4,y}} = \frac{1}{\mathrm{N\delta_{btm,y}+h_{btm,y}A_y}} \quad (7.10i)$$

$$\mathrm{R_{6,y}} = \frac{1}{\mathrm{N\delta_{top,y}+h_{top,y}A_y}} \quad (7.10j)$$

$$\mathrm{R_{5,y}} = \frac{1}{\mathrm{Nh_{btm,y}A_y}} \quad (7.10k)$$

$$\mathrm{R_{7,y} = R_{8,y}} = \frac{1}{\mathrm{\dot{m}c_{p,f}}} \quad (7.10l)$$

$$\mathrm{h_{btm,y}} = \frac{\mathrm{Nu_{btm,y}k_f}}{\mathrm{D_h}} \quad (7.10m)$$

$$\mathrm{h_{top,y}} = \frac{\mathrm{Nu_{top,y}k_f}}{\mathrm{D_h}} \quad (7.10n)$$

Where $\mathrm{D_h} = 2(\mathrm{W_{ch}H_{ch}})/(\mathrm{W_{ch}} + \mathrm{H_{ch}})$ is the hydraulic diameter of the channels.

It should be noticed that, in Eq. (7.10), variables $\mathrm{t}, \mathrm{W_{ch}}, \mathrm{H_{ch}}, \mathrm{W}$ and y are the design parameters of DL-MCHS. The unknown variables $\mathrm{Nu_{btm,y}}$ and $\mathrm{Nu_{top,y}}$ are the Nusselt numbers for the convection at the fluid-solid interface at the bottom and top channel, respectively.

For the bottom fluid channel, the heat is transferred from four solid side walls into fluid. While for the top fluid channel, the heat is transferred from three solid side walls only into fluid as the top wall is considered as insulated wall. $\mathrm{Nu_{btm,y}}$ can be solved using the correlation proposed by Lee et at. [115]

with four-sided heating condition as follows:

$$\mathrm{Nu}_{4,y} = \frac{1}{\mathrm{C}_1(y^*)^{\mathrm{C}_2}+\mathrm{C}_3} + \mathrm{C}_4 \tag{7.11}$$

Where $y^* = y/(\mathrm{RePrD_h})$is the dimensionless axial distance, $\mathrm{Re} = \frac{\rho_f v D_h}{\mu}$ is the Reynold's number , $\mathrm{Pr} = \frac{C_{p,f}\mu}{k_f}$ is the Prandtl number and μ is the the dynamic viscosity of the fluid.

The coefficients in Eq. (7.11) are given as follows:

$$\mathrm{C}_1 = -3.122 \times 10^{-3}\alpha^3 + 2.435 \times 10^{-2}\alpha^2 + 2.143 \times 10^{-1}\alpha + 7.325 \tag{7.12a}$$

$$\mathrm{C}_2 = 6.412 \times 10^{-1} \tag{7.12b}$$

$$\mathrm{C}_3 = 1.589 \times 10^{-4}\alpha^2 - 2.603 \times 10^{-3}\alpha + 2.444 \times 10^{-2} \tag{7.12c}$$

$$\mathrm{C}_4 = 7.148 - 1.328 \times \frac{10^{-1}}{\alpha} - 5.936/\alpha^3 \tag{7.12d}$$

where α is the channel aspect ratio. $\mathrm{Nu_{top,y}}$ can be solved using correlation proposed by Lee et al. [115] for three-sided heating condition as follows:

$$\mathrm{Nu_{top,y}} = \mathrm{Nu_{4,y}} \times (\mathrm{Nu_{\infty,3}}/\mathrm{Nu_{\infty,4}}) \tag{7.13}$$

where $\mathrm{Nu_{\infty,3}}$ and $\mathrm{Nu_{\infty,4}}$ are the Nusselt numbers for fully developed flow for 3-sided heating and 4-sided heating conditions, respectively, which are expressed as follows:

$$Nu_{\infty,3} = 8.235(1 - \frac{1.883}{\alpha} + \frac{3.767}{\alpha^2} - \frac{5.814}{\alpha^3} + \frac{5.361}{\alpha^4} - \frac{2.0}{\alpha^5}) \tag{7.14}$$

$$\mathrm{Nu_{\infty,4}} = 8.235(1 - \frac{2.041}{\alpha} + \frac{3.0853}{\alpha^2} - \frac{2.4765}{\alpha^3} + \frac{1.0578}{\alpha^4} - \frac{0.1861}{\alpha^5}) \tag{7.15}$$

7.3 Comparison of correlation and simulation results for DL-MCHS.

Figure 7-3 presents the comparison of local max temperature difference ΔT_y along y direction between correlation and simulation results for DL-MCHS with different channel width, W_{ch} of 50μm, 100μm, 150μm and 200μm. The results of ΔT_y for correlation and simulation were obtained respectively based on the following two equations:

- $$\Delta \mathrm{T_{y,corr}} = \mathrm{R_y} \cdot \mathrm{q''} \cdot \mathrm{NyW} \tag{7.16}$$

$$\Delta T_{y,simu} = T_{y,max} - T_{f,in} \tag{7.17}$$

where $T_{y,max}$ is the local maximum temperature long flow direction obtained by simulation.

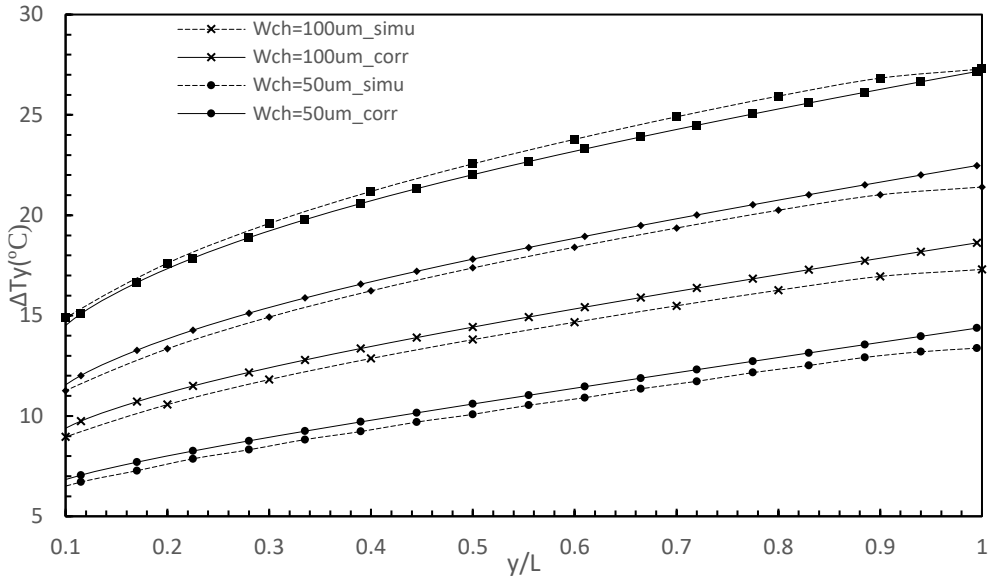


Figure 7-3 The comparison of ΔT_y for DL-MCHS with different W_{ch}.

It can also be seen in Figure 7-3 that value of $\Delta T_{y,,corr}$ is very close to the value of $\Delta T_{y,simu}$ for different values of W_{ch}. This indicates that the proposed correlated R_y may be employed to predict the temperature distributions along the flow direction for DL-MCHS

7.4 Nu correlation for tapered MCHS.

The following genialized correlation for local Nusselt number as a function of axial distance and channel outlet width is generated for different channel inlet width of 50μm, 100μm, 150μm and 200μm.through MATLAB curve fitting function. The constants used in Equation (7.18) are shown in

Table *7-1*. Good R^2 of 0.9837, 0.9774, 0.9805 and 0.9802 is found for W_i of 50μm, 100μm, 150μm and 200μ, respectively. Good agreement can be found in the comparison of generated local Nu through simulation and correlated local Nu for different W_i as shown in Figure 7-4 to Figure 7-7.

$$Nu_y = c_1 + c_2x + c_3y + c_4x^2 + c_5xy + c_6y^2 + c_7x^3 + c_8x^2y + c_9xy^2 + c_{10}x^4 + c_{11}x^3y + c_{12}x^2y^2 + c_{13}x^5 + c_{14}x^4y + c_{15}x^3y^2 \quad (7.18)$$

Table 7-1 The constant used in Eq. (7.18) for different W_i and corresponding R^2.

$\mathbf{W_i}$(μm)	$\mathbf{c_1}$	$\mathbf{c_2}$	$\mathbf{c_3}$	$\mathbf{c_4}$	$\mathbf{c_5}$	$\mathbf{c_6}$
50	3.02E+01	-3.15E-02	-1.10E-02	1.47E-05	-3.33E-06	3.68E-05
100	5.53E+00	-1.70E-02	3.90E-01	1.19E-05	-2.48E-04	-1.23E-03
150	1.28E-02	-1.11E-02	3.87E-01	9.63E-06	-2.68E-04	-1.01E-03
200	3.44E+00	-1.06E-02	2.38E-01	8.30E-06	-1.91E-04	-3.41E-04

$\mathbf{W_i}$	c_7	c_8	c_9	c_{10}	c_{11}	c_{12}
50	-3.02E-09	-1.03E-09	1.87E-08	2.82E-13	1.48E-13	-7.81E-14
100	-2.88E-09	5.23E-08	7.12E-07	2.94E-13	-4.42E-12	-1.24E-10
150	-2.54E-09	6.28E-08	5.97E-07	2.74E-13	-6.00E-12	-1.08E-10
200	-2.19E-09	5.23E-08	2.30E-07	2.40E-13	-5.70E-12	-4.91E-11

$\mathbf{W_i}$	c_{13}	c_{14}	c_{15}	R^2
50	-9.79E-18	-5.74E-18	-4.41E-17	0.9837
100	-1.07E-17	1.11E-16	7.10E-15	0.9774
150	-1.03E-17	1.82E-16	6.44E-15	0.9805
200	-9.14E-18	1.97E-16	3.44E-15	0.9802

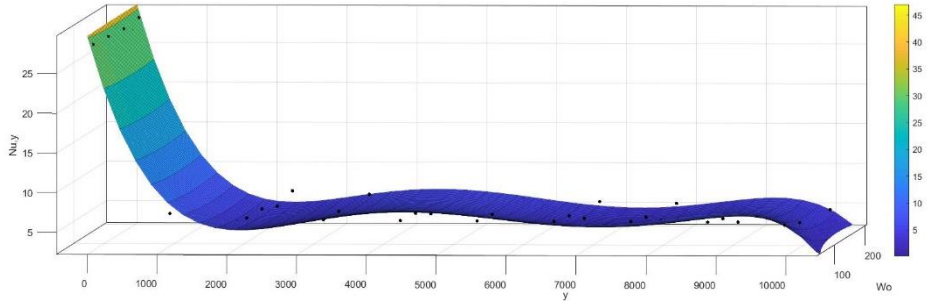


Figure 7-4 The comparison between generated and correlated Nu_y for W_i=50μm.

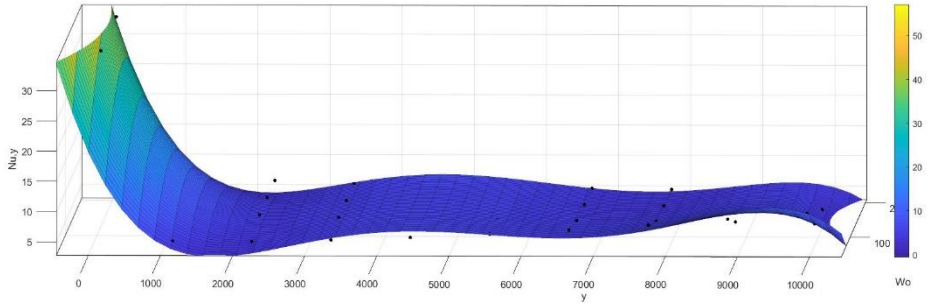


Figure 7-5 The comparison between generated and correlated Nu_y for W_i=100μm.

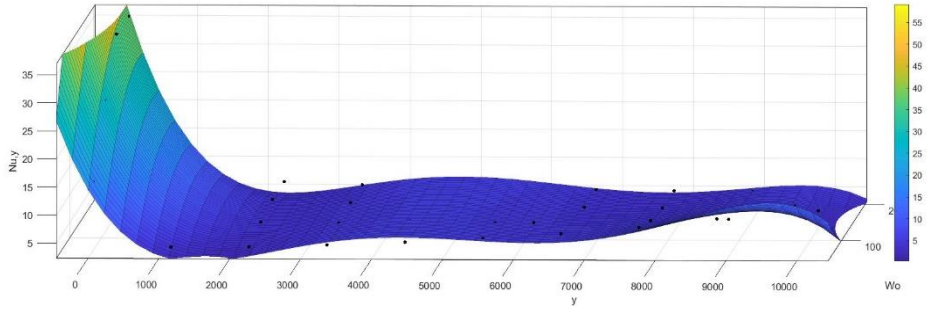


Figure 7-6 The comparison between generated and correlated Nu_y for W_i=150μm.

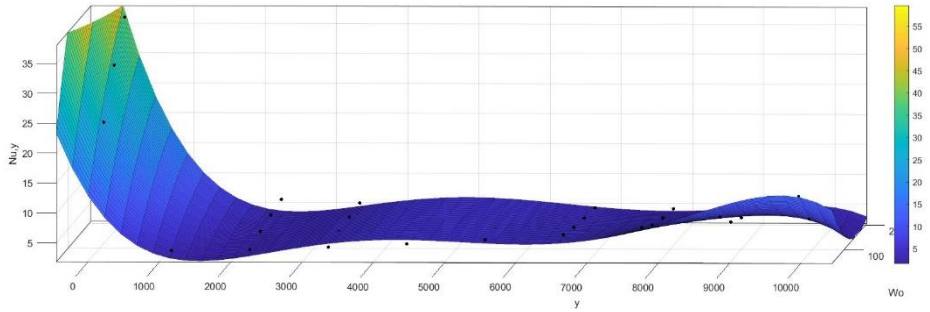


Figure 7-7 The comparison between generated and correlated Nu_y for W_i=200μm.

7.5 Conclusion

In present study, a thermal resistance network for DL-MCHS has been obtained. Modification has been carried on an existing thermal resistance network by imposing Delta-wye conversion. A correlation has been obtained from the modified thermal resistance network and solved to predict the local mean thermal resistance. Compared with ΔT_y obtained through numerical simulation results, the results of the proposed correlation results show good agreement, which indicates that this correlation could be used to predict the local temperature along the flow direction for DL-MCHS with different channel width. At last, the corelation of local Nu in terms of axial distance and channel outlet width for different channel inlet width has been proposed. Good agreement between generated and correlated local Nu was found and Good R^2 of 0.9837, 0.9774, 0.9805 and 0.9802 is found for W_i of 50μm, 100μm, 150μm and 200μm.

Chapter 8. Conclusion and recommendation for future work

8.1 Conclusion

The present study focusing on improving the heat transfer performance for microchannel heat sink and trying to find the design with best thermal-hydraulic performance. In order to achieve this, a novel multi-layered MCHS with tapered channel profile and with different flow configurations has been proposed. The numerical method used to solve 3D conjugate model and governing equations in this study is the finite element method built in Ansys Fluent software. Validations of previous experimental and numerical work and grid independence test has been conducted to ensure the accuracy of the numerical results. The thermal and hydraulic performance for each flow configuration was numerically investigated for 8 different channel designs at Re ranging from 100-1000. Then the parametric study has been conducted to evaluate the effect of different design parameters on thermal and hydraulic performance at fixed volumetric flow rate. The design with best thermal-hydraulic performance has been chosen based on Figure of Merit (FOM). For both double and three layered MCHS, the parallel flow design always presents better thermal-hydraulic performance as compared to counter flow designs. Hence, the thermal resistance network based on DL-MCHS with parallel flow has been proposed. Based on numerical results, the tapered channel design shows great improvement in thermal and thermal-hydraulic performance as compared with straight channel design, which provides an excellent solution for high-density integrated circuits' heat-dissipation problem. The details of major findings are listed below:

For DL-MCHS with parallel and counter flow:

- The DL-MCHS with converging channel design presents higher Nu as compared with straight channel design with same W_o, the increment of Nu for design 2,3 and 4 compares to design 1 is 22.48%, 38.34% and 49.38% for parallel flow and 33.69%, 57.03% and 71.74%

for counter flow when Re=100, respectively.

- The DL-MCHS with diverging channel design presents higher Nu as compared with straight channel design with same W_i. For diverging designs in both flow configurations, the increment of Nu for design 5,6 and 7 compares to design 8 is 10.62%, 11.11% and 8.02% for parallel flow and 10.62%, 11.11, 7.72% for counter flow when Re=1000, respectively.

- Based on the performance of overall thermal resistance alone, the optimal geometrical design of DL-MCHS has lowest value of W_o and W_i and highest value of H_c i.e., $W_i = W_o = 400\mu m$, $H_{ch} = 400\mu m$.
- The designs with counter flow configuration always have better thermal performance than the designs with parallel flow configuration when Q is large and the difference become more significant with the decrease of W_i, the maximum difference of 0.05K/W (21.67%) can be found at design with $W_i = 50\mu m$ $W_o = 200\mu m$ at $H_{ch} = 375\mu m$.
- The design with counter flow configuration has better temperature uniformity compare to the design with parallel flow configuration based on the temperature along the base surface.
- The effect of H_{ch} on thermal performance is small.
- The DL-MCHS with parallel flow always shows better thermal-hydraulic performance as compared with counter flow with exact channel dimensions, maximum difference of 0.12 (12.13%) is found between parallel and counter flow configuration for design with W_i=50μm W_o=50μm.

- For the optimization of thermal-hydraulic performance (considering both thermal resistance and pumping power), the design with W_i=150μm and W_o=200μm presents the highest value of FOM (1.68 for PF and 1.55 for CF) and design with W_i=50μm and W_o=50μm presents the lowest value (1 for PF and 0.88 for CF).

For DL-MCHS with alternating flow:

- The R_t decreases and $\triangle P$ increases with the increase of Re.

- For diverging designs, the Nu increases up to 37.45%, 63.71% and 81.56% for design 5,6 and 7 as compared to straight channel design with same W_i of 50μm for Re=100, respectively.
- For converging design, the Nu increase up to 13.94%, 12.6% and 8.78% for design 2,3,4 as compared to the straight channel design with same W_o of 50μm for Re=1000.
- The design with small inlet channel width or outlet channel width gives lower thermal resistance but results in high pressure drop.
- The DL-MCHS with alternating flow configuration shows better thermal performance (lower thermal resistance) for the case of higher channel inlet size or smaller channel outlet size as compared to the DL-MCHS with parallel flow configuration.
- The DL-MCHS with alternating flow configuration shows largely similar results of thermal resistance as compared to the DL-MCHS with counter flow configuration
- The DL-MCHS with alternating flow design with small inlet channel width or small outlet channel width gives better temperature uniformity. The optimum DL-MCHS with alternating flow with channel design has the lowest temperature difference of 3.297°C.
- The optimum DL-MCHS with alternating flow and tapered channel show about 76% better in thermo-hydraulic performance as compared with benchmark of DL-MCHS with straight channel design with inlet and outlet channel size of $50\mu m$.

For three-layered MCHS:

- For low value of channel inlet size (converging channel profile) in three-layered MCHS, CF1 flow configuration gives the lowest value of R_t
- For high value of channel inlet size (converging channel profile), parallel flow configuration gives the lowest value of R_t
- The counter flow configuration alters the temperature variation pattern of the parallel flow by moving the peak temperature location toward the center of the channel, giving better temperature uniformity.

- The three-layered MCHS with CF1 flow configuration demonstrate best temperature uniformity with lowest peak temperature for the case of straight and converging channel profile.
- The three-layered MCHS design with W_i=150μm and W_o=200μm has best thermal-hydraulic performance and optimum design shows about 69%,75%,76% and 77% better in thermal-hydraulic performance for PF, CF1, CF2 and CF3 as compared with base case, respectively.
- The PF shows better thermal-hydraulic performance and the enhancement can up to 14.41%,14.81% and 11.72% as compared with CF1, CF2 and CF3, respectively.

For correlation for multi-layered MCHS:

- Good agreement of was ΔT_y found between proposed correlation results and generated numerical simulation results, which indicates that this correlation could be used predict the local temperature along the flow direction for DL-MCHS with different channel width.
- The correlation of local Nusselt in terms of axial distance and channel outlet width for different channel inlet width has been proposed. Good agreement between generated and correlation local Nusselt was found and Good R^2 of 0.9837, 0.9774, 0.9805 and 0.9802 was found for W_i of 50μm, 100μm, 150μm and 200μm.

8.2 Future work

The future work possibilities are lister in this section:

1. This study is focusing on numerical investigation only, the experimental study can be conducted and compared with the existing numerical study.
2. From literature review, it's clear that the experimental work for multi-layered MCHS is limited. The challenge is mainly due to difficult of manufacturing single layered MCHS with complex shape

in good precision and the method to stack single-layered MCHS to multi-layered MCHS without much heat loss between layers. Hence, the technique to manufacture the heat sink and method to stack layers need to be explored.

3. In present study, for all cases investigated, each channel has exactly same geometry and inlet velocity. The numerical study on multi-layered MCHS with different channel dimensions and/or with different inlet velocity between layers can be conducted. The parametric study can be conducted to find the design with best thermal-performance.

4. In present study, the substrate material used is silicon and coolant used is water. More substrate materials (phase change material, porous medium or combination of these two) and more coolant types (different nanofluids) can be applied.

5. The current study proposed the correlation of thermal resistance network for multi-layered MCHS with parallel flow configuration and with tapered channel design. It uses the fin theory and assumed that the heat transferred from channel bottom surface to top surface and from inlet to outlet, which is not applicable for counter/alternating flow configurations due to the flow direction difference. Hence, a new correlation based on multi-layered MCHS with counter/alternating flow can be conducted.

Reference

[1] G. Moore, “Moore’s Law, Electronics,” *Electronics*, vol. 38, no. 8, p. 114, 1965,

[2] A. Hales and X. Jiang, “A review of piezoelectric fans for low energy cooling of power electronics,” *Appl. Energy*, vol. 215, no. January, pp. 321–337, 2018,

[3] H. Li *et al.*, “A comprehensive review of heat transfer enhancement and flow characteristics in the concentric pipe heat exchanger,” *Powder Technol.*, vol. 397, p. 117037, 2022,

[4] X. Wang *et al.*, “A review on data centre cooling system using heat pipe technology,” *Sustain. Comput. Informatics Syst.*, vol. 35, no. September 2019, p. 100774, 2022,

[5] D. B. Tuckerman and R. F. W. Pease, “High-Performance Heat Sinking for VLSI,” *IEEE Electron Device Lett.*, vol. EDL-2, no. 5, pp. 126–129, 1981,

[6] W. Qu and I. Mudawar, “Experimental and numerical study of pressure drop and heat transfer in a single-phase micro-channel heat sink,” *Int. J. Heat Mass Transf.*, vol. 45, no. 12, pp. 2549–2565, 2002,

[7] K. Vafai and L. Zhu, “Analysis of two-layered micro-channel heat sink concept in electronic cooling,” *Int. J. Heat Mass Transf.*, vol. 42, no. 12, pp. 2287–2297, 1999,

[8] S. G. Kandlikar and W. J. Grande, “Evolution of microchannel flow passages-thermohydraulic performance and fabrication technology,” *Heat Transf. Eng.*, vol. 24, no. 1, pp. 3–17, 2003,

[9] W. A. L. Peiyi Wu, “Measurement of friction factors for the flow of gases in very fine channels used for microminiature Joule-Thomson refrigerators,” *Cryogenics (Guildf).*, vol. 23, no. 5, pp. 273–277, 1983,

[10] W. A. L. Peiyi Wu, “Measurement of the heat transfer characteristics of gas flow in fine channel heat exchangers used for microminiature refrigerators,” *Cryogenics (Guildf).*, vol. 24, no. 8, pp. 415–420, 1984,

[11] P. S. Lee, S. V. Garimella, and D. Liu, “Investigation of heat transfer in rectangular

microchannels," *Int. J. Heat Mass Transf.*, vol. 48, no. 9, pp. 1688–1704, 2005,

[12] J. Zhou, X. Chen, Q. Zhao, M. Lu, D. Hu, and Q. Li, "Flow thermohydraulic characterization of hierarchical-manifold microchannel heat sink with uniform flow distribution," *Appl. Therm. Eng.*, vol. 198, no. April, p. 117510, 2021,

[13] A. J. Shkarah, M. Y. Bin Sulaiman, M. R. B. H. Ayob, and H. Togun, "A 3D numerical study of heat transfer in a single-phase micro-channel heat sink using graphene, aluminum and silicon as substrates," *Int. Commun. Heat Mass Transf.*, vol. 48, pp. 108–115, 2013,

[14] M. M. Mansoor, K. C. Wong, and M. Siddique, "Numerical investigation of fluid flow and heat transfer under high heat flux using rectangular micro-channels," *Int. Commun. Heat Mass Transf.*, vol. 39, no. 2, pp. 291–297, 2012,

[15] D. Deng, W. Wan, Y. Tang, Z. Wan, and D. Liang, "Experimental investigations on flow boiling performance of reentrant and rectangular microchannels - A comparative study," *Int. J. Heat Mass Transf.*, vol. 82, pp. 435–446, 2015,

[16] R. Zheng, Y. Wu, Y. Li, G. Wang, G. Ding, and Y. Sun, "Development of a hierarchical microchannel heat sink with flow field reconstruction and low thermal resistance for high heat flux dissipation," *Int. J. Heat Mass Transf.*, vol. 182, 2022,

[17] J. Pandey, A. Husain, M. Zahid Ansari, and N. Al-Azri, "Comparison of the parallel microchannel and Pin-Fin heat Sinks: An experimental study," *Mater. Today Proc.*, vol. 56, pp. 845–850, 2022,

[18] X. Ji, X. Yang, Y. Zhang, Y. Zhang, and J. Wei, "Experimental study of ultralow flow resistance fractal microchannel heat sinks for electronics cooling," *Int. J. Therm. Sci.*, vol. 179, no. April, p. 107723, 2022,

[19] F. Zhang, B. Wu, and B. Du, "Heat transfer optimization based on finned microchannel heat sink," *Int. J. Therm. Sci.*, vol. 172, no. November 2021, 2022,

[20] M. Parlak, A. Özsunar, and A. Koşar, "High aspect ratio microchannel heat sink optimization

under thermally developing flow conditions based on minimum power consumption," *Appl. Therm. Eng.*, vol. 201, no. May 2021, 2022,

[21] L. Zeng, D. Deng, N. Zhong, and G. Zheng, "Thermal and flow performance in microchannel heat sink with open-ring pin fins," *Int. J. Mech. Sci.*, vol. 200, no. April, p. 106445, 2021,

[22] M. J. Kohl, S. I. Abdel-Khalik, S. M. Jeter, and D. L. Sadowski, "An experimental investigation of microchannel flow with internal pressure measurements," *Int. J. Heat Mass Transf.*, vol. 48, no. 8, pp. 1518–1533, 2005,

[23] H. Y. Wu and P. Cheng, "An experimental study of convective heat transfer in silicon microchannels with different surface conditions," *Int. J. Heat Mass Transf.*, vol. 46, no. 14, pp. 2547–2556, 2003,

[24] Q. Weilin, G. M. Mala, and L. Dongqing, "Hydraulic diameter Confirmation of Trapezoidal channel.pdf," vol. 43, 2000.

[25] W. Qu, G. M. Mala, and D. Li, "Heat transfer for water flow in trapezoidal silicon microchannels," *Int. J. Heat Mass Transf.*, vol. 43, no. 21, pp. 3925–3936, 2000,

[26] G. Wang, D. Niu, F. Xie, Y. Wang, X. Zhao, and G. Ding, "Experimental and numerical investigation of a microchannel heat sink (MCHS) with micro-scale ribs and grooves for chip cooling," *Appl. Therm. Eng.*, vol. 85, pp. 61–70, 2015,

[27] E. M. Dede, "Optimization and design of a multipass branching microchannel heat sink for electronics cooling," *J. Electron. Packag. Trans. ASME*, vol. 134, no. 4, pp. 1–10, 2012,

[28] E. M. Dede and Y. Liu, "Experimental and numerical investigation of a multi-pass branching microchannel heat sink," *Appl. Therm. Eng.*, vol. 55, no. 1–2, pp. 51–60, 2013,

[29] X. Wei, Y. Joshi, and M. K. Patterson, "Experimental and numerical study of a stacked microchannel heat sink for liquid cooling of microelectronic devices," *J. Heat Transfer*, vol. 129, no. 10, pp. 1432–1444, 2007,

[30] B. Lu, W. J. Meng, and F. Mei, "Experimental investigation of Cu-based, double-layered,

microchannel heat exchangers," *J. Micromechanics Microengineering*, vol. 23, no. 3, 2013,

[31] G. Xia, D. Ma, Y. Zhai, Y. Li, R. Liu, and M. Du, "Experimental and numerical study of fluid flow and heat transfer characteristics in microchannel heat sink with complex structure," *Energy Convers. Manag.*, vol. 105, pp. 848–857, 2015,

[32] Z. Dai, Z. Zheng, D. F. Fletcher, and B. S. Haynes, "Experimental study of transient behaviour of laminar flow in zigzag semi-circular microchannels," *Exp. Therm. Fluid Sci.*, vol. 68, pp. 644–651, 2015,

[33] V. S. Duryodhan, S. G. Singh, and A. Agrawal, "Liquid flow through converging microchannels and a comparison with diverging microchannels," *J. Micromechanics Microengineering*, vol. 24, no. 12, 2014,

[34] V. S. Duryodhan, A. Singh, S. G. Singh, and A. Agrawal, "Convective heat transfer in diverging and converging microchannels," *Int. J. Heat Mass Transf.*, vol. 80, pp. 424–438, 2015,

[35] V. S. Duryodhan, A. Singh, S. G. Singh, and A. Agrawal, "A simple and novel way of maintaining constant wall temperature in microdevices," *Sci. Rep.*, vol. 6, no. October 2015, pp. 1–15, 2016,

[36] A. Monavari, J. Jamaati, and M. Bahiraei, "Thermohydraulic performance of a nanofluid in a microchannel heat sink: Use of different microchannels for change in process intensity," *J. Taiwan Inst. Chem. Eng.*, vol. 125, pp. 1–14, 2021,

[37] M. R. Sohel, R. Saidur, M. F. M. Sabri, M. Kamalisarvestani, M. M. Elias, and A. Ijam, "Investigating the heat transfer performance and thermophysical properties of nanofluids in a circular micro-channel," *Int. Commun. Heat Mass Transf.*, vol. 42, pp. 75–81, 2013,

[38] W. Ling, W. Zhou, C. Liu, F. Zhou, D. Yuan, and J. Huang, "Structure and geometric dimension optimization of interlaced microchannel for heat transfer performance enhancement," *Appl. Therm. Eng.*, vol. 170, no. January, p. 115011, 2020,

[39] G. D. Xia, J. Jiang, J. Wang, Y. L. Zhai, and D. D. Ma, “Effects of different geometric structures on fluid flow and heat transfer performance in microchannel heat sinks,” *Int. J. Heat Mass Transf.*, vol. 80, pp. 439–447, 2015,

[40] M. Balaj, E. Roohi, and H. Akhlaghi, “Effects of shear work on non-equilibrium heat transfer characteristics of rarefied gas flows through micro/nanochannels,” *Int. J. Heat Mass Transf.*, vol. 83, pp. 69–74, 2015,

[41] M. Ghasemian, Z. Najafian Ashrafi, M. Goharkhah, and M. Ashjaee, “Heat transfer characteristics of Fe3O4 ferrofluid flowing in a mini channel under constant and alternating magnetic fields,” *J. Magn. Magn. Mater.*, vol. 381, pp. 158–167, 2015,

[42] M. Pan, Y. Tang, L. Pan, and L. Lu, “Optimal design of complex manifold geometries for uniform flow distribution between microchannels,” *Chem. Eng. J.*, vol. 137, no. 2, pp. 339–346, 2008,

[43] Q. Zhu *et al.*, “Heat transfer enhancement for microchannel heat sink by strengthening fluids mixing with backward right-angled trapezoidal grooves in channel sidewalls,” *Int. Commun. Heat Mass Transf.*, vol. 135, no. May, p. 106106, 2022,

[44] Q. Zhu, R. Su, H. Xia, J. Zeng, and J. Chen, “Numerical simulation study of thermal and hydraulic characteristics of laminar flow in microchannel heat sink with water droplet cavities and different rib columns,” *Int. J. Therm. Sci.*, vol. 172, no. PB, p. 107319, 2022,

[45] Z. Zhan *et al.*, “Numerical study on heat transfer enhancement by viscoelastic fluid pulsating laminar flow in rectangular microchannel heat sinks,” *Appl. Therm. Eng.*, vol. 213, no. December 2021, p. 118734, 2022,

[46] Y. Cheng *et al.*, “Multi-objective optimization of thermal-hydraulic performance in a microchannel heat sink with offset ribs using the fuzzy grey approach,” *Appl. Therm. Eng.*, vol. 201, no. PA, p. 117748, 2022,

[47] R. A and S. Chakraborty, “Estimation of the thermohydraulic performance of a microchannel heat sink with gradual and sudden variation of the flow passage,” *Int. J. Heat Mass Transf.*,

vol. 190, p. 122776, 2022,

[48] X. Liu *et al.*, “Thermal and hydraulic performances of the wavy microchannel heat sink with fan-shaped ribs on the sidewall,” *Int. J. Therm. Sci.*, vol. 179, no. February, p. 107688, 2022,

[49] H. A. Kose, A. Yildizeli, and S. Cadirci, “Parametric study and optimization of microchannel heat sinks with various shapes,” *Appl. Therm. Eng.*, vol. 211, no. March, p. 118368, 2022,

[50] H. Bhatt, H. Bist, H. Gola, and M. Zunaid, “Variation of heat transfer characteristics of a microchannel heat sink with geometry,” *Mater. Today Proc.*, vol. 56, pp. 936–942, 2022,

[51] J. Zhou, M. Lu, Q. Zhao, D. Hu, H. Qin, and X. Chen, “Thermal design of microchannel heat sinks using a contour extraction based on topology optimization (CEBTO) method,” *Int. J. Heat Mass Transf.*, vol. 189, p. 122703, 2022,

[52] Y. Pan, R. Zhao, Y. Nian, and W. Cheng, “Study on the flow and heat transfer characteristics of pin-fin manifold microchannel heat sink,” *Int. J. Heat Mass Transf.*, vol. 183, 2022,

[53] M. Jamshidmofid and M. Bahiraei, “Thermohydraulic assessment of a novel hybrid nanofluid containing cobalt oxide-decorated reduced graphene oxide nanocomposite in a microchannel heat sink with sinusoidal cavities and rectangular ribs,” *Int. Commun. Heat Mass Transf.*, vol. 131, no. December 2021, p. 105769, 2022,

[54] M. Khan, S. Z. Shuja, B. S. Yilbas, and H. Al-Qahtani, “A case study on innovative design and assessment of a microchannel heat sink with various turbulators arrangements,” *Case Stud. Therm. Eng.*, vol. 31, no. January, p. 101816, 2022,

[55] M. R. Hajmohammadi, M. Bahrami, and M. Ahmadian-Elmi, “Thermal performance improvement of microchannel heat sinks by utilizing variable cross-section microchannels filled with porous media,” *Int. Commun. Heat Mass Transf.*, vol. 126, no. May, p. 105360, 2021,

[56] D. Ansari and J. H. Jeong, “A silicon-diamond microchannel heat sink for die-level hotspot thermal management,” *Appl. Therm. Eng.*, vol. 194, no. May, p. 117131, 2021,

[57] S. D. Farahani, A. D. Farahani, and E. Hajian, “Effect of PCM and porous media/nanofluid on the thermal efficiency of microchannel heat sinks,” *Int. Commun. Heat Mass Transf.*, vol. 127, p. 105546, 2021,

[58] A. M. Ali, M. Angelino, and A. Rona, “Numerical analysis on the thermal performance of microchannel heat sinks with Al2O3 nanofluid and various fins,” *Appl. Therm. Eng.*, vol. 198, no. August, p. 117458, 2021,

[59] M. Mieczkowski, P. Furmański, and P. Łapka, “Optimization of a microchannel heat sink using entropy minimization and genetic aggregation algorithm,” *Appl. Therm. Eng.*, vol. 191, no. September 2020, 2021,

[60] S. Pourhammati and S. Hossainpour, “Improving the hydrothermal characteristics of wavy microchannel heat sink by modification of wavelength and wave amplitude,” *Int. Commun. Heat Mass Transf.*, vol. 130, no. November 2021, p. 105805, 2022,

[61] J. Qiu, J. Zhou, Q. Zhao, H. Qin, and X. Chen, “Numerical investigation of flow boiling characteristics in cobweb-shaped microchannel heat sink,” *Case Stud. Therm. Eng.*, vol. 28, no. October, p. 101677, 2021,

[62] A. M. Ali, A. Rona, H. T. Kadhim, M. Angelino, and S. Gao, “Thermo-hydraulic performance of a circular microchannel heat sink using swirl flow and nanofluid,” *Appl. Therm. Eng.*, vol. 191, no. March, p. 116817, 2021,

[63] S. Liu, W. Xie, Q. Wang, Y. Liu, and N. Hu, “Thermal performance of a central-jetting microchannel heat sink designed for a high-power laser crystal,” *Int. J. Heat Mass Transf.*, vol. 185, p. 122409, 2022,

[64] M. S. Lori and K. Vafai, “Heat transfer and fluid flow analysis of microchannel heat sinks with periodic vertical porous ribs,” *Appl. Therm. Eng.*, vol. 205, no. December 2021, p. 118059, 2022,

[65] Q. Zhu *et al.*, “Fluid flow and heat transfer characteristics of microchannel heat sinks with different groove shapes,” *Int. J. Therm. Sci.*, vol. 161, no. October 2020, p. 106721, 2021,

[66] Q. Zhu *et al.*, “Computational study of rib shape and configuration for heat transfer and fluid flow characteristics of microchannel heat sinks with fan-shaped cavities,” *Appl. Therm. Eng.*, vol. 195, no. May, p. 117171, 2021,

[67] Q. Zhu *et al.*, “Characteristics of heat transfer and fluid flow in microchannel heat sinks with rectangular grooves and different shaped ribs,” *Alexandria Eng. J.*, vol. 59, no. 6, pp. 4593–4609, 2020,

[68] S. L. Wang *et al.*, “Heat transfer enhancement of symmetric and parallel wavy microchannel heat sinks with secondary branch design,” *Int. J. Therm. Sci.*, vol. 171, no. October 2020, 2022,

[69] Y. Alihosseini, M. Zabetian Targhi, and M. Mahdi Heyhat, “Thermo-hydraulic performance of wavy microchannel heat sink with oblique grooved finned,” *Appl. Therm. Eng.*, vol. 189, no. February, p. 116719, 2021,

[70] J. F. Zhong, S. N. Sedeh, Y. P. Lv, B. Arzani, and D. Toghraie, “Investigation of Ferro-nanofluid flow within a porous ribbed microchannel heat sink using single-phase and two-phase approaches in the presence of constant magnetic field,” *Powder Technol.*, vol. 387, pp. 251–260, 2021,

[71] F. Liu and D. Jing, “Hydrothermal performances of symmetric and asymmetric divergent-convergent microchannel heat sinks,” *Int. Commun. Heat Mass Transf.*, vol. 127, no. August, p. 105566, 2021,

[72] J. Pfahler, J. Harley, H. Bau, and J. N. Zemel, “Gas and liquid flow in small channels,” *Am. Soc. Mech. Eng. Dyn. Syst. Control Div. DSC*, vol. 32, no. June 2016, pp. 49–60, 1991.

[73] J. Harley and H. Bau, “Channels Liquid,” 1989.

[74] B. Xu, K. T. Ooi, N. T. Wong, and W. K. Choi, “Experimental investigation of flow friction for liquid flow in microchannels,” *Int. Commun. Heat Mass Transf.*, vol. 27, no. 8, pp. 1165–1176, 2000,

[75] D. Deng, Y. Tang, D. Liang, H. He, and S. Yang, “Flow boiling characteristics in porous heat

sink with reentrant microchannels," *Int. J. Heat Mass Transf.*, vol. 70, pp. 463–477, 2014,

[76] T. Hung, W. Yan, and W. Li, "Analysis of heat transfer characteristics of double-layered microchannel heat sink," *Int. J. Heat Mass Transf.*, vol. 55, no. 11–12, pp. 3090–3099, 2012,

[77] K. C. Wong and F. N. A. Muezzin, "Heat transfer of a parallel flow two-layered microchannel heat sink," *Int. Commun. Heat Mass Transf.*, vol. 49, pp. 136–140, 2013,

[78] M. L. Levac, H. M. Soliman, and S. J. Ormiston, "Three-dimensional analysis of fluid flow and heat transfer in single- and two-layered micro-channel heat sinks," pp. 1375–1383, 2008.

[79] G. Xie, Y. Liu, B. Sunden, and W. Zhang, "Computational Study and Optimization of Laminar Heat Transfer and Pressure Loss of Double-Layer Microchannels for Chip Liquid Cooling," *J. Therm. Sci. Eng. Appl.*, vol. 5, no. 1, pp. 1–9, 2013,

[80] H. Shen, Y. Zhang, C. Wang, and G. Xie, "Comparative study for convective heat transfer of counter- flow wavy double-layer microchannel heat sinks in staggered arrangement," *Appl. Therm. Eng.*, vol. 137, no. January, pp. 228–237, 2018,

[81] H. Shen, G. Xie, and C. Wang, "Thermal performance and entropy generation of novel X-structured double layered microchannel heat sinks," *J. Taiwan Inst. Chem. Eng.*, vol. 111, pp. 90–104, 2020,

[82] H. Shen, G. Xie, and C. Wang, "Heat transfer and thermodynamic analysis by introducing multiple alternation structures into double-layer microchannel heat sinks," *Int. J. Therm. Sci.*, vol. 145, no. February, p. 105975, 2019,

[83] H. Shen, G. Xie, and C. Wang, "The numerical simulation with staggered alternation locations and multi- fl ow directions on the thermal performance of double-layer microchannel heat sinks," *Appl. Therm. Eng.*, vol. 163, no. March, p. 114332, 2019,

[84] T. C. Hung, W. M. Yan, X. D. Wang, and Y. X. Huang, "Optimal design of geometric parameters of double-layered microchannel heat sinks," *Int. J. Heat Mass Transf.*, vol. 55, no. 11–12, pp. 3262–3272, 2012,

[85] L. Lin, Y. Y. Chen, X. X. Zhang, and X. D. Wang, “Optimization of geometry and flow rate distribution for double-layer microchannel heat sink,” *Int. J. Therm. Sci.*, vol. 78, pp. 158–168, 2014,

[86] S. Chamoli, R. Lu, H. Chen, Y. Cheng, and P. Yu, “Numerical optimization of design parameters for a modified double-layer microchannel heat sink,” *Int. J. Heat Mass Transf.*, vol. 138, pp. 373–389, 2019,

[87] C. Leng, X. D. Wang, T. H. Wang, and W. M. Yan, “Optimization of thermal resistance and bottom wall temperature uniformity for double-layered microchannel heat sink,” *Energy Convers. Manag.*, vol. 93, pp. 141–150, 2015,

[88] K. Kulkarni, A. Afzal, and K. Y. Kim, “Multi-objective optimization of a double-layered microchannel heat sink with temperature-dependent fluid properties,” *Appl. Therm. Eng.*, vol. 99, pp. 262–272, 2016,

[89] C. Leng, X. D. Wang, T. H. Wang, and W. M. Yan, “Multi-parameter optimization of flow and heat transfer for a novel double-layered microchannel heat sink,” *Int. J. Heat Mass Transf.*, vol. 84, pp. 359–369, 2015,

[90] K. Derakhshanpour, R. Kamali, and M. Eslami, “Improving performance of single and double-layered microchannel heat sinks by cylindrical ribs: A numerical investigation of geometric parameters,” *Int. Commun. Heat Mass Transf.*, vol. 126, p. 105440, 2021,

[91] Y. Zhai, G. Xia, Z. Li, and H. Wang, “A novel flow arrangement of staggered flow in double-layered microchannel heat sinks for microelectronic cooling,” *Int. Commun. Heat Mass Transf.*, vol. 79, pp. 98–104, 2016,

[92] C. Leng, X. D. Wang, and T. H. Wang, “An improved design of double-layered microchannel heat sink with truncated top channels,” *Appl. Therm. Eng.*, vol. 79, pp. 54–62, 2015,

[93] D. Debbarma, K. M. Pandey, and A. Paul, “Numerical study on double layered micro channel heat sink with partly diverged channel in top layer,” *Mater. Today Proc.*, vol. 45, pp. 6542–6546, 2020,

[94] S. Wang, X. Li, X. Wang, and G. Lu, “Flow and heat transfer characteristics in double-layered microchannel heat sinks with porous fi ns,” *Int. Commun. Heat Mass Transf.*, vol. 93, no. March, pp. 41–47, 2018,

[95] A. Ghahremannezhad, H. Xu, M. Alhuyi, M. Hossein, and K. Vafai, “Effect of porous substrates on thermohydraulic performance enhancement of double layer microchannel heat sinks,” *Int. J. Heat Mass Transf.*, vol. 131, pp. 52–63, 2019,

[96] X. Li, S. Wang, X. Wang, and T. Wang, “Selected porous-ribs design for performance improvement in double-layered microchannel heat sinks,” *Int. J. Therm. Sci.*, vol. 137, no. November 2018, pp. 616–626, 2019,

[97] T. Wang, H. Wu, J. Meng, and W. Yan, “Optimization of a double-layered microchannel heat sink with semi-porous-ribs by multi-objective genetic algorithm,” vol. 149, 2020,

[98] T. C. Hung and W. M. Yan, “Enhancement of thermal performance in double-layered microchannel heat sink with nanofluids,” *Int. J. Heat Mass Transf.*, vol. 55, no. 11–12, pp. 3225–3238, 2012,

[99] M. R. Hajmohammadi and I. Toghraei, “Optimal design and thermal performance improvement of a double-layered microchannel heat sink by introducing Al 2 O 3 nano-particles into the water,” *Physica A*, vol. 505, pp. 328–344, 2018,

[100] A. Sakanova, S. Yin, J. Zhao, J. M. Wu, and K. C. Leong, “Optimization and comparison of double-layer and double-side micro-channel heat sinks with nanofluid for power electronics cooling,” *Appl. Therm. Eng.*, vol. 65, no. 1–2, pp. 124–134, 2014,

[101] H. E. Ahmed, M. I. Ahmed, I. M. F. Seder, and B. H. Salman, “Experimental investigation for sequential triangular double-layered microchannel heat sink with nanofluids,” *Int. Commun. Heat Mass Transf.*, vol. 77, pp. 104–115, 2016,

[102] S. Sarvar-ardeh, R. Rafee, and S. Rashidi, “Hybrid nano fluids with temperature-dependent properties for use in double-layered microchannel heat sink ; hydrothermal investigation,” *J. Taiwan Inst. Chem. Eng.*, vol. 124, pp. 53–62, 2021,

[103] A. A. A. Arani *et al.*, “Heat transfer improvement of water/single-wall carbon nanotubes (SWCNT) nanofluid in a novel design of a truncated double-layered microchannel heat sink,” *Int. J. Heat Mass Transf.*, vol. 113, pp. 780–795, 2017,

[104] Y. Zhai, Z. Li, H. Wang, and J. Xu, “Thermodynamic analysis of the effect of channel geometry on heat transfer in double-layered microchannel heat sinks,” *Energy Convers. Manag.*, vol. 143, pp. 431–439, 2017,

[105] Y. Zhai, Z. Li, H. Wang, and J. Xu, “Analysis of field synergy principle and the relationship between secondary flow and heat transfer in double-layered microchannels with cavities and ribs,” *Int. J. Heat Mass Transf.*, vol. 101, pp. 190–197, 2016,

[106] Y. L. Zhai, G. D. Xia, X. F. Liu, and J. Wang, “Characteristics of entropy generation and heat transfer in double-layered micro heat sinks with complex structure,” *Energy Convers. Manag.*, vol. 103, pp. 477–486, 2015,

[107] K. C. Wong and M. L. Ang, “Thermal hydraulic performance of a double-layer microchannel heat sink with channel contraction,” *Int. Commun. Heat Mass Transf.*, vol. 81, pp. 269–275, 2017,

[108] D. Debbarma, K. M. Pandey, and A. Paul, “Numerical investigation on the impact of protrusions mounted on sidewalls of double layered micro channel heat sink,” *Mater. Today Proc.*, vol. 45, pp. 7001–7005, 2020,

[109] H. I. Elqady *et al.*, “Concentrator photovoltaic thermal management using a new design of double-layer microchannel heat sink,” *Sol. Energy*, vol. 220, no. April, pp. 552–570, 2021,

[110] G. Xie, Z. Chen, B. Sunden, and W. Zhang, “Numerical predictions of the flow and thermal performance of water-cooled single-layer and double-layer wavy microchannel heat sinks,” *Numer. Heat Transf. Part A Appl.*, vol. 63, no. 3, pp. 201–225, 2013,

[111] G. Xie, Z. Chen, B. Sunden, and W. Zhang, “Comparative study of the flow and thermal performance of liquid-cooling parallel-flow and counter-flow double-layer wavy microchannel heat sinks,” *Numer. Heat Transf. Part A Appl.*, vol. 64, no. 1, pp. 30–55, 2013,

[112] Y. J. Cheng, “Numerical simulation of stacked microchannel heat sink with mixing-enhanced passive structure,” *Int. Commun. Heat Mass Transf.*, vol. 34, no. 3, pp. 295–303, 2007,

[113] P. Srivastava, R. Ishwarlal, and A. Dewan, “A study on thermal characteristics of double-layered microchannel heat sink : Effects of bifurcation and flow configuration,” *Int. J. Therm. Sci.*, vol. 162, no. December 2020, p. 106791, 2021,

[114] R. K. Shah and A. L. London, “Chapter II - Differential Equations and Boundary Conditions,” R. K. Shah and A. L. B. T.-L. F. F. C. in D. London, Eds. Academic Press, 1978, pp. 5–36.

[115] P. S. Lee and S. V. Garimella, “Thermally developing flow and heat transfer in rectangular microchannels of different aspect ratios,” *Int. J. Heat Mass Transf.*, vol. 49, no. 17–18, pp. 3060–3067, 2006,

[116] F. P. Incropera, J. S. Kerby, D. F. Moffatt, and S. Ramadhyani, “Convection heat transfer from discrete heat sources in a rectangular channel,” *Int. J. Heat Mass Transf.*, vol. 29, no. 7, pp. 1051–1058, 1986,

[117] B. X. Wang and X. F. Peng, “Experimental investigation on liquid forced-convection heat transfer through microchannels,” *Int. J. Heat Mass Transf.*, vol. 37, no. SUPPL. 1, pp. 73–82, 1994,

[118] X. F. Peng and B. X. Wang, “Forced convection and flow boiling heat transfer for liquid flowing through microchannels,” *Int. J. Heat Mass Transf.*, vol. 36, no. 14, pp. 3421–3427, 1993,

[119] X. F. Peng and G. P. Peterson, “Convective heat transfer and flow friction for water flow in microchannel structures,” *Int. J. Heat Mass Transf.*, vol. 39, no. 12, pp. 2599–2608, 1996,

[120] M. Mital, “Semi-analytical investigation of electronics cooling using developing nanofluid flow in rectangular microchannels,” *Appl. Therm. Eng.*, vol. 52, no. 2, pp. 321–327, 2013,

[121] T. Yilmaz and E. Cihan, “General equation for heat transfer for laminar flow in ducts of arbitrary cross-sections,” *Int. J. Heat Mass Transf.*, vol. 36, no. 13, pp. 3265–3270, 1993,

[122] Y. Zhai, G. Xia, Z. Li, and H. Wang, “Experimental investigation and empirical correlations of single and laminar convective heat transfer in microchannel heat sinks,” *Exp. Therm. Fluid Sci.*, vol. 83, pp. 207–214, 2017,

[123] Z. Li, X. Huai, Y. Tao, and H. Chen, “Effects of thermal property variations on the liquid flow and heat transfer in microchannel heat sinks,” *Appl. Therm. Eng.*, vol. 27, no. 17–18, pp. 2803–2814, 2007,

[124] X. Wei and Y. Joshi, “Stacked microChannel heat sinks for liquid cooling of microelectronic components,” *J. Electron. Packag. Trans. ASME*, vol. 126, no. 1, pp. 60–66, 2004,

[125] L. Sun, J. Li, H. Xu, J. Ma, and H. Peng, “Numerical study on heat transfer and flow characteristics of novel microchannel heat sinks,” *Int. J. Therm. Sci.*, vol. 176, no. February, p. 107535, 2022,

[126] A. Bar-Cohen and P. Wang, “Thermal management of on-chip hot spot,” *J. Heat Transfer*, vol. 134, no. 5, pp. 1–11, 2012,

[127] S. G. Kandlikar *et al.*, “Heat transfer in microchannels - 2012 status and research needs,” *J. Heat Transfer*, vol. 135, no. 9, pp. 1–18, 2013,

[128] T. D. Nguyen *et al.*, “Design and thermomechanical analysis of a cell-integrated, tapered channel heat sink concept for prismatic battery cells,” *Appl. Therm. Eng.*, vol. 189, no. January, p. 116676, 2021,